KneeHub_DU Documentation
Cleveland State University

Release 1

William Zaylor, Neda Abdollahi, Jason P. Halloran

Aug 24, 2018

CONTENTS

ONE

MODEL CREATION SUMMARY

This section summarizes the steps involved in creating a finite element knee model. The summary includes links to other chapters where specific details are provided. This chapter also describes the inputs and outputs of each step.

These steps apply to the DU data set. The documentaiton for the OpenKnee(s) data set can be found in a separate document.

Additionally, ligaments and tendons are modeled as bundles of springs, however the steps for modeling these tissues as a continuum are also documented. This additional documentation is included to prevent excessive use of revisions if it is decided to represent ligaments and/or tendons as a continuum.

1.1 Image Segmentation and Reconstruction

The MR images are used to define two types of data

1. Label maps
2. Insertion sites (for spring representation)

Label maps are used to represent 3D geometry, and that geometry is reconstructed into surfaces. The insertion sites are used to define ligament and tendon geometry that are modeled as bundles of springs. The ligaments and tendons that are modeled as bundles of springs do not need label maps or surface models.

The segmentation process is described in the *image segmentation* (page 8) section, and the reconstruction process is described in the *geometric reconstruction* (page 45) section. The process used to define ligament and tendon insertion sites and geometry are described in the *ligament and tendon meshing* (page 52) section.

Ligaments and tendons are modeld as bundles of springs. One spring is defined by connecting one insertion point to another. Multiple springs are used to represent a ligament, and these springs are linearly distributed across the insertion area. To achieve this, the user places two points at the margins of each insertion area (4 total for each ligament/tendon). The insertion areas as identified using literature descriptions of *soft tissue anatomy* (page 16). The specific details on how this process are described in the *ligament and tendon meshing* (page 52) section.

If in the future, a ligament and/or tendon is being modeled as a continuum, then the geometry should be *segmented* (page 8) and *reconstructed* (page 45) like the other geometry.

1.1.1 Segmentation Inputs

- **MR images**
  - The CT images supplied with the DU data set are not used.

1.1.2 Segmentation Outputs

The outputs of segmentation are label maps that are defined from the MR images.

- **Label maps**
  - Femur
  - Tibia
  - Patella
  - Femur cartilage
  - Tibia cartilage
  - Patella cartilage
  - Medial meniscus
  - Lateral meniscus
- **Insertion sites for ligament/tendon spring model (4 points defined with respect to the MR image coordinate system)**

  - Ligaments
  - Tendons

1.1.3 Reconstruction Inputs

The label maps that are output from segmentation are the inputs for *geometric reconstruction* (page 45). These inputs are the label maps for the femur, tibia, patella, cartilage, and medial and lateral meniscus. Ligaments and tendons are modeled as bundles of springs, therefore they do not have label maps, and they are not reconstructed into surfaces.

If in the future, a ligament and/or tendon is being modeled as a continuum, then ligament/tendon label maps created during *segmentation* (page 8) should be reconstructed into surfaces.

1.1.4 Reconstruction Outputs

Geometric reconstruction uses the label maps to define surfaces. One surface is created for each label map, and these surfaces are saved as .stl files.

- Femur surface .stl
- Tibia surface .stl
- Patella surface .stl
- Femur cartilage surface .stl
- Medial tibial cartilage surface .stl
- Lateral tibial cartilage surface .stl
- Patella cartilage surface .stl
- Medial meniscus surface .stl
- Lateral meniscus surface .stl

1.2 Mesh Creation

The surfaces that were created during the *Image Segmentation and Reconstruction* (page 1) are used to create the solid meshes that are used in the finite element model. The bones and cartilage are modeled as rigid bodies, so the surfaces created for the femur, tibia, and patella are used as the finite element meshes for those geometries. The cartilage is being modeled using an elastic foundation model (*[LKST15]* (page 93),:cite:*halloran_comparison_2005*), so the meshes for the femoral cartilage, tibial cartilage (medial and lateral) and the patellar cartilage are being converted into quadrilateral dominated surfaces. The menisci are modeled as solids, and the surfaces are used to create hexahedral meshes, and the hexahedral meshes are used in the finite element model. If in the future, a ligament and/or tendon is being modeled as a continuum, then the geometry should also be meshed using hexahedral elements following the same procedure as used for meshing the menisci.

Specific details on the meshing process are described in the *meniscus meshing* (page 50) and *cartilage meshing* (page 51) sections.

The insertion points for the ligaments and tendons are used to define the individual fibers that connect the insertion sites. The insertion sites are used to define the initial ligament and tendon geometry. See the *ligament and tendon meshing* (page 52) section for more details on ligament and tendon mesh creation.

Note that the number of elements used in the ligament, cartilage, and menisci geometry will be determined with convergence studies.

1.2.1 Meshing Inputs

- **Solid Geometry**
    - Medial meniscus surface (.stl)
    - Lateral meniscus surface (.stl)
- **Elastic Foundation Geometry**
    - Femur cartilage surface (.stl)
    - Medial tibial cartilage surface (.stl)
    - Lateral tibial cartilage surface (.stl)
- **Rigid Geometry**
    - Femur surface (.stl)
    - Tibia surface (.stl)
    - Patella surface (.stl)
- **Ligament and Tendon Geometry**
    - Insertion sites (4 points defined with respect to the MR image coordinate system)
    - Desired number of fibers for each ligament and tendon
    - Desired number of "cross elements" for each ligament and tendon (see *ligament and tendon meshing* (page 52) for more information)

1.2.2 Meshing Outputs

- **Solid Geometry**
    - Medial meniscus hexahedral mesh (abaqus .inp file)

- – Lateral meniscus hexahedral mesh (abaqus .inp file)

- **Elastic Foundation Geometry (rigid)**

    - – Femur cartilage quadrilateral dominated mesh (abaqus .inp file)

    - – Medial tibial cartilage quadrilateral dominated mesh (abaqus .inp file)

    - – Lateral tibial cartilage quadrilateral dominated mesh (abaqus .inp file)

    - – Patellar cartilage quadrilateral dominated mesh (abaqus .inp file)

- **Rigid Geometry**

    - – Femur triangular surface mesh (abaqus .inp file)

    - – Tibia triangular surface mesh (abaqus .inp file)

    - – Patella triangular surface mesh (abaqus .inp file)

- **Initial Ligament and Tendon Geometry**

    - – Ligament spring mesh (abaqus .inp file, one file for each ligament)

    - – Tendon spring mesh (abaqus .inp file, one file for each tendon)

1.3 Reference Simulation

The initial ligament and tendon meshes are defined by connecting insertion points with straight lines, and they may overclose the bones, cartilage, and menisci. A *reference simulation* is used to make the ligaments and tendons wrap around any bodies that they may initially overclose. The purpose of the *reference simulation* is to modify the node positions of the initial ligament and tendon meshes to account for wrapping. The *reference state mesh* (page 54) and *reference simulation boundary conditions* (page 74) sections describes this process in more detail.
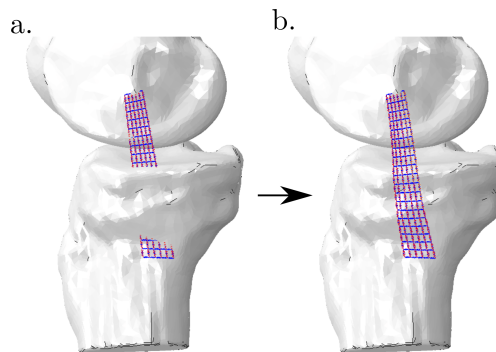
Fig. 1.1: An example of (a) the initial mesh that is defined from insertion point to insertion point data, and (b) the reference state where the ligament's mesh wrapped around the femur and tibia surfaces. Note that this is used as an example, and not used to describe the insertion locations or size of any specific ligament.

1.3.1 Reference Simulation Inputs

- **Solid Geometry**

    - – Medial meniscus hexahedral mesh (abaqus .inp file)

    - – Lateral meniscus hexahedral mesh (abaqus .inp file)

- **Rigid Geometry**

- Femur cartilage mesh (abaqus .inp file)

- Medial tibial cartilage mesh (abaqus .inp file)

- Lateral tibial cartilage mesh (abaqus .inp file)

- Femur triangular surface mesh (abaqus .inp file)

- Tibia triangular surface mesh (abaqus .inp file)

- Patella triangular surface mesh (abaqus .inp file)

- **Initial Ligament and Tendon Geometry**

  - Ligament spring mesh (abaqus .inp file, one file for each ligament)

  - Tendon spring mesh (abaqus .inp file, one file for each tendon)

1.3.2 Reference Simulation Outputs

- **Updated Ligament and Tendon Geometry (new node positions)**

  - Ligament spring mesh (abaqus .inp file, one file for each ligament)

  - Tendon spring mesh (abaqus .inp file, one file for each tendon)

1.4 Coordinate Systems

The rigid body coordinate systems are defined for the femur, tibia, and patella. Specific details on those processes can be found in the *coordinate systems* (page 55) section.

These rigid body coordinate systems are used to define *connector elements*, and the nodes that compose the *connector elements*. These elements are used to assign boundary conditions and/or loads to the joint coordinate system, and to also measure joint motion with respect to the joint coordinate system. The specific information on *connector element* definition can be found in the *connector elements* (page 61) section.

1.4.1 Coordinate Systems Inputs

- **User selected points from MR images (used for initialization)**

  - Femoral landmarks

  - Tibial landmarks

  - Patellar landmarks

- **Digitized points**

  - Femur

  - Femoral articulating surface

  - Femoral landmarks

  - Tibia

  - Tibia articulating surface

  - Tibial landmarks

  - Patella

- – Patella articulating surface
- – Patellar landmarks
- **Surfaces (.stl)**
  - – Femur
  - – Femoral cartilage
  - – Tibia
  - – Tibial cartilage
  - – Patella
  - – Patellar cartilage

1.4.2 Coordinate Systems Outputs

- Connector element definitions (abaqus .inp file)

1.5 Interactions and Ties

Rigid ties are used to simulate insertions of the ligament, tendons, and meniscal attachments. Similarly, the cartilage is rigidly tied to the corresponding bone. Interactions are used to define contact between different bodies.

This section does not have specific inputs or outputs. The ties and interactions are described in the *interactions and ties* (page 70) section, and the sequence with interactions are activated are described in the *simulation steps* (page 74) section.

1.6 Simulation Steps and Boundary Conditions

The different steps used in a FEA simulation, and boundary conditions are described in the *simulation steps and boundary conditions* (page 74) section.

In general, the passive flexion simulation starts with applying a nominal 20 N load to the quadricep along the quadricep's *line of action* (page 63), while the femur and tibia are fixed. This is followed by the femur being flexed from it's initial position to 0 degrees flexion. The 20 N quadricep load is maintained, and a 20 N compressive load is also applied to the femur throughout this step.

The last step in the passive flexion simulation flexes the femur about it's medial-lateral axis from 0 to 90 degrees. There is a nominal 20 N compressive load applied to the joint to maintain joint contact. Similarly, there is a nominal 20 N load applied to the quadricep to maintain contact between the femur and the patella.

1.7 Model Outputs

The model outputs are measured from the finite element simulation results. Custom Python scrits are used to read/extract the desired results from the simulation's results file. The outputs are described in the *Model Outputs* (page 85) section.

The main output variables are:

- Contact (area, force, and pressure)

- Joint kinematics

- Ligament forces

TWO

IMAGE SEGMENTATION

2.1 Introduction

This section contains the process of partitioning an MR image into multiple segments(sets of pixels, i.e. Label Map). In this process a label is assigned to each pixel in an MR image so that pixels with the same label represent a specific structure (e.g. bone, ligament, cartilage, etc). These segments will be used to create the volumetric reconstruction of the desired tissue or bone.

To familiarize yourself with the segmentation software and procedure, first review *Loading Data into Slicer* (page 9), *Segmentation Procedure* (page 10), *Label Map Smoothing* (page 13) and *Generate Triangulated Surface (STL) from Label Map* (page 13)) sections then move on to *Tissue Specific Procedure* (page 14) section for guidline on suggested steps for segmentation of bones, cartilage and soft tissues.

2.2 Prerequisite

3D Slicer: 3D Slicer is an open source software platform for medical image informatics, image processing, and three-dimensional visualization https://www.slicer.org/ .

2.3 Inputs

One set of DICOM file (.dcm files) including 112 slices of 3D T2-weighted MRI with fat suppression and sagittal plane resolution of 0.35 mm. Download the Denver group data from the following link: https://simtk.org/frs/?group_id=1061

Specimen/Sample Labeling protocols

Labeling protocols will be followed for each structure, which allows use of pre- and post-processing procedures to be generically applied after segmentation.

- DU02: Denver Group Specimen 2
- Bone:
    - **FMB**: Femur
    - **TBB**: Tibia
    - **FBB**: Fibula
    - **PTB**: Patella
- Cartilage:
    - **FMC**: Femoral Cartilage

- **TBC**: Tibial Cartilage
- **PTC**: Patellar Cartilage
- Ligaments:
    - *amAcl* (page 16): Anteromedial Bundle of Anterior Cruciate Ligamnet
    - *plAcl* (page 16): Posterolateral Bundle of Anterior Cruciate Ligamnet
    - *alPcl* (page 18): Anterolateral Bundle of Posterior Cruciate Ligament
    - *pmPcl* (page 18): Posteromedial Bundle of Posterior Cruciate Ligament
    - *sMclProx* (page 21): Proximal Fibers in Superficial Bundle of Medial Collateral Ligament
    - *sMclDist* (page 21): Distal Fibers in Superficial Bundle of Medial Collateral Ligament
    - *dMcl* (page 21): Deep Bundle of Medial Collateral Ligament
    - *lcl* (page 24): Lateral Collateral Ligament
    - *all* (page 26): Anterolateral Ligament
    - *pfl* (page 27): Popliteofibular Ligament
    - *oplMid* (page 27): Middle Portion of Oblique Popliteal Ligament
    - *pMFL* (page 38): Posterior Meniscofemoral Ligament (Ligament of Wrisberg)
    - *aMFL* (page 38): Anterior Meniscofemoral Ligament (Ligament of Humphrey)
    - *Mpfl* (page 29): Medial Patellofemoral Ligament
    - *Lpfl* (page 30): Lateral Patellofemoral Ligament

2.4 Loading Data into Slicer

Detailed procedures for loading the above described MRI data sets are given to help reduce the uncertainty for reproducibility across groups. Note the segmentation procedure, which applies to each tissue (*Tissue Specific Procedure* (page 14)), is described below. In Slicer to load DICOM files (for loading Denver data):

- Click `File > DICOM`.
- On the top left of the window click on the `Import` and navigate to the desired dictory and hit `Import`. Yo can import multiple sets of DICOM data in to the slicer.
- Select the desired DICOM file in the DICOM browser and click `load`.
- To re-open the DICOM browser, from the `Modules` drop-down menu go to DICOM module and click on `Show DICOM Browser`.

Load segmented label maps:

- Click `data` button from the top toolbar section or go to `File > Add Data`.
- Click `Choose File(s) to Add`, select desired label map file (.nrrd or .nii).
- Check the `Show Options` box on top right of the window. A couple of checkboxes will appear in front of the name of the file you have selected. For label maps always check the `LabelMap` box.
- Click `Open`.

2.4.1 Notes

Following points will be useful throughout the segmentation procedure.

1. Display the slice view controller window by moving your mouse over the pin icon on the top left corner of any of the slice viewer you want. The panel may be opened persistently by clicking on the pin icon.

- you will see 3 layers (`L`,`F`,`B`) specific options (If you can not see layers option click on the double arrow icon for showing all the options).

- Layer labeled as "`L`" is the current Label Map Volume that you are editing. You can switch between available Label Maps using the drop-down menu. The visibility of the Label Map can be changed using the spinbox widget, from 0.0 (transparent) to 1.0 (opaque). You can toggle between showing the Label Map with regions outlined or filled using the square icon next to the spinbox.

- Layer labeled as "`B`" is the Background Layer. In the `Editor` module the background gray-scale is known as the `Master Volume` since it is used as the input for `Editor` module tools (e.g. `PaintEffect`, `DrawEffect`,etc). Note that you can load multiple MRI sets into Slicer (e.g. those that are cartilage specific or ligament specific). Any of these MR images can be used as the background layer, you can toggle between them using the background layer drop-down menu. For example one may wish to create the label map volume based on a high resolution MRI and then edit it while looking at a low resolution MRI. If you are doing so, make sure that you first create your label map based on the `Master Volume` you have already chose in the `Editor` module.

- Layer labeled as "`F`" is the Foreground Layer. Two label maps can be overlayed on the MRI in order to compare label map boundaries between two different structures. The label map you want to edit should be set as the label layer (`L`). The other label map can be loaded as the foreground layer (`F`). You can control the opacity of the Foreground label using the spinbox opacity widget next to it.

2. In the lower left corner of each slice viewer, three layers mentioned above and their assigned image/label are being displayed.

3. `Crosshair` options are available for precise cross-correlation between slice viewers. Click on the `Crosshair` drop-down menu in the toolbar. It provides a set of options for customizing the appearance and behavior of the `crosshair` across all slice viewer windows. Hold `Shift` and move mouse in a slice view to position the Crosshair in all slice viewers.

4. It's recommended to save your work frequently, to avoid repeating all the tedious work through program crashes. Click on `Save` icon on the toolbar, a list of different files with different names and formats will appear. By default, Slicer will select the scene and any modified data sets. You can change this selection using checkboxes in the leftmost column or through three shortcuts icon on the top left of the panel. Make sure to change the directory of each file in the directory column. To save label map volumes you have to make sure to select the file with the same name as your `Merge Volume` in the `Editor` module with .nrrd or .nii format.

2.5 Segmentation Procedure

2.5.1 Manual Segmentation

- After loading a volume (MR images) enter the `Editor` module from the toolbar. `Editor` module is used for manipulating label map volumes.

- If this is the first time entering `Editor`, you will be prompted to choose a color table. Select the `GenericAnatomyColors`. If this is not the first time, the result of previous editing will be automatically selected when you enter `Editor` module.

- Under the `Create and Select Label Maps` tab, there is a `Master Volume` drop-down menu. The MRI set displaying in slice viewers is automatically selected as the `Master Volume`. You can change it using the drop-down menu.

- If your background is named "x1", the label will be automatically named "x1-label". You can create a new one under the `Merge Volume` drop-down menu and then click `Create a new LableMapVolume`. If you have loaded a previously segmented label map, make sure that the label map being edited in the slice viewers is the same as the Merge Volume.

- Highlight the anatomy of interest in every slice, in each image orientation as appropriate (coronal, sagittal, axial).

    - If you want to segment multiple structures from one MRI, it is better to create separate label maps for each of them. Before start highlighting the structure of interest, under `Create and Select Label Maps` tab and in `Per-Structure Volumes` section click the `Add Structure`. You will be prompted to choose a color (label value) based on the Color Table selected when the Merge Volume was created. In such cases the Merge Volume will contain all the structures (label maps).

- Different tools are available in Editor module to highlight anatomy of interest:

    - Use the `Paint Effect` (under `Edit Selected Label Map` tab, third icon from left, on the top row) with an appropriate/largest radius, to fill in the area using a brush. Select the `Sphere` checkbox to also applies the radius to slices above and below the current slice. In this case you have to be careful on your brush size since it will also paint in other slices and it may overlap with other structures. To avoid this issue try not to highlight areas very close to boundaries of anatomy of interest and after you are done highlighting, make sure to go through all slices and check for overlaps. In general, spherical brush is a handy tool for segmenting big structures (e.g. femur and tibia). It will help you saving a lot of time doing highlighting.

    - Use the eraser (under `Edit Selected Label Map` tab, second icon from left, on the top row) to change the behaviour of the tool, e.g. brush or pencil, to erase rather than draw.

    - Use the Draw Effect (under `Edit Selected Label Map` tab, forth icon from left, on the top row) to draw the boundaries of the area. By dragging mouse right click lay down a continuous line to outline the structure of interest (use "x" key to delete the last point added) and then left click to fill in the outline.

2.5.2 Grow Cut Segmentation

- Perform first three steps of *Manual Segmentation* (page 10)

- Choose the paint brush effect and highlight the anatomy of interest (L1) on roughly equally-spaced slices in each image plane orientation as appropriate (coronal, sagittal, axial)(Fig. 2.1)

- Under `Edit Selected Label Map` tab, change the label value (color) to highlight the area around the anatomy of interest (L2) on the slices you have also highlighted the anatomy itself(Fig. 2.1).

- In an image plane orientation other than the one you are highlighting in, cap the area around the anatomy of interest to prevent L1 label leakage (Fig. 2.2).

- Click the `GrowCutEffect` (third icon from left on the bottom row). Make sure the L1 label (associated with the anatomy of interest) is selected under the `Label` drop-down menu and then hit the `Apply` button. Slicer window graphics will freeze until the grow cut algorithm is complete.

- Remove the L2 label color (colors around the anatomy of interest) using `ChangeLabelEffect`. Choose the L2 label as the selected Label and also as the `Input Color` and choose background label (black color) as the `Output Color` and click the `Apply` button.
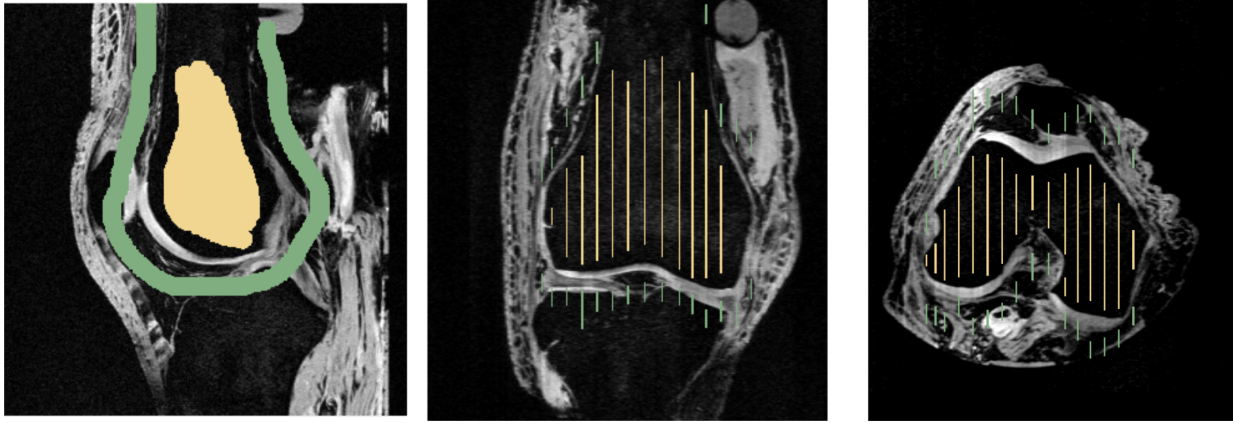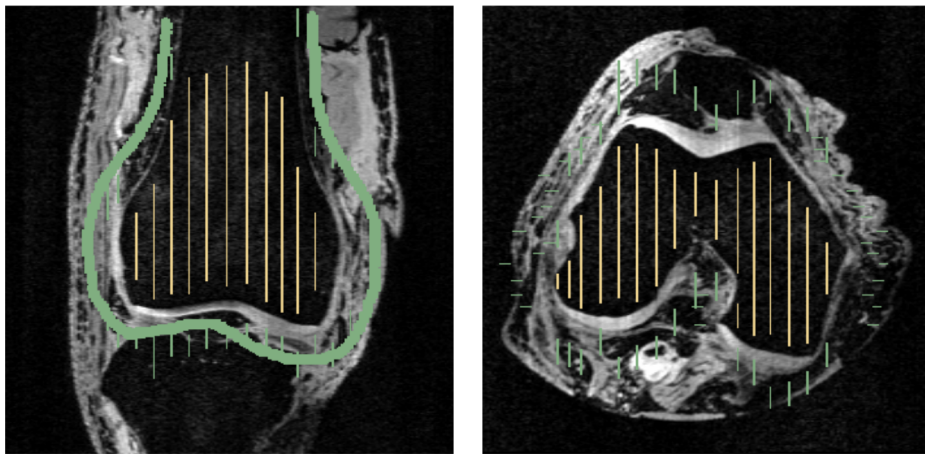
Fig. 2.1: Grow Cut Segmentation.

Fig. 2.2: Grow Cut Segmentation, after performing label leakage control.

2.5.3 Notes

Some shortcuts in `Editor` module:

- **f** , move to next slice

- **b** , move to previous slice

- **z** , undo

- **y** , redo

- **Shift** , scroll other slices to mouse location

- **h** , toggle the crosshair and put it into navigator mode

- **e** , toggles from the current color to 0 and back (use this while painting or drawing to quickly erase if you go over the line)

- **c** , show color picker

- **Escape** , cancel current effect

- **p** , select Paint effect

- **d** , select Draw effect

- **w** , select Wand effect

- **r** , select Rectangle effect

- **Space** , bring up tool selection window at current mouse location

- **- or _** , shrink the current radius by 20%

- **+ or =** , grow the current radius by 20%

2.6 Label Map Smoothing

Following smoothing step will be performed to remove the noises and outliers remaining from the grow cut segmentation step. This smoothing procedure is on the voxel level and will preserve the volume.

- From the `Modules` drop-down menu, select `Surface Models > Label Map Smoothing`.

- Set Gaussian Smoothing Parameters, Sigma based on image resolution (e.g. 0.7 for cartilage MRI, resolution = 0.35 x 0.35 x 0.7 mm).

- From `Input Volume` drop-down menu, select desired label map.

- From `Output Volume` drop-down menu, select `Create new Volume as...`.

- Enter new name as desired, click `OK`.

- Click `Apply`.

2.7 Generate Triangulated Surface (STL) from Label Map

- From the `Modules` drop-down menu, select `Surface Models > Model Maker`.

- Under `IO` tab, from `Input Volume` drop-down menu, select desired label map.

- In `Models` drop-down menu, either `Create new ModelHierarchy as...` (e.g. default is 'Models'), or select an existing Model Hierarchy. All models can be generated under the same or separate model hierarchies.

- Under `Create Multiple` tab, specify a desired `Model Name` for the selected label map.

- For creating raw STL models:

  - Under `Model Maker Parameters` tab, set `Smooth` to zero.

  - Under `Model Maker Parameters` tab, set `Decimate` to zero.

- Click Apply button.

- Enter the `Editor` module and select the `MakeModelEffect` (second icon from right on the bottom row) under `Edit Selected Label Map` tab.

- Set desired label map as the `Merge Volume`. If no smoothing is desired, deselect `Smooth Model`.

- Click Apply button.

- A 3D model of the label map will appear on the 3D view window. Roll your mouse over the pushpin icon on the blue bar across top of the 3D viewer window to open the configuration panel.

- Click on the `Save` icon on the toolbar. By default, 3D models will be saved with .vtk format. you can change it from the `File Format` drop-down menu in front of the file name. Make sure to choose the desired directory for saving the file.

2.8 Output

Output of the segmentation procedure is the triangulated surface representation of the tissue of the interest (.STL) in the raw and unfiltered format.

2.9 Tissue Specific Procedure

In the following sections segmentation procedure for bones, cartilage and soft tissues will be specifically described.

2.9.1 Bone & Cartilage Segmentation Procedure

Input: Cartilage MRI

Procedure:

- Perform *Grow Cut Segmentation* (page 11) on desired bone.

- Perform *Label Map Smoothing* (page 13) to remove Grow Cut boundary noise.

- Perform *Manual Segmentation* (page 10) to more accurately define bone/cartilage boundary. It will be helpful to overlay the General Purpose MRI (as the Foreground label) on the Cartilage MRI in order to get a more accurate boundary definition.

- Iteratively repeat last two steps until boundary is as desired.

It is better to perform cartilage segmentation along with the bone segmentation. This way you can use bone boundaries to define cartilage boundaries, just remember to define a separate label map volume for the cartilage.

2.9.2 Soft Tissue Segmentation Procedure

Input: Connective Tissue MRI (MRL)

Procedure:

- Load sagittal ligament MRI

- Perform *Manual Segmentation* (page 10)

- Perform *Label Map Smoothing* (page 13)

- In order to have a high resolution segmentation volume from a low resolution MRI, one can open Cartilage MRI and Connective Tissue MRI in different viewer windows. When windows are linked Slicer uses interpolation for coupled viewing and you can use Cartilage MRI as the `Master Volume` and segment the soft tissue on the interpolated MRI.

- Alternatively, You can segment the tissue on the Connective Tissue MRI and then lay the label map over the Cartilage MRI (as the `Foreground Layer`, make sure to increase the opacity, the default is zero) Create a new label map as the `Merge Volume` and start to segment the soft tissue. Use the Connective Tissue MRI label map as a guideline for the boundaries of the tissue.

SOFT TISSUE ANATOMY

This section is a annotated bibliography for the soft tissue anatomy that is represented in the knee models. It is used to provide a description of the soft tissue anatomy that is being modeled.

Note: Many of the descriptions are copy and pasted from the literature. Citations are included in the descriptions, however they are not properly quoted. This documentation is for internal use only, and descriptions should be quoted or revised before publication.

Tibiofemoral:

3.1 ACL Anatomy

This section describes the ACL anatomy, including the bundles represented in the model and the femoral and tibial insertion sites.

3.1.1 General Description

- **Femoral insertion: posterior part of the inner surface of the lateral femoral condyle** *[DBA+06]* **(page 89)**

    – Size can vary from 11 to 44 mm across ('across' not defined) *[DBA+06]* (page 89)

- **Tibial insertion: a fossa located anterior and lateral to the medial tibial spine. Fibers 'fan out' as they approach the tibial**

    – The fosa is approximately 11 mm wide (range of 8 to 12 mm), and the anterior-posterior length is 17 mm (range, 14–21 mm) *[DBA+06]* (page 89)

- Length: 22 to 41 mm (mean 32 mm) *[DBA+06]* (page 89)

This lab models the ACL as two distinct bundles, the anteromedial (amACL) and the posterolateral (plACL) bundles. These names are derived from their insertion on the tibial plateau.

3.1.2 amACL

- Femoral insertion: The most superior and anterior part of the insertion

- Tibial insertion: The most anteromedial aspect of the tibial insertion

- Length: 34 mm in extension (like most MR images used in the lab) *[DBA+06]* (page 89).
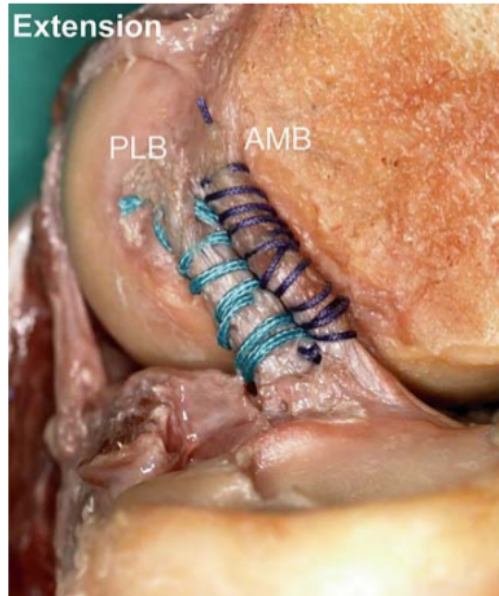
Fig. 3.1: The amACL (labeled AMB) and plACL (labeled PLB) bundles *[DBA+06]* (page 89).

Fig 3A–B. (A) This figure shows a lateral femoral condyle. The anteromedial bundle is located high and deep in the intercondylar fossa, whereas the postero-lateral bundle is located more low and shallow. Because arthroscopic surgery is normally performed with the knee in 90° of flexion, in the clinical literature the notch roof is considered high (anatomic description, anterior), the anterior rim is considered shallow, the posterior part is considered deep, and the posterior part is considered low. (B) The posterior end of the intercondylar fossa is marked by the intercondylar line (arrows). This line borders on the Facies poplitea (FP) of the distal femur. The AM origin is located at the transition of the intercondylar line to the articular cartilage.
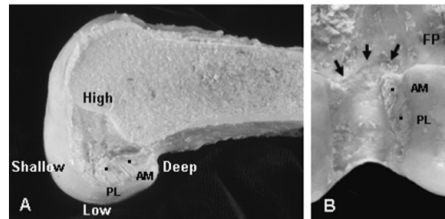
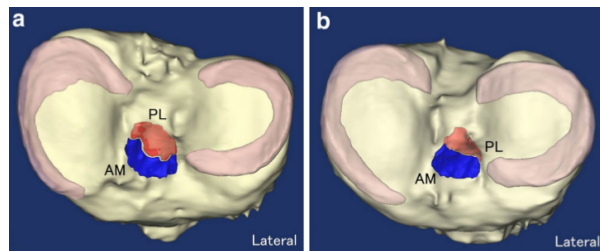Fig. 3.2: The amACL and plACL femoral insertions *[PZ07]* (page 89).

Fig. 3.3: General tibial insertions of the amACL and plACL bundles *[TLG+18]* (page 89).

Fig. 1 **a** Anteromedial (AM: blue) and posterolateral (PL: *red*) bundle fibres of the ACL are distinguished from each other at the tibial side, and the attachment is segmented from the sagittal MR images. **b** A 3D model of proximal left tibia with AM and PL insertion sites was created from the MRI slices using the Mimics® software. Medial meniscus is shown in this figure. **c** The lateral meniscus (LM) is segmented and shown in 3D. The overlap of ACL fibres and anterior horn of lateral meniscus (AHLM) is also segmented and reconstructed in 3D (*green* area indicated with *arrow*)
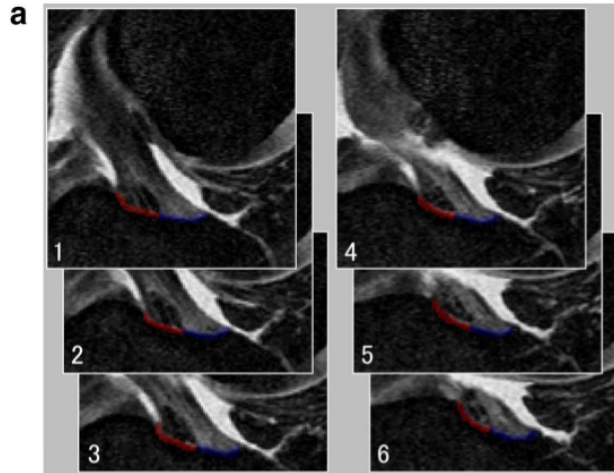
Fig. 3.4: Segmentation of the amACL and plACL bundles *[TLG+18]* (page 89). This shows one way to differentiate between the AM and PL bundles in the MR images.

Note:

When modeling the ligament as a bundle of nonlinear springs that are linearly mapped across the insertion site:

- The femur's proximal point corresponds with the tibia's more anteromedial point
- The femur's distal point corresponds with the tibia's more posterolateral point

---

3.1.3 plACL

- Femoral insertion: The most distal and posterior part of the insertion
- Tibial insertion: The most posterolateral aspect of the tibial insertion
- Length: 22.5 mm in extension (like most MR images used in the lab) *[DBA+06]* (page 89).

Note:

When modeling the ligament as a bundle of nonlinear springs that are linearly mapped across the insertion site:

- The femur's proximal point corresponds with the tibia's more anterior point
- The femur's distal point corresponds with the tibia's more posterior point

---

3.2 PCL Anatomy

This section describes the PCL anatomy, including the bundles represented in the model and the femoral and tibial insertion sites.

3.2.1 General Description

- Femoral insertion: The femoral insertion can span from the trochlear notch to the inner surface of the medial femoral condyle. The femoral attachment of the PCL extends more than 20 mm in an anterior–posterior (AP) direction across the roof and medial side of the femoral intercondylar notch *[AGBE05]* (page 89).

- Tibial insertion: posterior aspect of the tibia, between two prominences which are the posterior aspects of the medial and tibial plateau *[AZW+12]* (page 89).

The lab models the PCL as two functional bundles, the anterolateral (alPCL) and posteromedial (pmPCL).
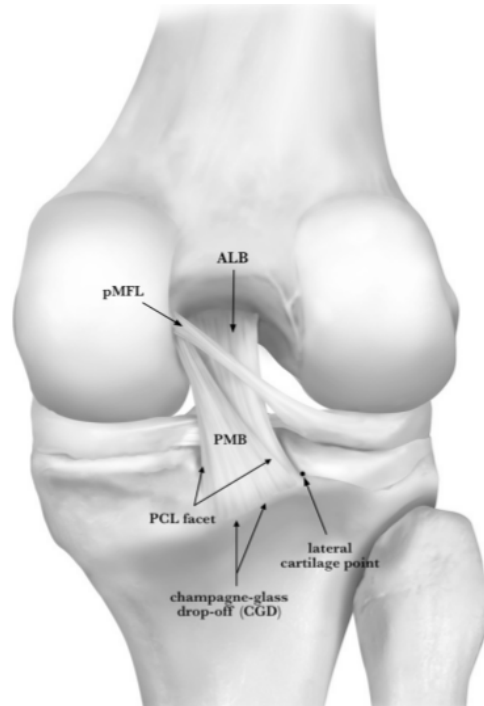
Fig. 3.5: The alPCL (labeled ALB) and pmPCL (labeled PMB) bundles *[AZW+12]* (page 89).

3.2.2 alPCL

- Femoral insertion: approximately 112 mm^2 in area, with the center being ~7.4 mm to the trochlear point, and ~7.9 mm from the distal articular cartilage Fig. 3.7 *[AZW+12]* (page 89).

- Tibial insertion: t approximately 88 mm^2 in area. The insertion is anterior to the pmPCL tibial insertion. The center of the insertion area is ~8.6 mm from the lateral cartilage point Fig. 3.9 *[AZW+12]* (page 89).

Note:

When modeling the ligament as a bundle of nonlinear springs that are linearly mapped across the insertion site:

- The femur's more anterior point corresponds with the tibia's more lateral point

- The femur's more posteriomedial point corresponds with the tibia's more medial point

Fig. 3.6: The alPCL (labeled ALB) and pmPCL (labeled PMB) femoral insertions for a right knee *[AZW+12]* (page 89).

Fig. 3.7: The alPCL (labeled ALB) and pmPCL (labeled PMB) femoral insertions for a right knee *[AZW+12]* (page 89).

Fig. 3.8: The alPCL (labeled ALB) and pmPCL (labeled PMB) tibial insertions for a right knee *[AZW+12]* (page 89).
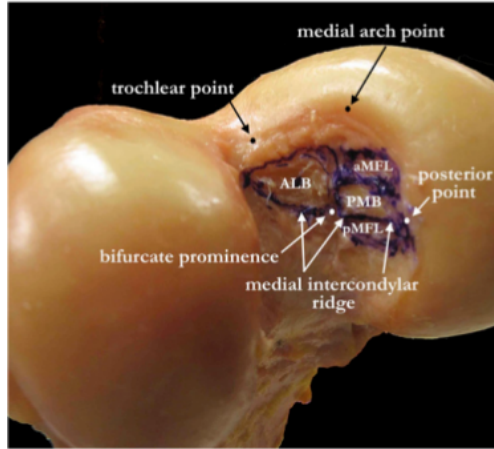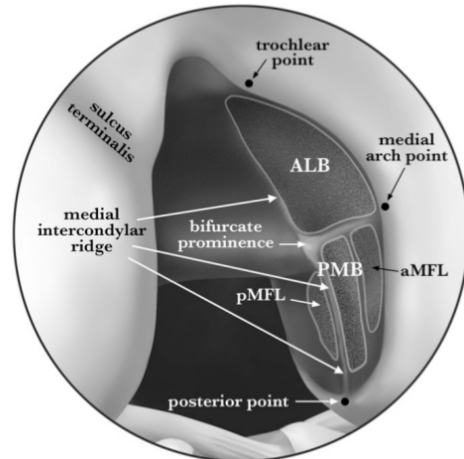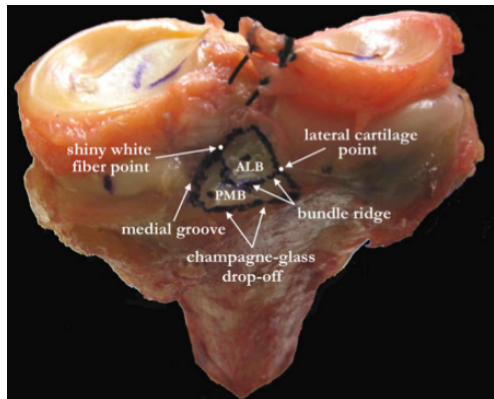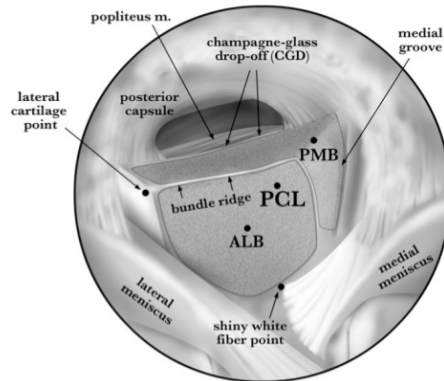
Fig. 3.9: The alPCL (labeled ALB) and pmPCL (labeled PMB) tibial insertions for a right knee *[AZW+12]* (page 89).

3.2.3 pmPCL

- Femoral insertion: approximately 60 mm^2 in area, with the center being about ~18.8 mm from the trochlear point and ~8.6 mm from the distal articular cartilage Fig. 3.7 *[AZW+12]* (page 89).

- Tibial insertion: approximately 105 mm^2 in area. The insertion is posterior to the alPCL tibial insertion Fig. 3.7 Fig. 3.6. *[AZW+12]* (page 89).

Note:

When modeling the ligament as a bundle of nonlinear springs that are linearly mapped across the insertion site:

- The femur's more anterior point corresponds with the tibia's more lateral point

- The femur's more posterior point corresponds with the tibia's more medial point

---

3.3 MCL Anatomy

This section describes the MCL anatomy, including the bundles represented in the model and the femoral and tibial insertion sites.

3.3.1 General Description

This lab models the MCL as three distinct bundles. Two of those bundles compose the superficial MCL (sMCL), and one bundle represents the deep MCL (dMCL). The sMCL has one femoral and two two tibial attachments *[LaP07]* (page 91), one tibial insertion is more proximal to the joint line (psMCL), and the other is more distal to the joint line (dsMCL). The tibial attachments are used to differentiate the two sMCL bundles.

3.3.2 Proximal sMCL

- Femoral insertion: the attachment is located in a depression that is slightly proximal and posterior to the medial femoral epicondyle. The center of the attachment side is 6.4 mm (3.9 to 9.6 mm) from the medial femoral epicondyle, and 26.8 mm (13.1 to 32.2 mm) from the femoral joint line (assumed to be in extension). The insertion area is approximately 94.1 mm^2 (60.1 to 143.8 mm^2) *[LaP07]* (page 91) (appendix).
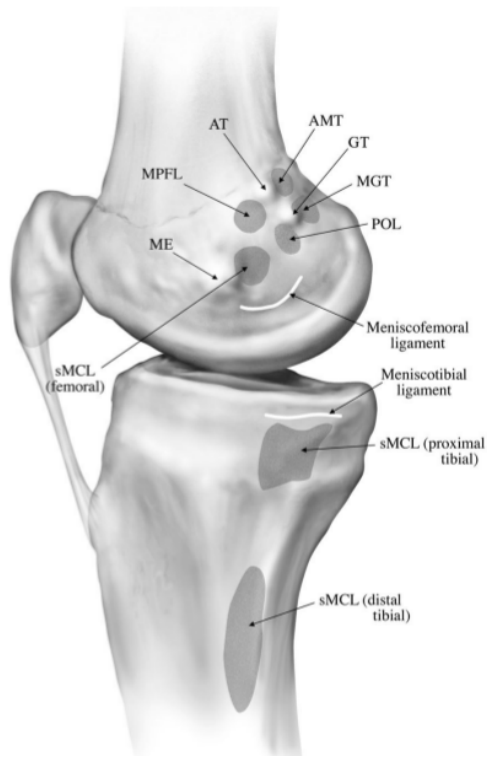
Fig. 3.10: The insertions of the MCL *[LaP07]* (page 91).
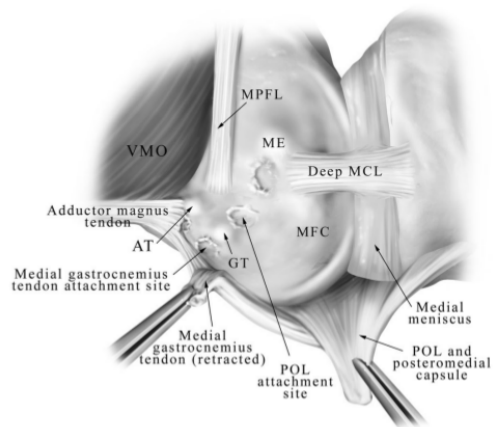
Fig. 3.11: The insertions of the dMCL *[LaP07]* (page 91).
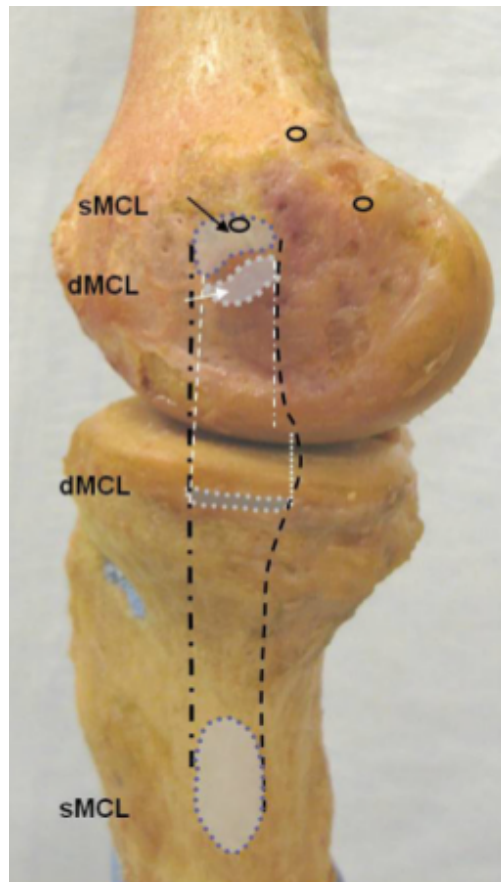
Fig. 3.12: The insertions of the dMCL *[LYG+10]* (page 89).

- Tibial insertion: the tibial insertion is described as connecting to the semimembranosus tendon, and the tendon inserts into the tibia. This is modeled as a direct attachement of the psMCL into the tibia (this describes the semimembranosus tendon tibial attachment from *[LaP07]* (page 91)). The center of the attachment is located 12.2 mm (8.8 to 15.3 mm) to the tibial joint line. The attachment area is approximately 221.5 mm^2 (104.7 to 609.2 mm^2).

3.3.3 Distal sMCL

- Femoral insertion: the attachment is located in a depression that is slightly proximal and posterior to the medial femoral epicondyle. The center of the attachment side is 6.4 mm (3.9 to 9.6 mm) from the medial femoral epicondyle, and 26.8 mm (13.1 to 32.2 mm) from the femoral joint line (assumed to be in extension). The insertion area is approximately 94.1 mm^2 (60.1 to 143.8 mm^2) *[LaP07]* (page 91) (appendix).

- Tibial insertion: just anterior to the posteromedial crest of the tibia. The distance from the center of the attachment to the joint line is approximately 61.2 mm (52.4 to 70.5 mm). The attachement area is approximately 294.3 mm^2 (212.4 to 356.8 mm^2) *[LaP07]* (page 91) (appendix).

3.3.4 Deep MCL

The deep MCL (dMCL) has an insertion into the medial meniscus *[LaP07]* (page 91)*[LYG+10]* (page 89). The definition of this insertion is described in *dMCL and Meniscus Ties* (page 72).

- Femoral insertion: width (anterior-posterior) 9.9 ± 3.2 mm, with an area of 71.9 ± 14.8 mm^2, and the center of the insertion area is 20.5 ± 4.2 mm from the femoral joint line, and 13.0 ± 2.7 mm from the medial femoral epicondyle *[LYG+10]* (page 89).

- Tibial insertion: width (anterior-posterior) 18.0 ± 4.0 mm, with an area of 63.6 ± 13.4 mm^2, and the center of the insertion area is 6.5 ± 1.3 mm inferior to the tibial joint line *[LYG+10]* (page 89).

Note: This section references *[LaP07]* (page 91), and the appendix for this article can be found on the journal's website. The appendix appears to be freely available, so a subscription to the journal is not needed.

3.4 LCL Anatomy

This section describes the LCL anatomy, including the femoral and fibular insertion sites.

3.4.1 General Description

- Femoral insertion: slightly superior and posterior to the lateral femoral epicondyle. There is a small bony depression that the ligament inserts into. The insertion area is approximately 48 mm^2 (range, 43 to 52 mm^2):cite:*laprade_posterolateral_2003*.

- Fibular insertion: Attaches to the lateral aspect of the fibular head. The insertion is approximately 28.4 mm (range 25.1 to 30.6 mm) from the apex of the fibular head. The insertion area is approximately 43 mm^2 (range, 39 to 50 mm^2) *[LLWE03]* (page 89).

- Length: 69.6 mm (range, 62.6 to 73.5) *[LLWE03]* (page 89).
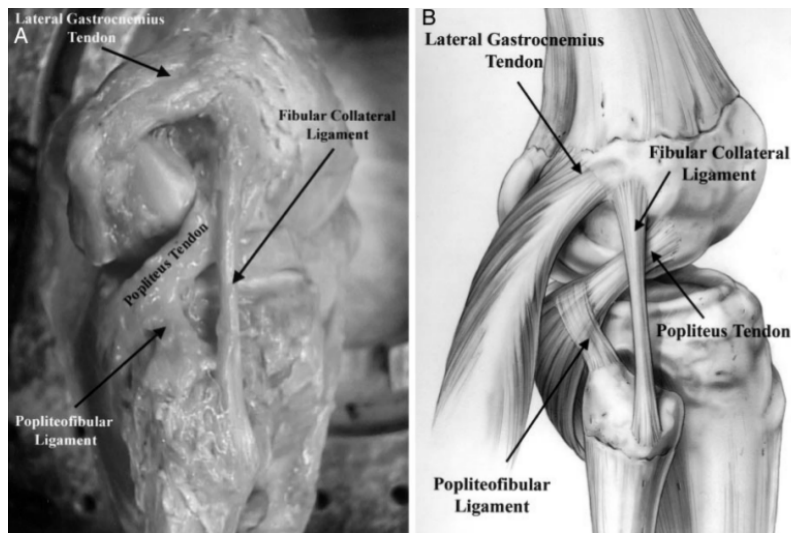
Fig. 3.13: The LCL (labeled *fibular collateral ligament*) anatomy for a right knee *[LLWE03]* (page 89).
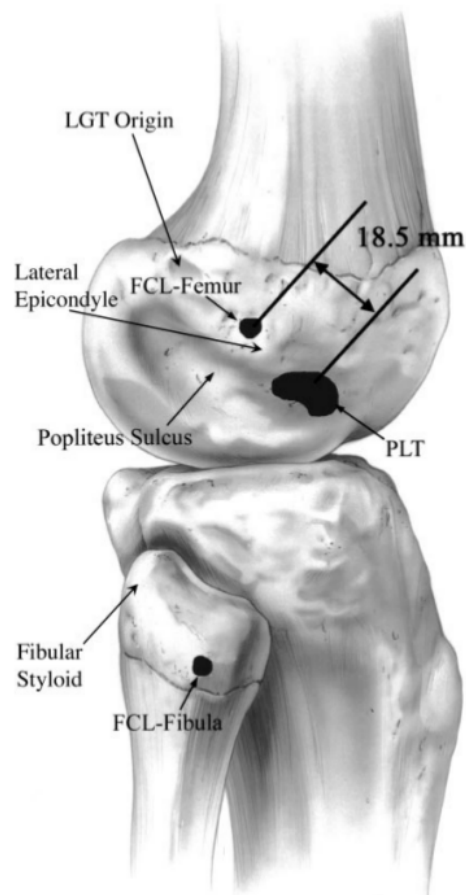
Fig. 3.14: The LCL (labeled *FCL*) anatomy for a right knee *[LLWE03]* (page 89).

3.5 ALL Anatomy

This section describes the anterolateral ligament (ALL) anatomy, including the femoral and tibial insertion sites.

3.5.1 General Description

- Femoral insertion: located on the prominence of the lateral femoral epicondyle, anterior to the socket from which the LCL originated, and proximal and posterior to the insertion of the popliteus tendon. The width is 8.3 $\pm$ 2.1 mm *[CVM+13]* (page 89).

- Tibial insertion: the width is 11.2 $\pm$ 2.5 mm, and the distance from the tibial articular cartilage and the insertion (assuming center) is 6.5 $\pm$ 1.4 mm. The distance from the center of the insertion to the fibular head is 23.2 $\pm$ 5.7 mm *[CVM+13]* (page 89).
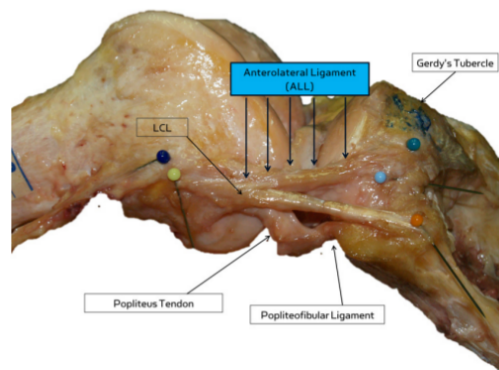
Fig. 3.15: The ALL anatomy for a right knee *[CVM+13]* (page 89).
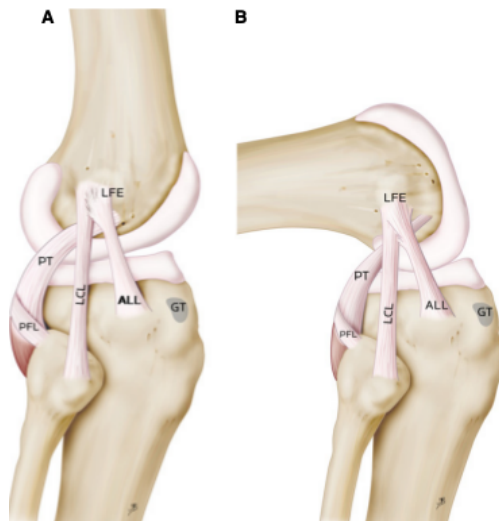
Fig. 3.16: The ALL anatomy for a right knee *[CVM+13]* (page 89).

3.6 PFL Anatomy

This section describes the popliteofibular ligament (PFL) anatomy, including the femoral and fibular insertion sites.

3.6.1 General Description

The popliteofibular ligament originates at the fibular styloid process and attaches to the popliteus tendon. The PFL courses proximodistally from the fibular attachment *[LLWE03]* (page 89) into the popliteus tendon, however this is not represented in the model. The model uses the popliteus tendon femoral insertion as the PFL's femoral insertion. The PFL/popliteus tendon is medial to the LCL.

- Femoral insertion: the femoral insertion of the popliteus tendon is used at the PFL's femoral insertion. The insertion is anterior to the LCL femoral attachment. The center of the insertion area is 15.8 mm (range, 11.2 to 18.6) from the lateral femoral epicondyle. The area of the insertion is 59 mm^2 (range,53 to 62) Fig. 3.18 *[LLWE03]* (page 89).

- Fibular insertion: near the tip of the fibular styloid process. The PFL is described as having separate anterior and posterior attachments *[LLWE03]* (page 89), however the model represents a single attachment.
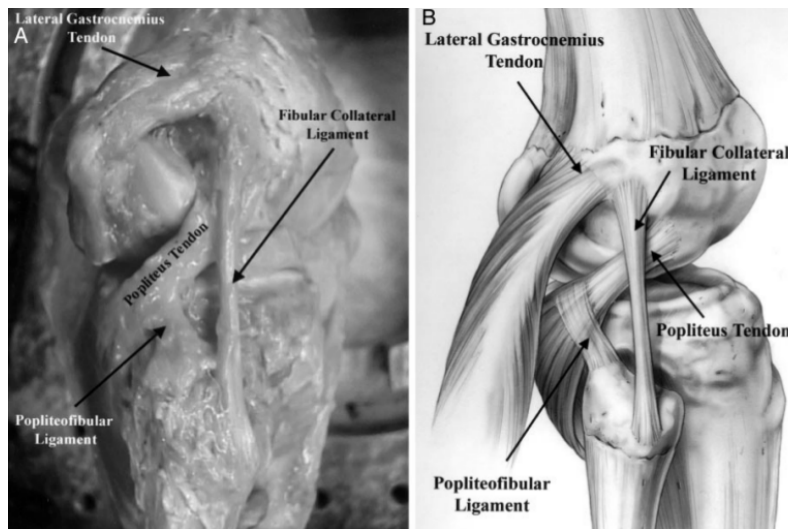
Fig. 3.17: The PFL anatomy for a right knee *[LLWE03]* (page 89).

3.7 OPL Anatomy

This section describes the oblique popliteal ligament anatomy, including the femoral and tibial insertion sites.

3.7.1 General Description

The OPL has two distal insertions, however the model represents the OPL as having only one tibial insertion that is just lateral to the PCL insertion. The medial aspect of the OPL is formed by "a confluence of the lateral expansion off the semimembranosus common tendon" *[LaP07]* (page 90). Given that the laxity tests do not activate the muscles, the medial aspect of the OPL is assumed to not be recruited throughout testing, and is not represented in the model.
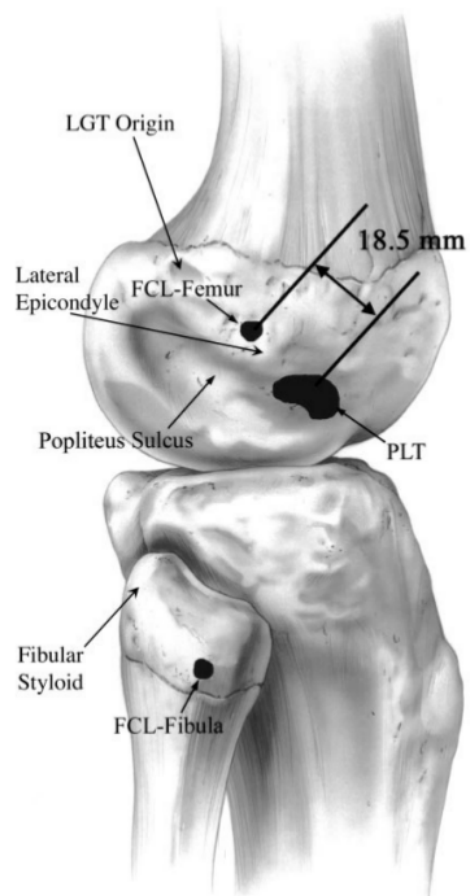
Fig. 3.18: The femoral insertion of the popliteus tendon (labeled *PLT*) *[LLWE03]* (page 89).

The OPL attaches proximally to an osseous or cartilaginous fabella, and blends into the posterolateral capsule at the posterolateral aspect of the distal part of the femur *[LaP07]* (page 90). The model does not represent the fabella, so the femoral attachment is taken as the attachment of the posterolateral jonit capsule to the

- Femoral insertion: inserts into the posterolateral joint capsule at the medial border of the lateral femoral condyle *[HSM+17]* (page 90). The model represents the femoral insertion site as on the lateral side of the lateral femoral condyle near the superior margin of the cartilage.

- Tibial insertion: lateral to the PCL tibial attachment, with an attachment length of 10.4mm (range, 7.0 to 14.0).
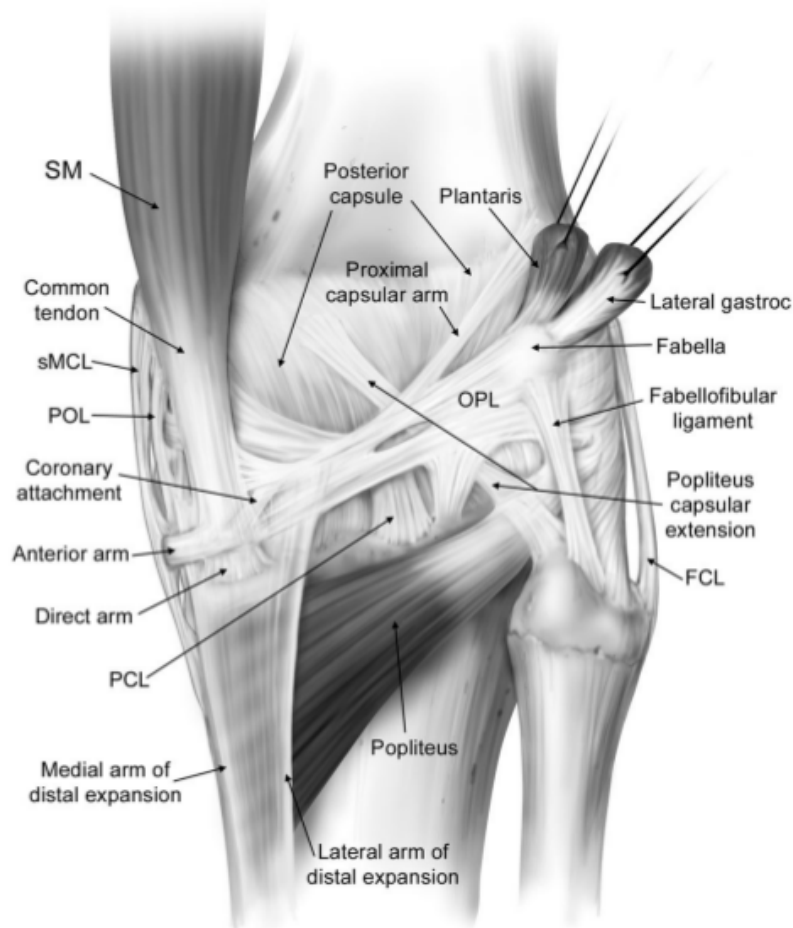
Fig. 3.19: The posterior view of a right knee showing the OPL *[LaP07]* (page 90).

Patellofemoral:

3.8 MPFL Anatomy

This section describes the medial patellofemoral ligament (MPFL) anatomy, including the femoral and patellar insertion sites.

3.8.1 General Description

The MPFL attaches at the medial epicondyle of the femur to the proximal part of the medial border of the patella.
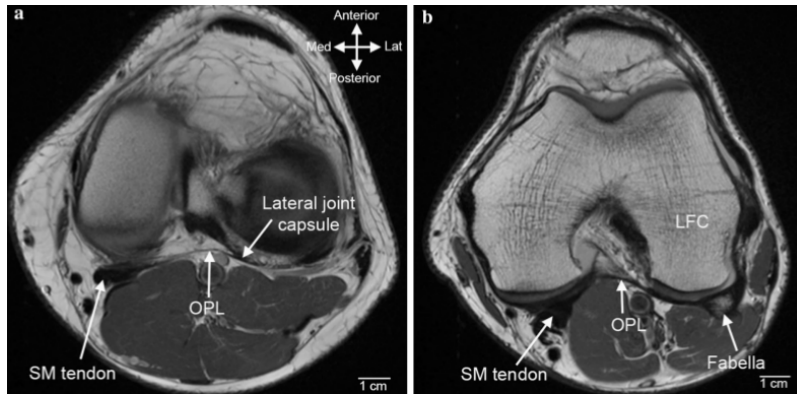
Fig. 3.20: Axial MR images showing the OPL *[HSM+17]* (page 90).

- Femoral insertion: attaches to the anterior aspect of the medial epicondyle, and the superior aspect of the MCL was in direct contact with the most inferior edge of the MPFL. Width (proximal to distal) is 15.4 mm (range, 11-20 mm) *[SDM04]* (page 90). The area of insertion site is 25.9 mm^2 (range, 22.7-29.2 mm^2) *[KCM+18]* (page 90).

- Patellar insertion: The vertical distance from the superior pole of the patella to the level of the superior edge of the MPFL is 6.1 mm (range, 0-13 mm). The vertical distance from the superior pole to the inferior edge of the MPFL is 23.1 mm (range, 15-29 mm). Width (proximal to distal) is 17 mm (range, 14-20 mm) *[SDM04]* (page 90). The area of patellar insertion site is 37.6 mm^2 (range, 26-49.2 mm^2) *[KCM+18]* (page 90).

- Length: 56.6 mm (range, 54.2-58.8 mm) *[KCM+18]* (page 90).

3.9 LPFL Anatomy

This section describes the lateral patellofemoral ligament (LPFL) anatomy, including the femoral and patellar insertion sites.

3.9.1 General Description

The lateral patellofemoral ligament is located in the deep retinacular layer. It is attached to the lateral patella as its widest part and anchored to the lateral femoral epicondyle with fan-like expansions *[CZE+17]* (page 90).

- Femoral insertion: The LPFL originated, on average, 2.6 mm distal (range, 13.1 mm proximal to 11.4 mm distal) and 10.8 mm anterior (range, 7.3 mm posterior to 14.9 mm anterior) to the lateral epicondyle. Overall, the absolute distance (Fig. 3.27) from the epicondyle was 14.5 mm (range, 10.6-20.6 mm). The average width of the femoral insertion is 11.7 mm (range, 9-13.9 mm) *[SDW+17]* (page 90).

- Patellar insertion: The LPFL insertion on to the patella is about 45% (range, 23.7%-58.4%) of its lateral articular surface and is in the middle third of the lateral patella. The average width of patellar insertion is 14.3 mm (range, 8.1-16.8 mm) *[SDW+17]* (page 90).

- Length: 23.2 mm (range, 12.4-40 mm) *[CZE+17]* (page 90).

3.10 Patellar Tendon Anatomy

This section describes the patellar tendon anatomy, including the tibial and patellar insertion sites.
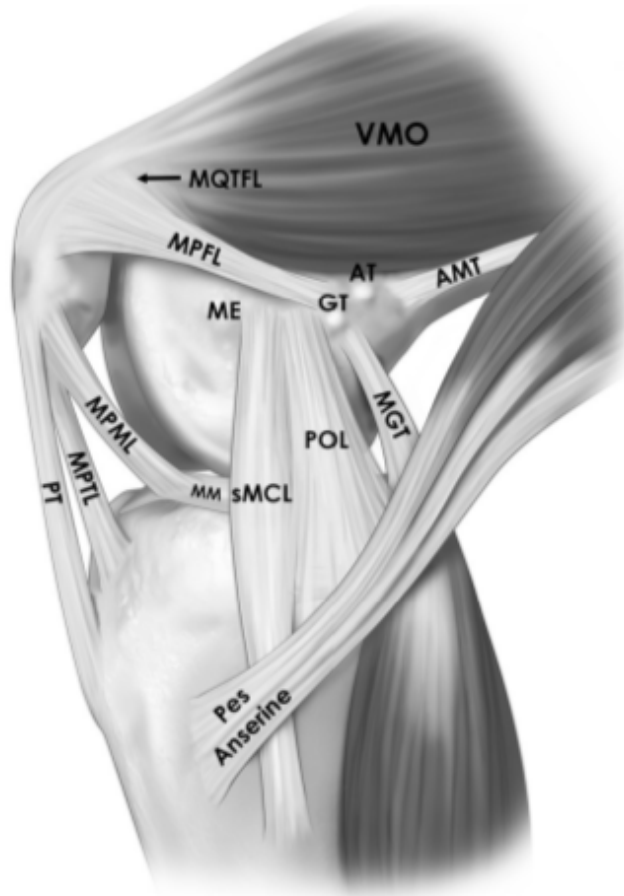
Fig. 3.21: The MPFL anatomy for a right knee *[KCM+18]* (page 90).
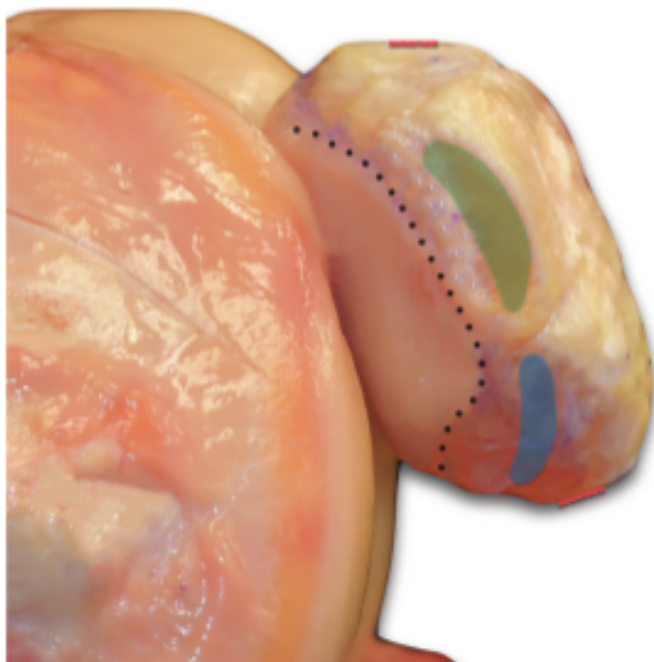
Fig. 3.22: Medial view of a left knee showing the patellar insertion site of MPFL (green) relative to the patellar articular cartilage (dotted line) *[KCM+18]* (page 90).
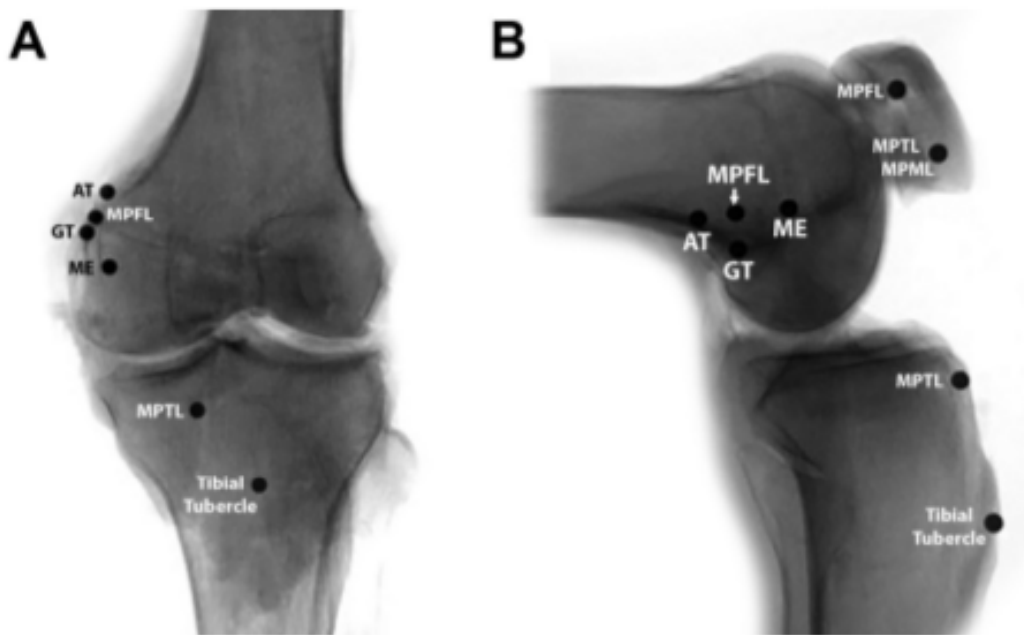
Fig. 3.23: Coronal and sagittal views of a left knee showing the positioning of the center of attachment of MPFL relative to the surgical relevant landmarks *[KCM+18]* (page 90).

Coronal View

	Mean Distance (95% CI), mm	Directionality
MPFL femoral attachment from		
Adductor Tubercle (AT)	9.2 (7.8-10.6)	Dsital
Gastrocneius Tubercle (GT)	3.5 (2.3-4.6)	Proximal
Medial Epicondyle (ME)	14.1 (10.8-17.5)	Proximal
Femoral Condylar line	36.5 (34.7-38.2)	Proximal

Sagittal View

	Mean Distance (95% CI), mm	Directionality
MPFL femoral attachment from		
Adductor Tubercle (AT)	9.7 (8.6-10.8)	Dsital
Gastrocneius Tubercle (GT)	10.4 (7.9-12.9)	Anterior
Medial Epicondyle (ME)	15.2 (12.8-17.6)	Proximal
Posterior Femoral Cortex Extension line	8.3 (5.1-11.5)	Anterior

Fig. 3.24: Radiographic measurements of the distances between MPFL attachment center and pertinent anatomic osseous landmarks on the femur on coronal and sagittal view *[KCM+18]* (page 90).
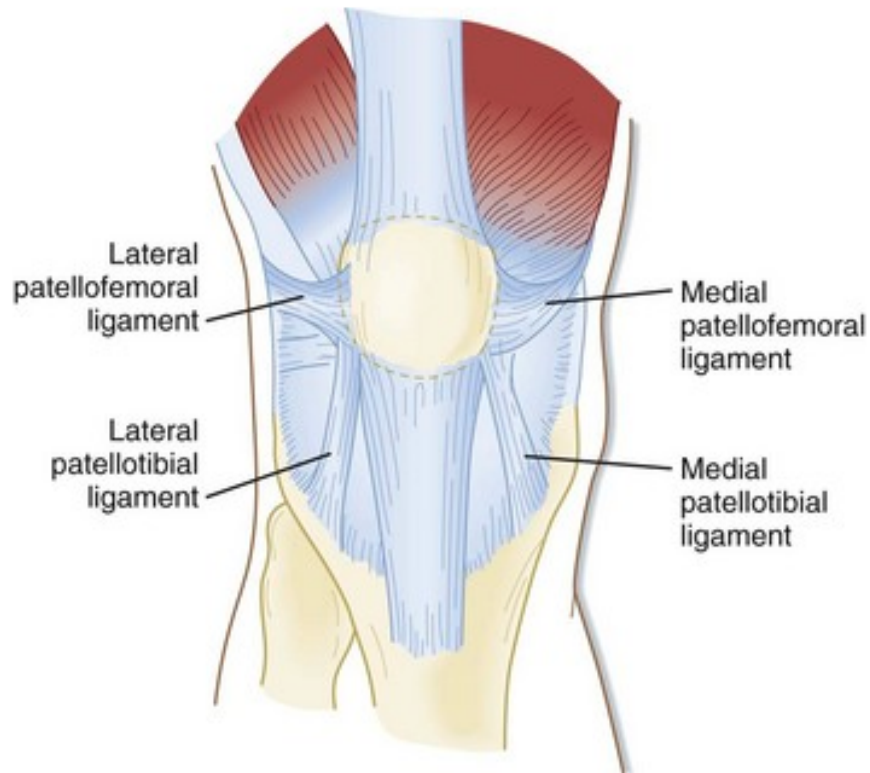
Fig. 3.25: The lateral patellofemoral ligament (LPFL) *[noa]* (page 90).
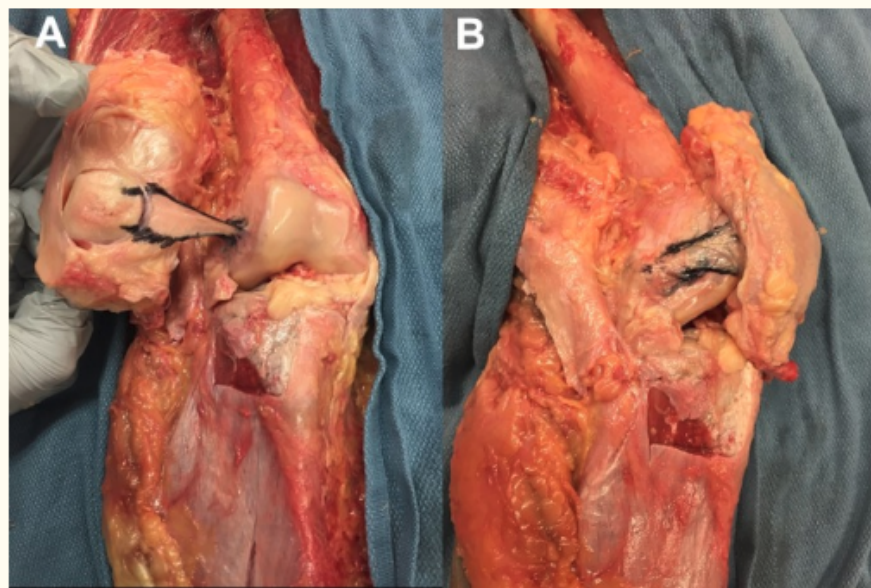
Fig. 3.26: LPFL outlined in a cadaveric specimen. (A) After disection, the patella is reflected laterally providing an intra-articular view of the LPFL (outlined in black). (B) Lateral image of the knee with the LPFL outlined in black *[SDW+17]* (page 90).
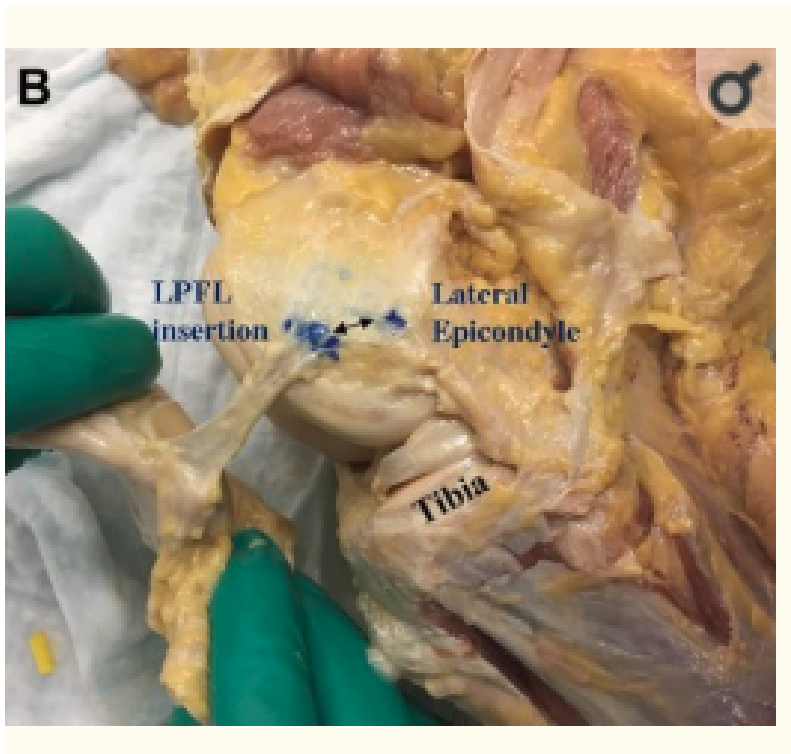
Fig. 3.27: Image showing the absolute distance (black double headed row) from the center of LPFL femoral insertion to the tip of the lateral epicondyle. In this case the femoral attachment was distal and anterior to the lateral epicondyle *[SDW+17]* (page 90).
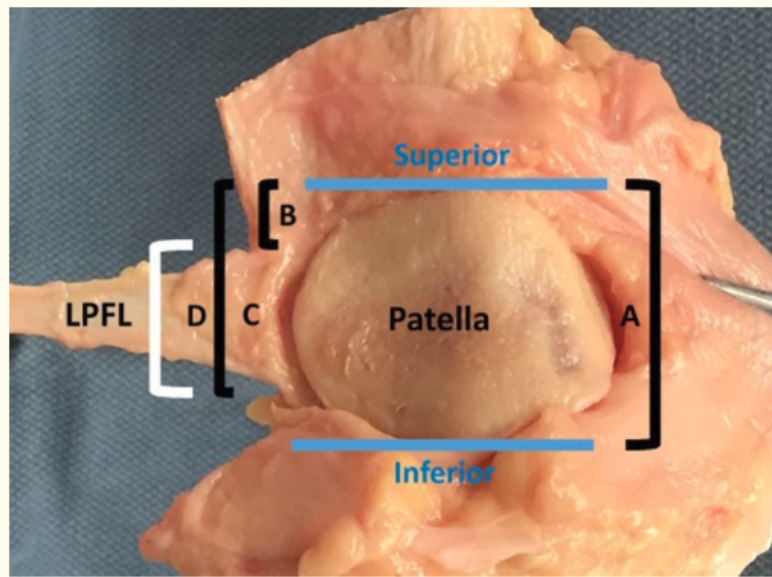
Fig. 3.28: Distance D is calculated to determine the width of the LPFL patellar insertion.

3.10.1 General Description

The patellar tendon (PT) extends from the inferior pole of the patella to the tibial tuberosity *[LAF12]* (page 90).

- Tibial insertion: is an irregular pentagonal shape with a medially directed superior apex and is widest proximally (Fig. 3.31). The mean tendon insertion width (Iw in Fig. 3.31) of 23.9 +/- 3.0 mm is nearly half that of the patella width at its greatest dimension (42 +/- 4.5 mm) *[DWP+14]* (page 90).

- Length: as the distance from the most proximal aspect of the attachment to the inferior pole of the patella is 52.88 +/- 7.56 mm *[NRLC+02]* (page 90).

3.11 Quadriceps Tendon Anatomy

This section describes the patellar insertion side anatomy of the quadriceps tendon.

3.11.1 General Description

The tendons of the four muscles that make up the quadriceps converge to one insertion on the superior aspect of the patella *[WJH09]* (page 90). The model represents these as one tendon.

- Patellar insertion: width 43.3+/-5.8 mm (range, 34.3 to 54.1 mm) *[LAF12]* (page 90).

Note: When defining the insertion site for the quadriceps, two proximal points should be defined (one medial and one lateral). These are used to calculate the line of action of the tendon in the image state.

Menisci:
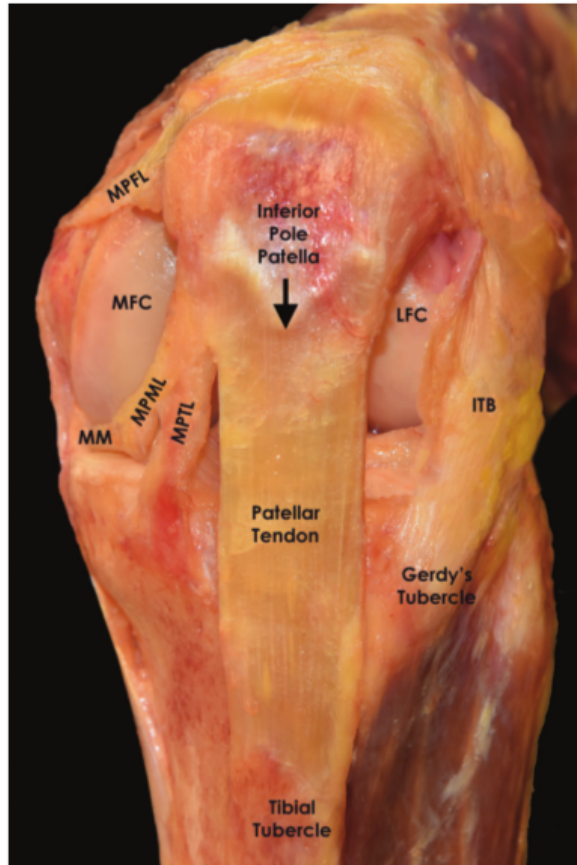
Fig. 3.29: Anterior view of a left knee at 90 degree flexion showing the attachments of the patellar tendon *[KCM+18]* (page 90).
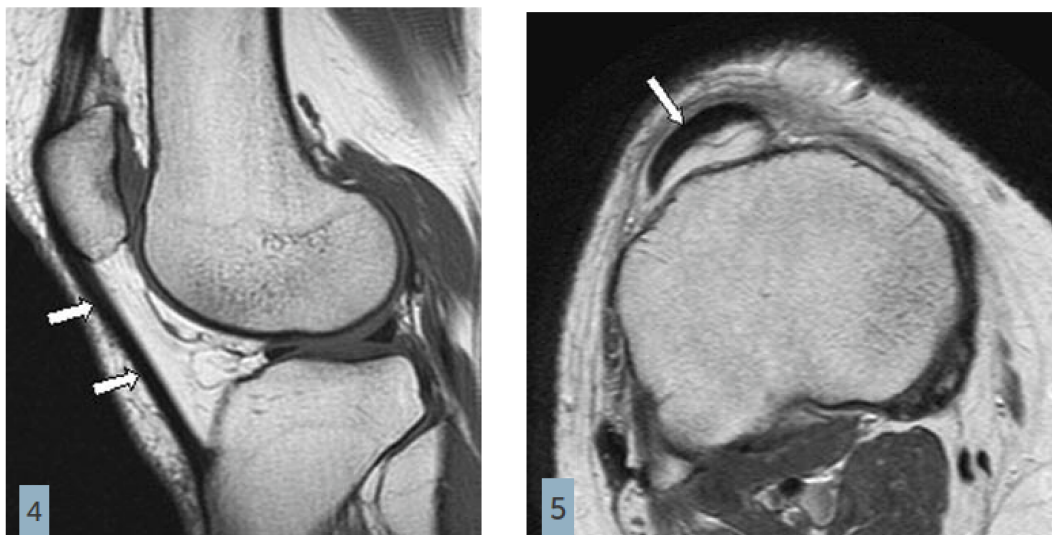
Fig. 3.30: A sagittal and axial MRI view of patellar tendon (arrow) *[noa06]* (page 90).
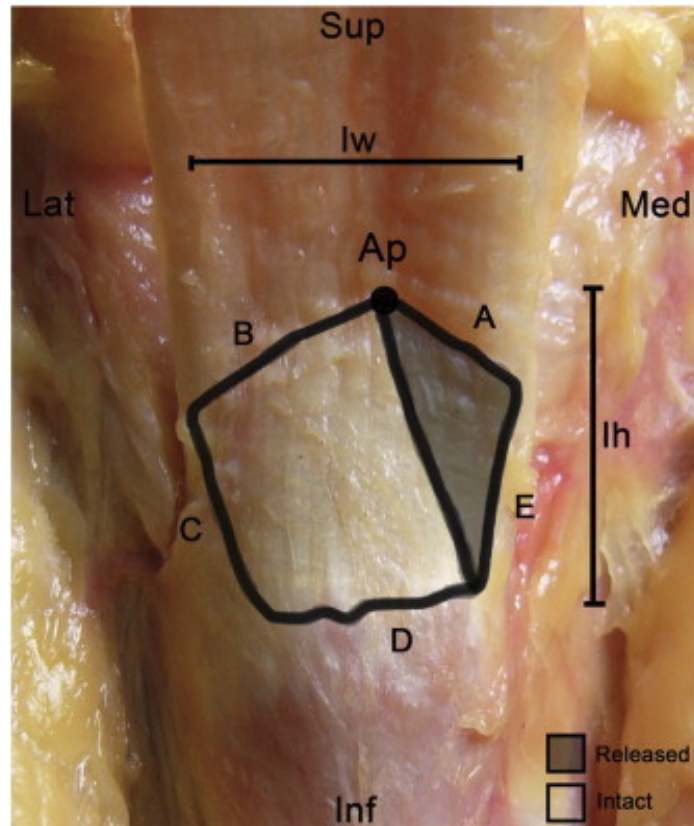
Fig. 3.31: Tibial insertion of patellar tendon in a right knee. Surface area landmarks are showing the Inserion Width (Iw), Insertion height(Ih), Superomedial edge length (A), Superolateral edge length (B), Lateral edge length (C), Inferior edge length (D) and Medial edge length (E) *[DWP+14]* (page 90).

3.12 aMFL Anatomy

This section describes the Anterior Meniscofemoral Ligament (aMFL) anatomy, including the femoral insertion sites.

3.12.1 General Description

The Anterior Meniscofemoral Ligament (aMFL), also known as ligament of Humphrey, arises from the posterior horn of the lateral meniscus, runs anterior to the PCL and inserts at the distal edge of the femoral PCL attachment *[noa18]* (page 91). The average ratio of the cross sectional area of Humphrey to that of the PCL within the same knee is 11.9% ± 5.7% *[KHC+94]* (page 91). This ligament may be confused for the PCL *[noa18]* (page 91).

- Femoral insertion: Inserts proximally to the inner aspect of the medial condyle of the femur, between the distal margin of the femoral attachment of the PCL and the edge of the condylar articular cartilage *[GSM+02]* (page 91).

- Meniscal insertion: The meniscal attachments of the pMFL followed its orientation in the sagittal plane and attaches to posterior horn of lateral meniscus. aMFL attachment to the meniscus is more anteriorly than pMFL *[GSM+02]* (page 91).

- length: 28.3 mm (range, 20.0-37.0 mm) *[YH91]* (page 91).
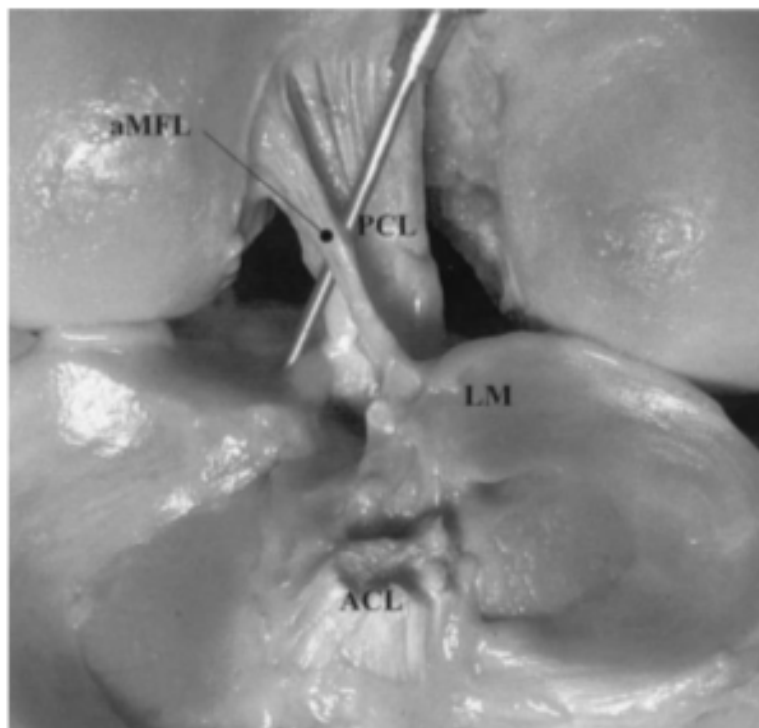
Fig. 3.32: Photograph showing an aMFL in a cadaver left knee. This clear view is provided by an anterior approach after removing the ACL and collateral ligaments *[GSM+02]* (page 91).

3.13 pMFL Anatomy

This section describes the Posterior Meniscofemoral Ligament (pMFL) anatomy, including the femoral insertion sites.
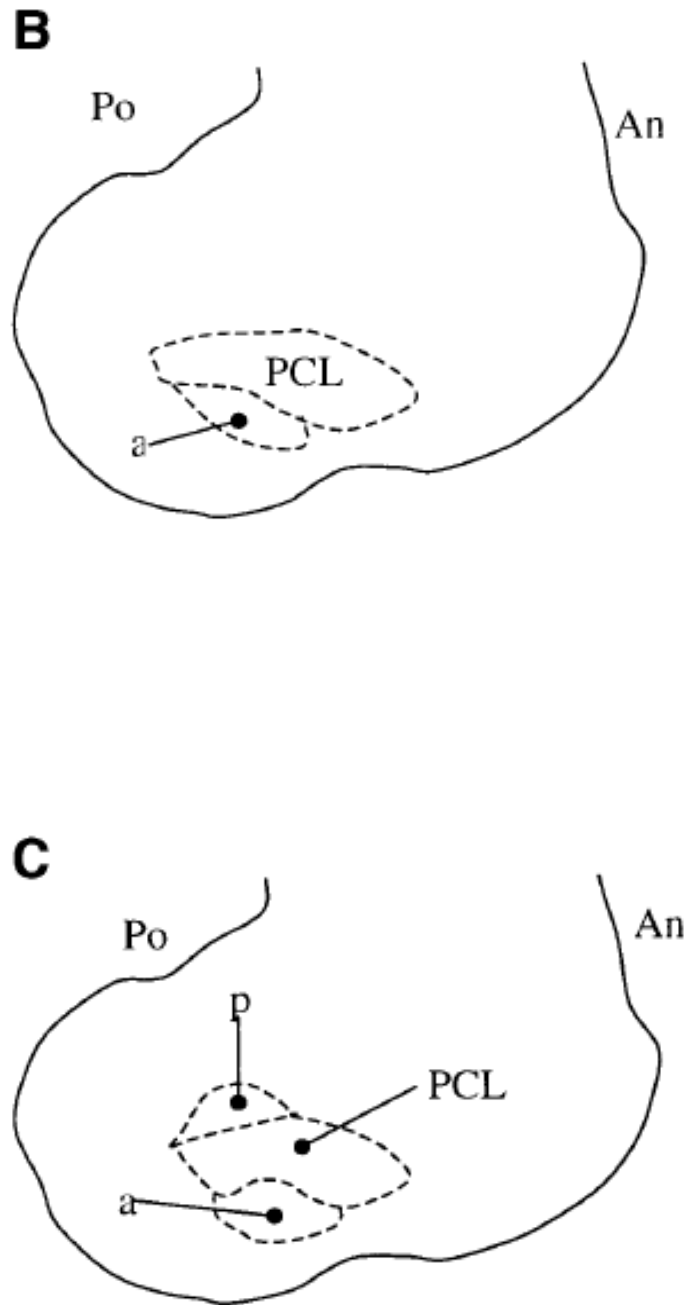
Fig. 3.33: Femoral insertion of aFML in relation to the insertion of the PCL. Diagrammatic views of the left lateral femoral condyle in sagittal section demonstrating its anterior (An) and posterior (Po) aspects. (B) Specimen with aMFL (a) and PCL. (C) Specimen with PCL and coexisting aMFL (a) and pMFL (p):cite:*gupte_review_2003*.

3.13.1 General Description

The Posterior Meniscofemoral Ligament (pMFL), also known as ligament of Wrisberg, extends from the posterior horn of lateral meniscus to medial femoral condyle and lies posterior to PCL. It is usually larger than ligament of Humphrey *[noa18]* (page 91). The average ratio of the cross sectional area of Wrisberg to that for the PCL within the same knee is $12.0 \pm 7.7\%$ *[KHC+94]* (page 91).

- Femoral insertion: It inserts at the medial part of the intercondylar notch near to insertion of the posteromedial band of the PCL. This is the reason why fibers of the pMFL and PCL sometimes intermingle *[noa18]* (page 91).

- Meniscal insertion: The meniscal attachments of the pMFL followed its orientation in the sagittal plane and attaches to posterior horn of lateral meniscus

- length: 31.2 mm (range, 27.0-40.0 mm) *[YH91]* (page 91).
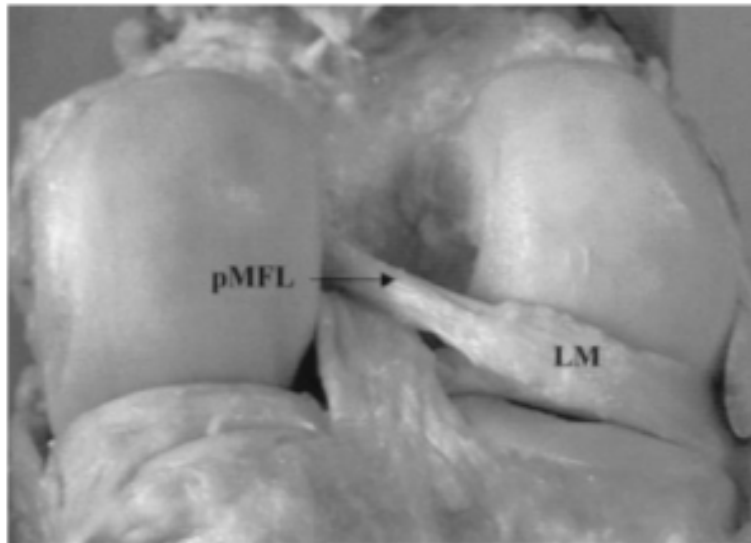
Fig. 3.34: Photograph of a pMFL in a cadaver right knee, as viewed after a posterior approach with the joint capsule removed. *[GSM+02]* (page 91).

3.14 Meniscal Horn Attachments

This section describes the anterior and posterior attachemnts of the medial and lateral menisci to the tibia.

3.14.1 General Description

The medial and lateral meniscus both have anterior and posterior attachment sites on the tibial plateau.

Lateral Meniscus

- Anterior insertion (alHorn): area of 140.7 mm^2 (+/- 30.0). The center of the attachment is approximately 7.1 mm (+/- 1.3) from the nearest edge of the lateral articular cartilage, and 13.4 mm (+/- 2.1) from the nearest edge of the posterior lateral meniscus attachment. *[LER+14]* (page 91)
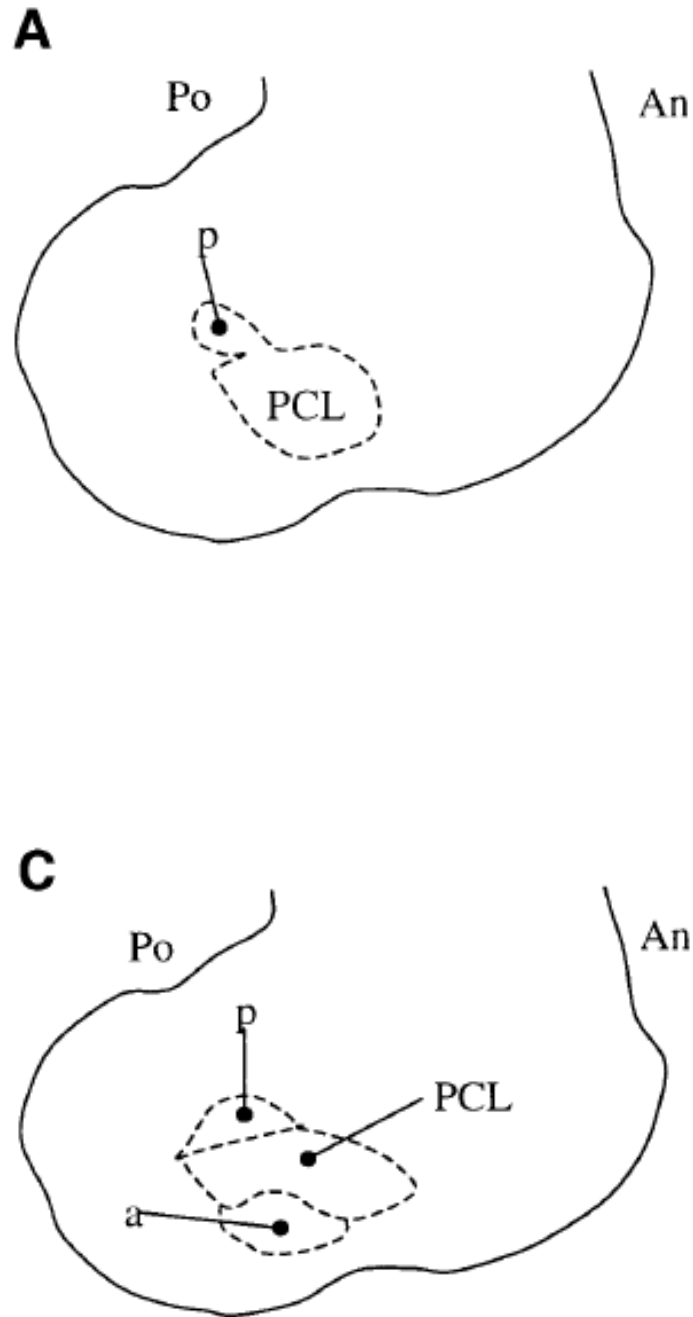
Fig. 3.35: Femoral insertion of pFML in relation to the insertion of the PCL. Diagrammatic views of the left lateral femoral condyle in sagittal section demonstrating its anterior (An) and posterior (Po) aspects. (A) Specimen with pMFL (p) and PCL. (C) Specimen with PCL and coexisting aMFL (a) and pMFL (p):cite:*gupte_review_2003*.
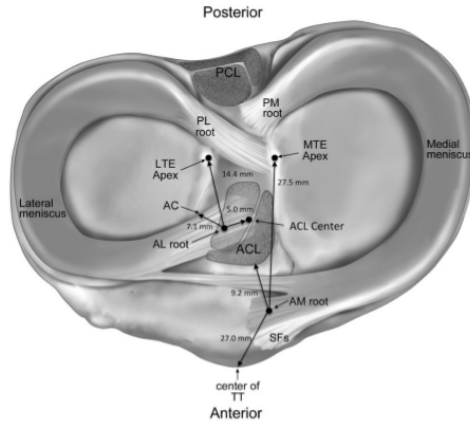
Fig. 3.36: The insertions of the meniscal horn attachments *[LER+14]* (page 91).
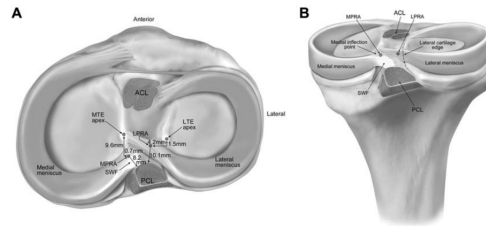
Fig. 3.37: The insertions of the meniscal horn attachments *[JCP+12]* (page 91).

- Posterior insertion (plHorn): area of 39.2 mm^2 (+/- 2.4). The center of the attachment is approximately 12.7 mm (+/- 1.1) from the nearest point on the PCL tibial insertion, and 10.1 mm (+/- 0.8) from the posterior edge of the anterior root attachment of lateral meniscus *[JCP+12]* (page 91).

Medial Meniscus

The anterior insertion of the medial meniscus (amHorn) is described as having a central dense root, and supplemental fiber extensions *[LER+14]* (page 91). The model will only include the central dense root of the attachment.

- Anterior insertion (amHorn): area of 56.3 mm^2 (+/- 14.9). The center of the attachment is approximately 7.6 mm (+/- 2.3) from the nearest edge of the medial articular cartilage, and 9.2 mm (+/- 2.7) from the nearest edge of the ACL insertion. *[LER+14]* (page 91)

- Posterior insertion (pmHorn): area of 30.4 mm^2 (+/- 2.9). The center of the attachment is approximately 8.2 mm (+/- 0.7) anterior of the most superior tibial attachment of the PCL, and 3.4 mm (+/- 0.4) lateral to the medial articular edge inflection point. *[JCP+12]* (page 91)

Tendons:

3.15 Biceps Femoris

This section describes the biceps femoris (BFM) anatomy, and the fibular attachment.

This anatomy is only modeled with the DU specimen because it is described as being loaded during patellofemoral testing in *[ASC+16]* (page 91). The OpenKnee(s) specimen does not have this tendon modeled because it is not loaded during the tibiofemoral or patellofemoral testing.

3.15.1 General Description

The biceps femoris is described as having several attachemnts to the tibia, and fibula. The tendons of the long and short head of the biceps femoris are described as coalescing, and first inserting into the fibula *[BA15]* (page 91). Three fibular insertions are described (proximal, distal, and medial). The proximal insertion is composed of both the long and short head of the biceps femoris. The distal and medial insertions are composed largely of the long and short head of the biceps femoris respectively.

The model includes the proximal fibular insertion of the BFM.

- Fibular insertion: 8.96 (95% confidence interval: 8.2-9.7) mm from the center of the fibular insertion to the tip of the fibular styloid process *[BA15]* (page 91). The area is 214.9 (95% CI 192.4-237.5) mm^2. The insertion is posterior to the LCL's fibular insertion.
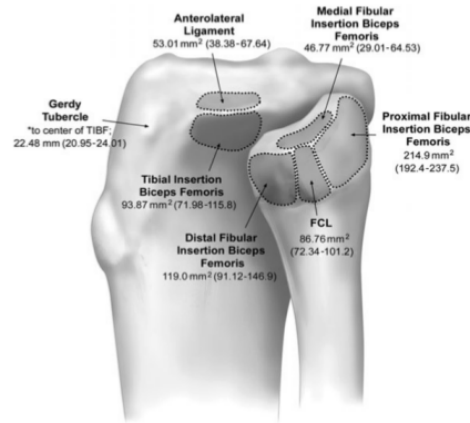
Fig. 3.38: The distal insertions of the BFM *[BA15]* (page 91). Note that the model only includes the proximal fibular attachement.

Note: When defining the insertion site for the biceps femoris, two proximal points should be defined to represent the line of action of the tendon in the image state.

3.16 Semimembranosus

This section describes the semimembranosus (SMT) anatomy, and the tibial attachment.

This anatomy is only modeled with the DU specimen because it is described as being loaded during patellofemoral testing in *[ASC+16]* (page 91). The OpenKnee(s) specimen does not have this tendon modeled because it is not loaded during the tibiofemoral or patellofemoral testing.

3.16.1 General Description

The semimembranosus tendon is described as having two arms that insert into the tibia, a direct arm and an anterior arm *[LaP07]* (page 91). The model includes the direct arm attachment, but not the anterior arm.

- Tibial insertion: proximal aspect of the posteromedial part of the tibia in a small groove just proximal to the tuberculum tendinis prominence. The center of the insertion area is 12.1 (range 9.2 to 14.9) mm distal to the tibial joint line. The insertion area is 107.4 (range 69.4 to 166.0) mm^2 *[LaP07]* (page 91).
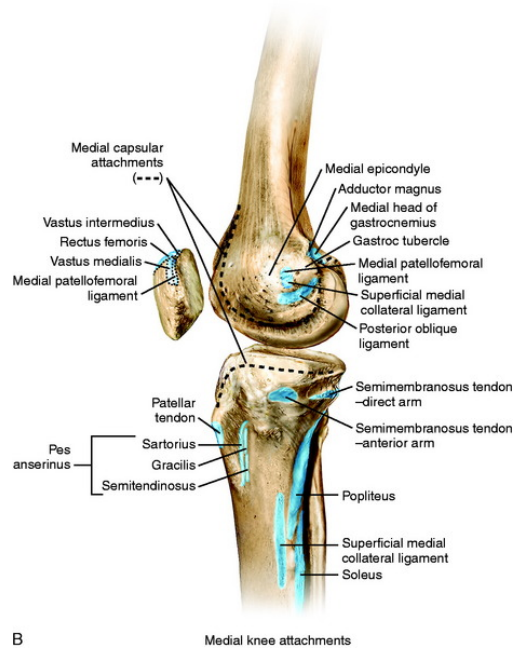
Fig. 3.39: The distal insertions of the SMT (https://clinicalgate.com/medial-and-anterior-knee-anatomy/). Note that the model only includes the insertion of the direct arm.

Note: When defining the insertion site for the semimembranosus, two proximal points should be defined to represent the line of action of the tendon in the image state.

GEOMETRIC RECONSTRUCTION

4.1 Introduction

In this section the surface representation of the tissue of interest (.stl) is used to construct the geometric representation of that tissue. The STL file is the output of the segmentation procedure in raw and unfiltered state. First a brief introduction to the software and tools that you will be using is proposed. Next, in the *Tissue Specific Procedure* (page 49) a guideline is presented for reconstruction of each tissue of interest.

4.2 Prerequisite

MeshLab: MeshLab is a free and open source software for processing and editing 3D triangular meshes. It provides a set of tools for editing, cleaning, inspecting, texturing and rendering of unstructured large 3D triangular meshes. It offers features for processing raw data produced by 3D digitization tools/devices (e.g. 3D Slicer) and for preparing 3D models https://www..meshlab.net/ .

4.3 Loading Data into MeshLab

Input: Triangulated Surface representation of the tissue of interest in stl format (.stl).

- Click `File > Import Mesh`

- Select the desired .stl file. You can select multiple non-contiguous files by holding `Ctrl` or selecting contiguous ones by holding `Shift`.

- Click `Open`.

4.3.1 Notes

1. There is no `Undo` in MeshLab. Please save your work frequently and after every successful step, before losing it during program crashes (which unfortunately occurs a lot!) or applying a wrong filter!

2. In the toolbar panel on top of the MeshLab main interface, click on the `Show Layer Dialog` button, a layer dialog will pop up on the right side of the window. You can get plenty of information about the project from this dialog.

- On the upper part you have a list of all files/meshes you have already loaded into MeshLab, the highlighted one in this section is the current layer. This is important since some of the operations of the MeshLab work only on the current layer. You can change the visibility of a layer by clicking on the eye icon next to each layer. If

you keep `Ctrl` button and then select the visibilty of a layer, all other layers will be switched off and the only visible one is the one you selected.

- In the middle part you can handle visualization and rendering modes of meshes. You can manage color, size and shading/lighting of points, edges and faces in each layer or you can apply your desired settings to all visible layers by checking the `apply to all visible layers` box on bottom of this section.

- The lower section is the feedback dialog. You can read there about all the things you have done, loaded and unloaded and also errors you have been encountered diring an operation.

4.4 Smoothing Procedure

In this section a couple of smoothing procedures will be described in detail and later, in the *Tissue Specific Procedure* (page 49) section a guideline will be provided for each specific tissue.

4.4.1 Laplacian Smoothing

- Select desired mesh from the layer dialog panel.
- Go to `Filters > Smoothing, Fairing and Deformation > Laplacian Smooth`.
- Set `Smoothing Steps` to whatever value is recommended in the *Tissue Specific Procedure* (page 49) section for your desired tissue.
- Make sure the `Affect only selected faces` box is unchecked.
- Click `Apply`.
  - Before hitting the `Apply` button you can check the `Preview` box to see how the smoothing will affect the mesh.

4.4.2 Surface Reconstruction

- Select desired mesh from the layer dialog panel.
- Go to `Filters > Remeshing, Simplification and Reconstruction > Surface Reconstruction: VCG`.
- Alter `Voxel Side, world unit`. Try different values, smaller number means less smoothing. It is recommended to set `world unit` value to a meaningful one relative to the original image resolution (e.g. for cartilage specific images with a resolution of 0.35 x 0.35 x 0.7 mm, use a world unit between 0.35 and 0.7 mm).
- Select `Post Merge Simplification`.
- Click `Apply`.

4.4.3 Taubin Smoothing

Taubin Smoothing procedure is very useful for smoothing vertices/nodes at sharply curved model edges.

- Select desired mesh from the layer dialog panel (It is better to select parts of the mesh with sharped edges, guideline for selection is provided in *Selecting Procedure* (page 47) section).
- Go to `Filters > Smoothing, Fairing and Deformation > Taubin Smoothing`.
- Select `Preview` to interactively display current smoothing parameters.

- It is suggested to set `Lambda` and `mu` to their default values (0.5 and -0.53 respectively). Alter them to get the best result.``Lambda`` should usually be between 0.3 to 1.2 to prevent having jagged meshes.

- Click `Apply`.

4.4.4 Iso Parametrization

- Before starting the `Iso Parametrization` procedure make sure that you have saved your work up to this point.

- Select desired mesh from the layer dialog panel.

- Go to `Filters > Remeshing, Simplification and Reconstruction > Iso Parameterization`.

- Use the default settings and click `Apply`.

Note: Sometimes, the Iso Parametrization will fail and cause Meshlab to crash. If this occurs:

- Deselect `Double Step` box in the `Iso Parametrization` window and click `Apply`.

- Or try an increased amount of smoothing (using *Laplacian Smoothing* (page 46) or *Surface Reconstruction* (page 46)) and/or *Downsizing* (page 48).

- After successfully applying the `Iso Parametrization`, navigate to `Filters > Remeshing, Simplification and Reconstruction > Iso Parameterization Remeshing`.

- Try default `Sampling Rate` = 10. Alter the `Sampling Rate` if it is needed (a higher number of sampling rate creates a higher density triangular surface mesh).

- Click `Apply`.

4.5 Selecting Procedure

To select a specific portion of surface there are different tools you can use:

- Click on `Select Faces in a rectangular region` icon in the toolbar panel on top of the MeshLab main interface. With this tool you can select faces in a rectangular region. This tool select visible and invisible faces in this rectangular region (if you turn your model you will see that it has also selected all the faces on the other side of the model in this rectangular region). it takes a little bit of exercise to make the right selection of faces. You have to play with navigation to put the model in the proper position to make the right selection.

  - If during the selection process you wanted to move the model to a more suitable position to see other sides of the model, press `Esc` button to switch to navigation mode. Now you can rotate the model. To switch back to selecting tool, press `Esc` button again. If you want to exit from the selecting tool permanently you have to click again on its icon in the toolbar panel.

  - If you press `Ctrl` key, a plus sign will apear next to the mouse cursor. Now you can add new selection to the one that has been previously made.

  - If you press the `Shift` key, a minus sign will apear next to the mouse cursor. Now you can subtract part of already selected region.

- Click on `Z-painting` tool in the toolbar panel. A window will pop up. On the left side of the window click on the red head brush and click on the surface of the geometry you want to paint. you can adjust brush size using the `Size` widget. Paint tool only select visible surfaces and also you don not need to hit `Ctrl` key to select multiple regions. It automatically adds new selection to previous one.

- Under `Filters` menu there is a submenu devoted only to selections. There are several ways to select desired regions in a mesh processing style rather than directly interacting with the model and manually tuning it. Their names usually explains their action so they are easy to implement. For example, if you have small disconnected fragments of stl in your model, go to `Filters > Selection > Select small disconnected component`.

4.6 Downsizing

In order to simplify the mesh by reducing number of faces:

- Go to `Filters > Remeshing, Simplification and Reconstruction > Quadric Edge Collapse Decimation`.

- It is suggested to change the visualization mode to flat lines (click on `Wireframe` icon in the toolbar panel) to see the density change of the triangles.

- Change the `Quality threshold`. The higher the value is, your original model's shape will be preserved. Suggest value is 0.4.

- Click `Apply`.

4.7 Cleaning and Repairing

After performing all the smoothing process, we have to make sure that the model is manifold (all edges have exactly two incident triangles. All vertices have exactly one cycle of incident triangles. All triangles in the mesh are consistently oriented). In the visualization and rendering modes section (middle part of layer dialog), click on the `Edge decorators` icon (last icon from the right). A list of `On` and `Off` switches will appear. Switch on the `No-Manif Verts` and `Boundary Edges`. A box will pop up in the top left corner showing how many of each of these exist in the model. If the numbers are zero skip to step 7 otherwise:

1. Switch on `No-Manif Edges` as well.

2. Area relating to these vertices and edges will be highlighted in the model. if you can not see the highlighted area, go to `Filters > Selection > Dilate Selection`, it will expand the current set of selected faces.

3. Use your preferred selection tool from the *Selecting Procedure* (page 47) section and select all the highlighted regions.

4. Select `Delete the current set of selected faces and all the vertices surrounded by that faces`.

5. Again, check the number of `No-Manif Verts`. If it is zero go to the next step to close the holes, otherwise:

- The remaining `No-Manif Verts` are the orphan nodes, to delete them go to `Filters > Cleaning and Repairing > Remove Unreferenced Vertices`.

6. Go to `Filters > Remeshing, Simplification and Reconstruction > Close Holes`. Leave default options and click `Apply`.

7. Go to `Filters > Cleaning and Repairing > Merge Close Vertices`. Change the `world unit` for the `Merging distance` based on how close the model's vertices should be. Use very small values (suggested value is 0.001). Click `Apply`.

8. Go to `Filter > Normals, Curvatures and Orientation > Re-Orient all faces coherently`. This modification is beneficial to the 3D meshing procedure. To see normals of faces navigate to `Render > Show Normal`

4.8 Exporting Data from MeshLab

To save your work:

- Select your desired layer from the layer dialog panel and go to `File > Export Mesh As`.

- Navigate to the desired directory for saving the mesh. Change the file type to `stl` format and hit `Save`.

- A window will pop up. Leave the default settings and click `OK`.

4.9 Tissue Specific Procedure

In the table below the specific order of smoothing procedures for each tissue and also the parameters related to each of these smoothing steps has been provided. It is required to perform the *Cleaning and Repairing* (page 48) procedure after doing all the smoothing steps below.

Tissue Name	**1.** *Laplacian Smoothing* (page 46)	**2.** *Surface Reconstruction* (page 46)	**3.** *Taubin Smoothing* (page 46)	**4.** *Iso Parametrization* (page 47)
Tibia Femur	20	0.7	0.5; -0.53	10
Patella	20	0.5	0.5; -0.53	7
Fibula	20	0.5	0.5; -0.53	5
Tibial Cartilage	20	0.35	0.5; -0.53	10
Femoral Cartilage	20	0.35	0.5; -0.53	15
Patellar Cartilage	20	0.35	0.5; -0.53	10
Meniscus	20	not needed	not needed	8

MODEL SETUP

Contents:

5.1 Mesh Creation

This section describes the procedures that are used to create the geometric mesh that is used in the finite element model.

Software

Table 5.1: Software used during mesh creation

Program Name	Version	link
IA_FEMesh		https://www.ccad.uiowa.edu/ MIMX/projects/IA-FEMesh
Meshlab	2016.12	https://www.ccad.uiowa.edu/ MIMX/projects/IA-FEMesh
3D Slicer	4.8.1	https://www.slicer.org/

5.1.1 Bone

Triangulated surface mesh is used to represent the geometry of bones in .stl format. If you have already followed all the steps in the *Geometric Reconstruction* (page 45) section, the .stl file you have is appropriately meshed otherwise, look at the *Tissue Specific Procedure* (page 49) section in *Geometric Reconstruction* (page 45) section and follow all the required step for smoothing and re-meshing of your tissue of interest and after that perform *Cleaning and Repairing* (page 48) process which is in *Geometric Reconstruction* (page 45) section aswell.

Table 5.2: Required data after bone segmentation

Description	Mesh Type	Comments
Femur surface	triangle	The osseous surface of the femur. This surface is hollow however it should be a closed surface.
Tibia surface	triangle	The osseous surface of the tibia. This surface is hollow however it should be a closed surface.
Patella surface	triangle	The osseous surface of the patella. This surface is hollow however it should be a closed surface.

5.1.2 Meniscus

Note: If in the future, a ligament and/or tendon is being modeled as a continuum, then the geometry should be *segmented* (page 8) and *reconstructed* (page 45), the meshed following these procedures.

Mesh Generation

Hexahedral elements are used to represent the geometry of the menisci. The smoothed .stl surfaces (described in *Geometric Reconstruction* (page 45)) are loaded into IA_FEMesh, and blocks are manually define and oriented around the surface (Fig. 5.1). The number of seed nodes along the axes of each block should be defined, and the specific number of seed points should be determined with a convergence analysis. Smoothing should not be used when generating the mesh (the mesh may be smoothed in later steps).
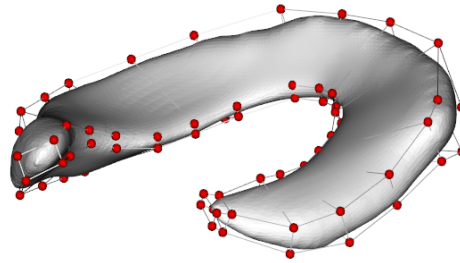
Fig. 5.1: An example of the blocks setup around a lateral meniscus surface.

5.1.3 Cartilage

The cartilage is being modeled using an elastic foundation model *[LKST15]* (page 93),:cite:*halloran_comparison_2005*. As such, only a surface mesh is needed. The triangular mesh that was created from the *segmentation and reconstruction* (page 1) steps is converted into a quadrilateral dominated mesh. This is performed using *MeshLab*, where there is an option to convert a triangular mesh into a quadrilateral dominated mesh. Using *MeshLab*, the triangular mesh (imported from the .stl file) is converted into a quadrilateral dominated mesh. The option for *Fewer Triangles* should be selected. Note that this creates a mesh that may have still have triangular elements.

The surfaces that are converted into quadrilaterl dominated meshes are:

- Femoral cartilage
- Tibial cartilage - medial
- Tibial cartilage - lateral
- Patellar cartilage

Mesh Quality

If the resulting mesh does not approximate the smoothed surface (i.e. the hex mesh has sharp points along surfaces that are smooth in the input surface), the mesh can be smoothed for 1 or 2 iterations using the `Elliptical` interpolation option. If the mesh still does not approximate the smoothed surface, then the number of seed nodes should be increased, and the surface should be remeshed.

After generating a mesh that matches the input geometry, the mesh should be imported into Abaqus to measure the mesh quality. Following the Abaqus documentation, the mesh should meet the criteria described in Table 5.3. If all

---

of the elements in the mesh do not have the desired quality metrics, then the blocks should be adjusted as needed, and the geometry should be remeshed. If the desired quality metrics are still not achieved after several iterations, then the affected geometry should be documented, and the mesh with the best quality elements should be used. Thin areas in the geometry, such as the inner rim of the meniscus, may not have elements with the desired quality.

Table 5.3: Hexahedral mesh quality metrics found in Abaqus 6.14 documentation, `Abaqus/CAE User's Guide` in section 17.6.1 `Verifying your mesh`

Metric	Value
Smaller face corner angle	10 deg
Larger face corner angle	160 deg
Aspect ratio	10

Meniscal Attachments

Similar to other studies (*[NBJvdG+17]* (page 93)), the meniscal attachments are modeled as bundles of nonlinear springs. The mensical attachments are defined in the same was as described in the *Ligaments and Tendons* (page 52) section. In short, insertion points are manually defined from the MR images, and these points are used to create the attachment's mesh (Fig. 5.2).

5.1.4 Ligaments and Tendons

Ligaments and tendons are represented as a bundle of nonlinear springs. Bundles are composed of a line of equally space fibers, where adjacent fibers are connected by tension only corss-springs Fig. 5.2.
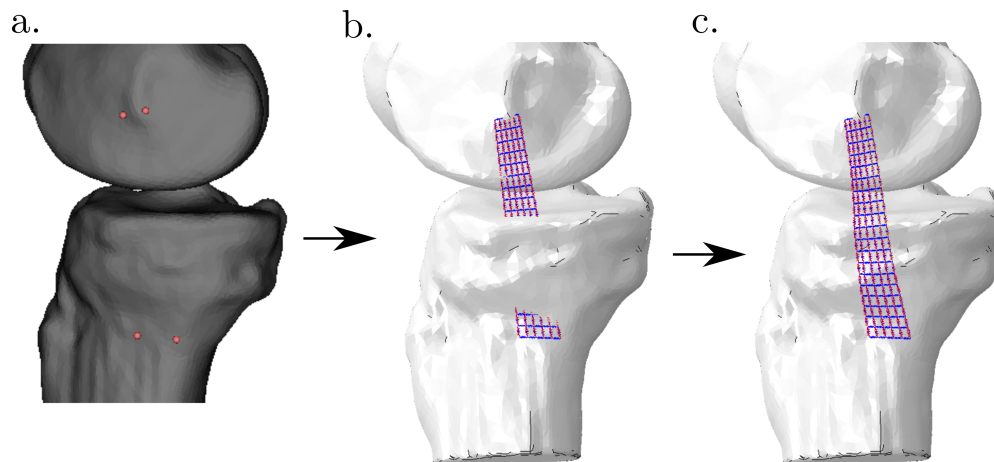
Fig. 5.2: An example of the (a) points used to define a ligament, (b) the point to point mesh that is generated from the four points, and (c) the mesh wrapping around the femur and tibia osseous surfaces. The example shows six ligament fibers that are oriented in the proximal-distal direction, and the connecting springs that are oriented in the anterior-posterior direction that make up a total of 20 divisions in the mesh. This is a medial view of a right knee. Note that this is used as an example, and not used to describe the insertion locations or size of any specific ligament.

Note: If in the future, a ligament and/or tendon is being modeled as a continuum, then the geometry should be *segmented* (page 8) and *reconstructed* (page 45), then meshed following the same proceedure as described for meshing the *menisci* (page 50).

Manually Defined Data

For each ligament/tendon mesh, there are two types of data that are manually defined by the user

1. Points that define both insertion areas Fig. 5.2 (a)

2. The correspondence of the points between insertion areas

The MR images are used to manually define the insertions of the ligaments/tendons. Using 3D Slicer, two points are manually placed in the MR image at the margins of the ligament/tendon's insertion area. These two points should form a line that bisects the insertion area. The literature should be used to confirm the relative locations of the insertions (Table 5.4), and when literature based measurements are available, the `ruler` tool in 3D Slicer should be used to verify the ligament/tendon insertion's size and location. The links in Table 5.4 contain the literature sources used to define the insertions, and measurements that were referenced to verify the insertion area size and location.

After the points that represent the ligament/tendon's insertion area have been defined (4 points total, 2 for each end of the ligament/tendon's insertion) the user should manually define the corresponding points between insertion sites. The corresponding points are used to define the fibers at the margins of the ligament/tendon's insertion area. For example, in Table 5.4, the anterior point on the tibia's insertion corresponds with the anterior point of the femur's insertion. Due to possible ambiguity, notes for corresponding points in the ACL and PCL bundles are provided on their anatomy description page Table 5.4.

Mesh Generation

Using the manually defined data, two inputs are needed to define the coarseness of the mesh. Appropriate values should be deter

1. Number of fibers Fig. 5.2

2. Number of divisions Fig. 5.2

The fibers at the margins of the insertion sites are defined using the manually defined points, and additional fibers are mapped between these fibers. The insertion points of the additional fibers are equally spaced between each manually defined point. Adjacent fibers are connected with tension only springs, and the locations of these springs are defined by evenly distributing the same number of points along the length of each fiber.

Due to the use of explicit analysis in Abaqus, there are mass elements defined at every node, and dashpot elements are defined to be in parallel with every spring element. The material properties of all the elements in the ligament mesh can be found here: *Initial Material Properties* (page 65).

Table 5.4: Ligaments and tendons included in the model, and links to the descriptions of their anatomy.

Description	File Type	Anatomy description
Anteromedial ACL (amACL)	Spring	*ACL Anatomy* (page 16)
Posteriolateral ACL (plACL)	Spring	*ACL Anatomy* (page 16)
Anterolateral PCL (alPCL)	Spring	*PCL Anatomy* (page 18)
Posteromedial PCL (pm-PCL)	Spring	*PCL Anatomy* (page 18)
Superficial MCL	Spring	*MCL Anatomy* (page 21)
Deep MCL	Spring	*MCL Anatomy* (page 21)
LCL	Spring	*LCL Anatomy* (page 24)
ALL	Spring	*ALL Anatomy* (page 26)
PFL	Spring	*PFL Anatomy* (page 27)
OPL	Spring	*OPL Anatomy* (page 27)
MPFL	Spring	*MPFL Anatomy* (page 29)
Quadriceps Tendon	Spring	*Quadriceps Tendon Anatomy* (page 35)
Patellar Tendon	Spring	PatellarTendonAnatomy

Reference State

The ligament spring meshes do not account for wrapping when they are defined. This could lead to unusual recruitment when defining ligament prestrain. Additionally, nodes that may be tied to the meniscus cannot be identified from the initial ligament spring mesh.

To account for ligament wrapping when setting up the FE model, an initial FE simulation will be used to define ligament node positions when wrapping is enforced (Fig. 5.3). The ligament meshing procedures will be used to define the mesh for the initial simulation, and the results of this simulation will be used to define the node positions in subsequent simulations (such as passive flexion).

Note: The joint in the reference state is in the same position/orientation as the image state. Ligament prestrain is defined with respect to the reference state, therefore prestrains are defined with respect to the position/orientation that the knee was in during imaging.

Method - Reference State

In the initial reference simulation, the femur, tibia, patella, menisci, and cartilage are rigid and fixed. This keeps those bodies in the same position as in the MR images. To prevent the ligaments from being slack, they will be assigned a uniform prestrain of -5%. The stiffness of the ligaments will not be changed from their normally assigned values (*Initial Material Properties* (page 65)).
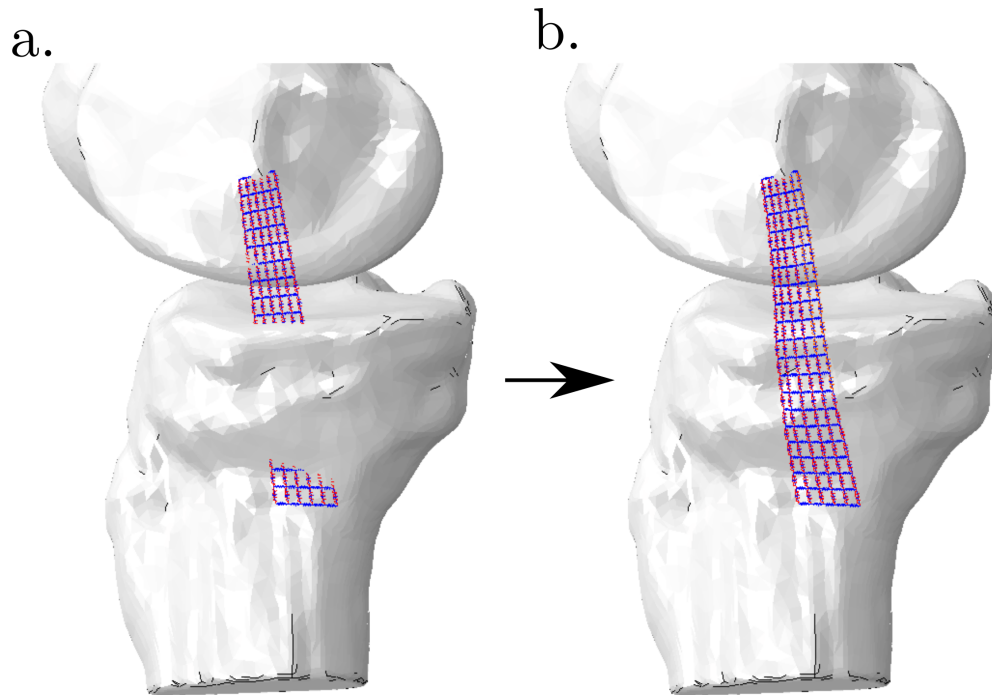
Fig. 5.3: An example of (a) the initial mesh that is defined from insertion point to insertion point data, and (b) the reference state where the ligament's mesh wrapped around the femur and tibia surfaces. Note that this is used as an example, and not used to describe the insertion locations or size of any specific ligament.

The simulation enforces contact between the ligaments and the femur, tibia, patella, menisci, and cartilage. The results of this simulation are used to define the initial ligament node positions for all subsequent simulations. These node positions are used when calculating fiber lengths which is used then assigning prestrain. Additionally, the node positions of the dMCL are used to define which nodes are tied to the medial meniscus (*dMCL and Meniscus Ties* (page 72)).

Note: The reference simulation should be performed after mesh convergence has been established.

Additionally, if there is a change in ligament or medial meniscus geometry, then the reference simulation should be re-run.

5.2 Coordinate Systems

This section describes the methods used to define the coordinate systems of the femur, tibia, and patella. These coordinate systems are used to describe tibiofemoral and patellofemoral kinematics.

This describes how the coordinate system is defined using the DU data set, which consists MR and CT images, as well as points that were digitized around the femur, tibia, and patella during testing. The digitized points include individual landmarks, and sets of points that were digitized around the osseous and articulating surfaces.

These methods define the digitized landmarks with respect to the MR image's coordinate system by using a registration procedure (described here: *DU Registration* (page 58)). The landmarks in the MR image coordinate system are used to define the fixed coordinate systems for the femur, tibia, and patella.

5.2.1 Femur (DU)

Five digitized landmarks around the distal femur and several digitized points around the femoral head are reported. Four of the distal points and the center of the femoral head are used to define the femur's fixed coordinate system. The center of the femoral head is calculated from the points digitized around the femoral head. This coordinate system is similar to that described by *[GS83]* (page 92).

Fiducial locations:

- F_1 = **Medial femoral epicondyle**
- F_2 = **Lateral femoral epicondyle**
- F_3 = **distal point between condyles**
- F_4 = **Posterior medial femoral condyle**
- F_5 = **Posterior lateral femoral conldyle**

Calculated location:

- F_6 = **Femoral head center**, calcualted by fitting a sphere to the points dititized around the femoral head

Origin: defined as F_3, the distal point between condyles.

The femoral superior-inferior axis (z_{SI}) points superiorly, and is defined as the unit vector that is parallel with the line that passes through the center of the femoral head (F_5) and the mid point between the medial and femoral condyles (F_3).

$$z_{SI} = \frac{F_6 - F_3}{||F_6 - F_3||}$$

The femoral anterior-posterior axis (y_{AP}) points anteriorly, and is defined as

$$y_{AP} = z_{SI} \times \bar{EF}$$

Where $\bar{EF}$ is a unit vector line that points to the right, and is parallel to the line that passes through the posterior medial (F_4) and posterior lateral (F_5) femoral condyles.

Note: For a right knee:

$$\bar{EF} = \frac{F_5 - F_4}{||F_5 - F_4||}$$

For a left knee:

$$\bar{EF} = \frac{F_4 - F_5}{||F_4 - F_5||}$$

The medial-lateral (x_{ML}) axis points to the right, and is defined with as the cross product between the y_{AP} and z_{SI} axes.

$$x_{AP} = y_{AP} \times z_{SI}$$

5.2.2 Tibia (DU)

Five digitized landmarks are reported, and four of these points are used to define the tibia's fixed coordinate system. This coordinate system is similar to that described by *[GS83]* (page 92).

Fiducial locations:

- T_1 = **Medial tibial plateau dwell point**
- T_2 = **Lateral tibial plateau dwell point**
- T_3 = Proximal tip of the medial spine of the tibial eminence (Not used in coordinate system definition)
- T_4 = **Center of the tibial eminence**
- T_5 = **Center of the distal intramedullary canal**

Origin: defined as T_4, the center of the tibial eminence.

The tibial superior-inferior axis (z_{SI}) points superiorly, and is defined as the unit vector that is parallel with the line that passes through the center of the distal intramedullary canal (T_5) and the center of the tibial eminence (T_4).

$$z_{SI} = \frac{T_4 - T_5}{||T_4 - T_5||}$$

The tibial anterior-posterior axis (y_{AP}) points anteriorly, and is defined as

$$y_{AP} = z_{SI} \times \bar{AB}$$

Where $\bar{AB}$ is a unit vector line that points to the right, and is parallel to the line that passes through the medial (T_1) and lateral (T_2) tibial plateau dwell points.

Note: For a right knee:

$$\bar{AB} = \frac{T_2 - T_1}{||T_2 - T_1||}$$

For a left knee:

$$\bar{AB} = \frac{T_1 - T_2}{||T_1 - T_2||}$$

The medial-lateral (x_{ML}) axis points to the right, and is defined with as the cross product between the y_{AP} and z_{SI} axes.

$$x_{AP} = y_{AP} \times z_{SI}$$

5.2.3 Patella (DU)

Five fiducial points are used to define the patella's fixed coordinate system. The article *[ASC+16]* (page 91) does not state the coordinate system used for the patella, so the patella's coordinate system is defined using the same procedure as the OpenKnee(s) data.

Four fiducial points are used to define the patella's fixed coordinate system.

Digitized anatomy:

- P_1 = Most medial point
- P_2 = Most lateral point
- P_3 = Most superior point
- P_4 = Most inferior point

Origin: defined as the midpoint between the medial (P_1) and lateral (P_2) points.

$$P_{OriginP} = \frac{P_1 + P_2}{2}$$

The medial-lateral (x_{ML}) points to the right. For a right knee x_{ML} is defined as the line passing through the lateral point (P_2) and the origin of the patella's coordinate system ($P_{OriginP}$. For a left knee x_{ML} is defined as the line passing through the medial point (P_1) and the origin of the patella's coordinate system ($P_{OriginP}$.

$$x_{ML-right} = \frac{P_2 - P_{OriginP}}{||P_2 - P_{OriginP}||}$$
$$x_{ML-left} = \frac{P_{OriginP} - P_1}{||P_{OriginP} - P_1||}$$

The anterior-posterior (y_{AP}) points anteriorly, and is defined as

$$y_{AP} = \bar{EF} \times x_{ML}$$

where $\bar{EF}$ is a unit vector that points superiorly and is parallel with a line that passes through the inferior (P_4) and superior (P_3) points.

$$\bar{EF} = \frac{P_3 - P_4}{||P_3 - P_4||}$$

The superior-inferior (z_{SI}) axis points superiorly, and is defined as the cross product between the medial-lateral axis (x_{ML}), and the anterior-posterior axis (y_{AP}).

$$z_{SI} = x_{ML} \times y_{AP}$$

5.3 Registration

This document describes how the physical femur, tibia, and patella coordinate systems are registered to their digital models. Registration is used to define the osseous coordinate systems with respect to the digital model's coordinate system. The digial models (usually surfaces) were defined using MR images, therefore the models are defined with respect to the MR image's coordinate system. The MR image's coordiante system will be referred to as the **image coordinate system**, and the digial models are initially defined with respect to this coordiante system.

At the end of the registration procedure, there will be femur, tibia, and patella coordinate systems that are defined with respect to to the image coordinate system.

5.3.1 DU Registration

During physical testing, several points around the femur, tibia, and patella were digitized.

This registration procedure registers points that were digitized during physical testing to the segmented osseous surfaces. The points that were digitized during physical testing were taken on the ossous parts of the anatomy, and specific anatomic landmarks were digitized to define the osseous coordinate system during testing. The transform that is used to register the digitized points to the osseous surface will be used to transform the digitized anatomic landmarks, and these transformed landmarks will be used to define the osseous coordinate system in the MR image coordinate system.

Method Overview

Optimization is used to minimize the total distance between the model's surface and the transformed points. Rotations and translations in the xyz directions (rx, ry, rz, tx, ty, tz) are the control variables that are used to define a transform, and the transform will be applied to the digitized points.

The optimization will likely have several local minima. In an attempt to avoid these issues, an informed initial guess for the transform (rx, ry, rz, tx, ty, tz) will be used. The initial guess will be informed by the osseous landmarks that were digitized during physical testing. Similar landmarks will be defined in the digital model, and these will be used to define the initial transform.

Note: that the digitized points may extend beyond the proximal/distal end of the femur/tibia surfaces. These points should be excluded from the optimization to prevent the registration from erroneously being more proximal/distal. These points should be excluded from the optimization to prevent them from influencing the optimization results.

Specific details on the segmented surfaces and digitized points that are included in the registration optimization are in each section below

Femur

Table 5.5: Femur registration data - DU registration

Description	File Type	Comments
Osseous femur points	txt	The points that were digitized during physical testing. *data-MD-DU02/DU02_raw_probed_points/Points_on_Femur/DU02_fem_Bone.txt*
Osseous landmarks	txt	Osseous landmarks that were digitized during physical testing to define the femoral coordinate system. *data-MD-DU02/DU02_raw_probed_points/Points_on_Femur/DU02_fem_GSPts.txt* Table 5.6
Femoral cartilage	txt	The points that were digitized during physical testing around the femur's articulating surface. *data-MD-DU02/DU02_raw_probed_points/Points_on_Femur/DU02_fem_artgeo.txt*
Osseous surface	stl	The segemented femoral surface
Femoral cartilage	stl	The segemented femoral cartilage surface
Image points	fcsv	The landmarks that were manually defined from the MR image

The digitized points around the osseous femur do not include any points on the distal end. Given that the articulating surface of the femur is an area of interest in the model, the femoral cartilage segmented surface and the digitized points around the femoral articulating surface (*data-MD-DU02/DU02_raw_probed_points/Points_on_Femur/DU02_fem_artgeo.txt*) will also be included in the optimization.

There is no description of the digitized points in *data-MD-DU02/DU02_raw_probed_points/Points_on_Femur/DU02_fem_GSPts.txt*, so the point descriptions were determined by plotting the digitized landmarks and the digitized femoral surface points (*DU02_fem_Bone.txt*). The descriptions can be found in Table 5.6.

Table 5.6: Point order description for DU02_fem_GSPts.txt - DU registration

Row number	Point description
1	Medial femoral epicondyle
2	Lateral femoral epicondyle
3	Distal point between condyles
4	Posterior medial femoral condyle
5	Posterior lateral femoral conldyle

Tibia

Table 5.7: Tibia registration data - DU registration

Description	File Type	Comments
Osseous tibia points	txt	The points that were digitized during physical testing. *data-MD-DU02/DU02_raw_probed_points/Points_on_Tibia/DU02_tib_bone.txt*
Osseous landmarks	txt	Osseous landmarks that were digitized during physical testing to define the tibial coordinate system. Table 5.8. *data-MD-DU02/DU02_raw_probed_points/Points_on_Tibia/DU02_tib_GSPts.txt*
Tibial cartilage	txt	The points that were digitized during physical testing around the tibia's articulating surface. *data-MD-DU02/DU02_raw_probed_points/Points_on_Tibia/DU02_tib_artgeo.txt*
Osseous surface	stl	The segmented tibial surface
Tibial cartilage	stl	The segmented tibla cartilage surface
Image points	fcsv	The landmarks that were manually defined from the MR image

The digitized points around the osseous tibia do not include any points on the proximal end. Given that the articulating surface of the tibia is an area of interest in the model, the tibial cartilage segmented surface and the digitized points around the tibial articulating surface (*data-MD-DU02/DU02_raw_probed_points/Points_on_Tibia/DU02_tib_artgeo.txt*) will also be included in the optimization.

There is no description of the digitized points in *data-MD-DU02/DU02_raw_probed_points/Points_on_Tibia/DU02_tib_GSPts.txt*, so the point descriptions were determined by plotting the digitized landmarks and the digitized tibial articulating surface (*DU02_tib_artgeo.txt*) and the PCL tibial insertion (*DU02_PCL_tib.txt*). The descriptions can be found in Table 5.8.

Table 5.8: Point order description for DU02_tib_GSPts.txt - DU registration

Row number	Point description
1	Medial tibial plateau dwell point
2	Lateral tibial plateau dwell point
3	Proximal tip of the medial spine of the tibial eminence
4	Center of the tibial eminence
5	Center of the distal intramedullary canal

Patella

There is no description of the digitized points in *data-MD-DU02/DU02_raw_probed_points/Points_on_Patella/DU02_latPFlig_pat.txt*, so the point descriptions were determined by plotting the digitized landmarks and the digitized patellar insertion of the quadracept tendon (*DU02_QuadTend_pat.txt*) and lateral patellofemoral ligament (*DU02_latPFlig_pat.txt*). These descriptions. The descriptions can be found in Table 5.9.

Table 5.9: Point order description for DU02_Pat_GSPts.txt - DU registration

Row number	Point description
1	Superior patella
2	Inferior patella
3	Medial patella
4	Lateral patella
5	Center of patella
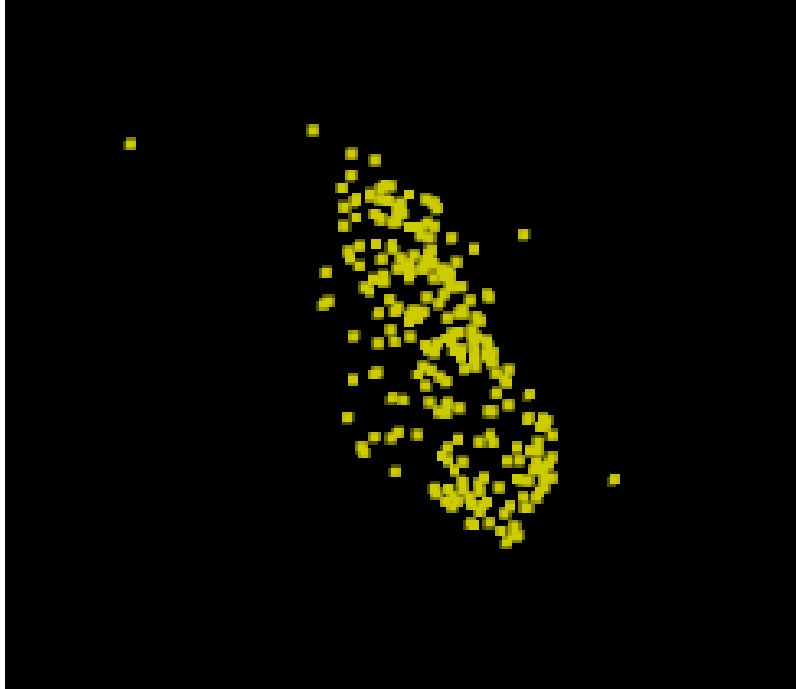
Fig. 5.4: The digitized points from the articulating surface of the patella.

5.4 Connector Elements

This document describes the way that connector elements are used in the FE model. Connector elements are used to define coordinate systems, and the line of action of the muscles (quadriceps, biceps femoris, and semimembranosus) in the FE model. These elements are used to apply external loads and to calculate kinematics throughout the FE simulation.

Two nodes are used to define a connector element, and the order that those nodes are specified in the Abaqus input file determine the positive direction.

All of the connector elements are cylindrical, meaning that they can only rotate and translate along one axis.

5.4.1 Tibiofemoral Coordinate System - Connectors

The fixed femoral and tibial *Coordinate Systems* (page 55) are used to define the connector elements that make up the tibiofemoral coordinate system in the FE model.

Nodes

Four nodes are used to define the three connector elements that compuse the tibiofemoral coordinate system.

- Node 1: The origin of the tibia's fixed coordinate system
- Node 2: The origin of the femur's fixed coordinate system
- Node 3: The point where the AP axis intersects the SI axis
- Node 4: The point there the AP axis intersects the ML axis
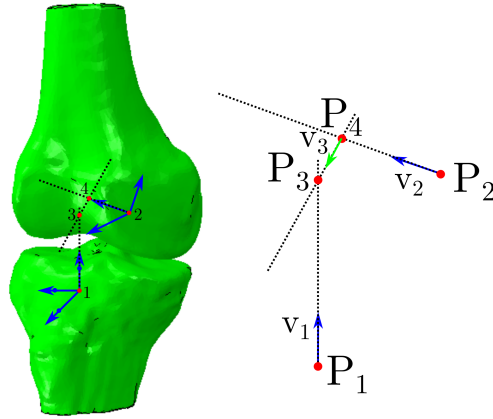
Fig. 5.5: The nodes that are used to define the connector elements.

Referring to Fig. 5.5, and using the line equation ($p_1 = p_0 + t\bar{v}$), the points that lie on the AP axis can be written as (noting that $\bar{v}_1$, $\bar{v}_2$, and $\bar{v}_3$ are unit vectors that are parallel with the x_{ML}, y_{AP} and z_{SI} axes respectively)

$$P_4 = P_2 + t_2\bar{v}_2$$
$$P_3 = P_4 + t_3\bar{v}_3$$
$$= P_2 + t_2\bar{v}_2 + t_3\bar{v}_3$$

Recognizing that P_3 can also be written as $P_3 = P_1 + t_1\bar{v}_1$, the following expression can be written

$$P_3 = P_1 + t_1\bar{v}_1$$
$$= P_2 + t_2\bar{v}_2 + t_3\bar{v}_3$$
$$P_1 + t_1\bar{v}_1 = P_2 + t_2\bar{v}_2 + t_3\bar{v}_3$$

Rearranging the above equation,

$$P_1 - P_2 = -t_1\bar{v}_1 + t_2\bar{v}_2 + t_3\bar{v}_3$$

Recognizing that the only unknown values in the above equation are t_1, t_2, and t_3, the above equation can be expressed in matrix form

$$\begin{bmatrix} -v_{11} & v_{21} & v_{31} \\ -v_{12} & v_{22} & v_{32} \\ -v_{13} & v_{23} & v_{33} \end{bmatrix} \begin{bmatrix} t_1 \\ t_2 \\ t_3 \end{bmatrix} = \begin{bmatrix} P_{11} - P_{21} \\ P_{12} - P_{22} \\ P_{13} - P_{23} \end{bmatrix}$$

where v_{ij} refers to the j index in unit vector i, and P_{kl} refers to the l index in point number k.

The values for t_i can be solved for in the above equation, and

$$P_3 = P_1 + t_1\bar{v}_1$$
$$P_4 = P_2 + t_1\bar{v}_2$$

Elements

The nodes are used to define the elements in the FE model. These elements are used to apply or measure kinematics, and apply external loads. The order that the nodes are defined in the Abaqus input file defines the positive direction of the element. A minimum of three elements are needed, however three additional elements are added to keep consistency in kinematic and load descriptions between right and left knees. For example, translation along the y_{AP}

axis has the same sign between left and right knees, however the same rotation about the y_{AP} (varus) has an opposite sign between left and right knees.

The specific ordering of the nodes will change between right and left knees, but the elements will contain the following nodes:

- Element 1: node 2 and node 4 - medial tibial translation and force

- Element 2: node 4 and node 3 - anterior tibial translation and force

- Element 3: node 1 and node 3 - superior tibial translation and force

- Element 4: node 2 and node 4 - extension rotation and moment

- Element 5: node 4 and node 3 - varus rotation and moment

- Element 6: node 1 and node 3 - internal tibial rotation and moment

Ties

Some of the nodes are tied to the femur and tibia geometry

- **Node 1: Tied to the tibia**
    - The node that is at the tibia's fixed coordinate system origin is rigidly tied to the tibia bone geometry
- **Node 2: Tied to the femur**
    - The node that is at the femur's fixed coordinate system origin is rigidly tied to the femur bone geometry

5.4.2 Patella Quadriceps Connectors - Connectors

Connector elements are used to apply external loading to the quadriceps tendon. In the absence of experimental data, the points manually placed in the MR images to define the quadriceps tendon are used to define the line of action of the quadriceps load (see *Ligaments and Tendons* (page 52) and *Quadriceps Tendon Anatomy* (page 35) for more information on point placement). One node on the connector element is tied to the femur's fixed coordinate system to allow it to move with the femur.

Nodes

Two nodes are defined from the points that were manually defined from the MR image during mesh creation (*Mesh creation - Ligaments and Tendons* (page 52)). There should be a total of four points defined in the MR image that correspond to the quadriceps tendon insertion in to the patella (medial and lateral margins), and two points that are more proximal along the tendon (medial and lateral). These points are used to define the spring representation of the quadriceps.

- P_1: the medial margin of the quadriceps tendon insertion into the patella

- P_2: the lateral margin of the quadriceps tendon insertion into the patella

- P_3: the medial margin of the quadriceps tendon proximal to the patella

- P_4: the lateral margin of the quadriceps tendon proximal to the patella

These points are used to calculate two more points that lie between P_1, P_2 and P_3, P_4.

$$P_5 = \frac{P_1 + P_2}{2}$$
$$P_6 = \frac{P_3 + P_4}{2}$$

A unit vector is defined that is parallel to the line that intersects P_5 and P_6,

$$\bar{v} = \frac{P_6 - P_5}{||P_6 - P_5||}$$

and a point is defined proximal to P_6 along the line of action,

$$P_7 = P_6 + 10.\bar{v}$$

- Node 1: P_6, the point proximal to the patella, at the midpoint between the points defined in the MR image P_3 and P_4
- Node 2: P_7, the point that is prixmal to P_6 along the line of of action defined with P_5 and P_6.

Elements

One connector element is defined with nodes 1 and 2.

Ties

- Node 1 is rigidly tied to the most proximal nodes in the quadricps mesh
- Node 2 is rigidly tied to the origin of the femur's fixed coordinate system

5.4.3 Femur and tibia fixed coordinate systems - Connectors

Connectors are placed on the fixed femur and tibia coordinate systems. These connectors can be used to apply loads or boundary conditions to the femur/tibia's fixed coordinate system.

Nodes

Connector elements are defined to be coincident with the axes of the femur and tibia fixed coordinate systems. Nodes are placed on each axis (6 total) and the origin of both coordinate systems is already defined.

Elements

A total of six elements are defined between the femur and tibia fixed coordinate systems. On each coordinate system, three elements are defined using the node that is defined at the origin, and the nodes that lie on each of the axes.

Ties

All of the nodes that lie on the femur's fixed coordinate system are rigidly tied to the femur's bone geometry. Similarly, all of the nodes that are on the tibia's fixed coordinate system are rigidly tied to the tibia's bone geometry.

5.4.4 Biceps Femoris Connectors

The current data set does not supply any external loading. The biceps femoris is not represented in the passive flexion model, therefore there are no connector elements defined for this anatomy. This is a placeholder for patellofemoral tests.

5.4.5 Semimembranosus Connectors

The current data set does not supply any external loading. The semimembranosus is not represented in the passive flexion model, therefore there are no connector elements defined for this anatomy. This is a placeholder for patellofemoral tests.

5.5 Initial Material Properties

This document describes the material properties that are applied to the geometry in the finite element knee model.

5.5.1 Ligaments and Tendons (spring representation)

The model includes 15 ligament bundles. Stiffness and reference strain of each of these bundles are summarized in Table 5.10. For each bundle, the stiffness was evenly divided between the springs included in that bundle. The number of springs will be determined with a convergence study.
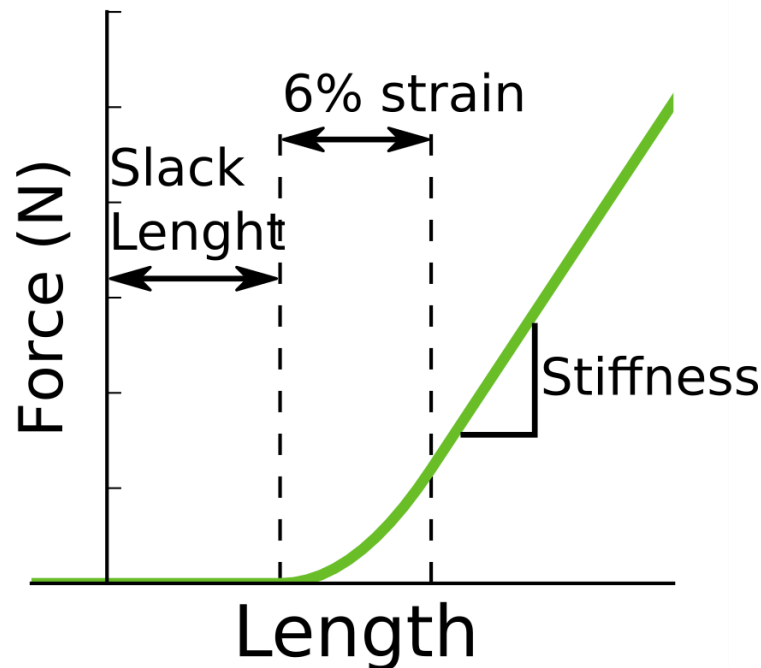
Fig. 5.6: The nonlinear force-length curve that is used to define ligament behavior.

Note that every ligament is modeled as having a toe region that ends at 6% strain.

Prestrain

Each ligament is modeled as a bundle of fibers and prestrain (Table 5.10) is defined with respect to each fiber's length in the *reference state* (page 54), therefore the prestrain is defined with respect to each fiber's length in the joint's position during imaging. The prestrain is used to define the slack length (Fig. 5.6).

Stiffness

Stiffness values (k_{eq}) (Table 5.10) define the ligament bundle's equivalent stiffness, where each fiber has the same stiffness. Each fiber in a ligament bundle with n fibers (Fig. 5.7) has a stiffness of $k_{fib} = k_{eq}/n$. Similarly, there are m springs (Fig. 5.7) that compose a fiber. Each spring in a fiber has the same stiffness value $k_{spr} = m/k_{fib}$.

Adjacent fibers in the ligament mesh are connected with *cross springs* (Fig. 5.7). There are $p = (n-1)(m+1)$ cross spring in a ligament mesh. each cross spring only carries tension forces, and has a constant stiffness of 10 N/mm.
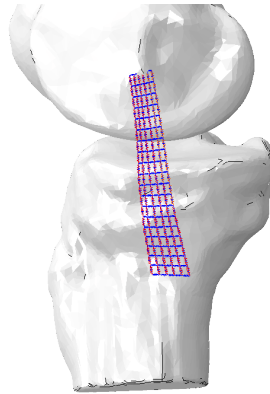
Fig. 5.7: An example of a ligament mesh with $n = 6$ fibers in parallel, and are oriented in the superior-inferior direction. Each fiber contains $m = 19$ springs in series. There are also $p = 100$ cross springs that are oriented in the anterior-posterior direction. The cross springs connect adjacent ligament fibers. Note that this is used as an example, and not used to describe the insertion locations or size of any specific ligament.

The literature normally reportes stiffness values in units of N/mm or N/ϵ. To avoid limiting potential sources, values for both unit types are used. Every spring in the finite element model has a force-displacement curve that is similar to Fig. 5.6. Ligaments with a stiffness with units of N/ϵ have the spring's stiffness converted to units of N/mm based on the spring's length in the *reference state* (page 54) and the assigned prestrain.

Table 5.10: Material properties of the ligament and tendons that are modeled as bundles of springs.

Tissue Name	Stiffness	Reference Strain	Comments
amAcl (page 16)	2120 (N/strain) [AW12] (page 92)	-0.01 [HCA+16] (page 93)	ACL stiffness magnitude from [AW12] (page 92) and amACL to plACL ratio from [KSL+16] (page 93)
plAcl (page 16)	2880 (N/strain) [AW12] (page 92)	-0.04 [HCA+16] (page 93)	ACL stiffness magnitude from [AW12] (page 92) and amACL to plACL ratio from [KSL+16] (page 93)
alPcl (page 18)	5625 (N/strain) [AW12] (page 92)	0.06 [HCA+16] (page 93)	PCL stiffness magnitude from [AW12] (page 92) and alPCL to pmPCL ratio from [KSL+16] (page 93)
pmPcl (page 18)	3375 (N/strain) [AW12] (page 92)	-0.03 [HCA+16] (page 93)	PCL stiffness magnitude from [AW12] (page 92) and alPCL to pmPCL ratio from [KSL+16] (page 93)
sMclProx (page 21)	1375 (N/strain) [AW12] (page 92)	0.07 [HCA+16] (page 93)	The average of the anterior middle and posterior MCL springs reported in [HCA+16] (page 93)
sMclDist (page 21)	1375 (N/strain) [AW12] (page 92)	0.07 [HCA+16] (page 93)	The average of the anterior middle and posterior MCL springs reported in [HCA+16] (page 93)
dMcl (page 21)	1000 (N/strain) [AW12] (page 92)	0.03 [AW12] (page 92)	
lcl (page 24)	2000 (N/strain) [AW12] (page 92)	0.05 [AW12] (page 92)	
all (page 26)	750 (N/strain) [EKH+15] (page 92)	0.05	The prestrain value is arbitrarily defined
pfl (page 27)	1000 (N/strain) [EKH+15] (page 92)	-0.02 [EKH+15] (page 92)	
oplMid (page 27)	1000 [EKH+15] (page 92)	-0.03 [EKH+15] (page 92)	
Mpfl (page 29)	29.4 (N/mm) [HHD+14] (page 92)	-0.05 [SVL+16] (page 93)	
Lpfl (page 30)	16 (N/mm) [MSIA09] (page 92)	0.01 [SVL+16] (page 93)	
PT (page 30)	4334 (N/mm) [HBMA+06] (page 92)	0.02 [SVL+16] (page 93)	
pMFL (page 38)	49 (N/mm) [KHC+94] (page 92)	0.0	The prestrain value is arbitrarily defined
aMFL (page 38)	49 (N/mm) [KHC+94] (page 92)	0.0	The prestrain value is arbitrarily defined
amHorn (page 40)	125 (N/mm) [ELS+14] (page 92)	0.0	The prestrain value is arbitrarily defined
pmHorn (page 40)	125 (N/mm) [ELS+14] (page 92)	0.0	The prestrain value is arbitrarily defined
alHorn (page 40)	150 (N/mm) [ELS+14] (page 92)	0.0	The prestrain value is arbitrarily defined
plHorn (page 40)	130 (N/mm) [ELS+14] (page 92)	0.0	The prestrain value is arbitrarily defined

5.5.2 Ligaments and Tendons (continuum representation)

If in the future, a ligament and/or tendon is being modeled as a continuum, the tissue will be modeled as a transversely isotropic material.

Fiber Direction

The fibers are assumed to be uniformly distributed in, and perfectly bonded to the matrix. The fiber directions are defined in the image state, and run along the length of the ligament. Similar to *[NBJvdG+17]* (page 93), the ACL and PCL are split into two fiber orientations each. These different orientations represent the amACL, plACL, alPCL, and pmPCL bundles of the ligament.

Material Model

Ligament/tensons will be modeled with a transversely isotropic hyperelastic material model. A Holzapfel-Gesser-Ogden *[NBJvdG+17]* (page 93) hyperelastic model will be used. The properties for the ligament and tendons are shown in Table 5.11. Tissues that were not modeled in *[NBJvdG+17]* (page 93) were assigned the same values as the MCL.

Table 5.11: Material properties of the ligament and tendons if they are modeled as a continuum. Note that all of the K_1 and K_2 come from [NBJvdG+17].

Tissue Name	K_1	K_2	prestrain	Comments
amAcl (page 16)	52.27	5.789	0.03 [NBJvdG+17] (page 93)	
plAcl (page 16)	52.27	5.789	0.03 [NBJvdG+17] (page 93)	
PCL	46.18	2.758	0.06 [HCA+16] (page 93)	
MCL (page 21)	41.21	5.351	0.07 [HCA+16] (page 93)	
dMcl (page 21)	41.21	5.351	0.03 [AW12] (page 92)	The K_1 K_2 values are taken from the MCL
lcl (page 24)	41.21	5.351	0.05 [AW12] (page 92)	
all (page 26)	41.21	5.351	0.05	The prestrain value is arbitrarily defined and the K_1 K_2 values are taken from the MCL
pfl (page 27)	41.21	5.351	-0.02 [EKH+15] (page 92)	The K_1 K_2 values are taken from the MCL
oplMid (page 27)	41.21	5.351	-0.03 [EKH+15] (page 92)	The K_1 K_2 values are taken from the MCL
Mpfl (page 29)	41.21	5.351	-0.05 [SVL+16] (page 93)	The K_1 K_2 values are taken from the MCL
Lpfl (page 30)	41.21	5.351	0.01 [SVL+16] (page 93)	The K_1 K_2 values are taken from the MCL
PT (page 30)	41.21	5.351	0.02 [SVL+16] (page 93)	The K_1 K_2 values are taken from the MCL
pMFL (page 38)	41.21	5.351	0.0	The prestrain value is arbitrarily defined and the K_1 K_2 values are taken from the MCL
aMFL (page 38)	41.21	5.351	0.0	The prestrain value is arbitrarily defined and the K_1 K_2 values are taken from the MCL
Meniscal Horns (page 40)	41.21	5.351	0.0	The prestrain value is arbitrarily defined and the K_1 K_2 values are taken from the MCL

Prestrain

A uniform prestrain will be assigned to the ligament/tendon [MEHW16] (page 93) with the prestrain values defined in Table 5.10.

5.5.3 Cartilage

The model includes 4 cartilage geometries. The cartilage is modeled using an elastic foundation model *[LKST15]* (page 93). Contact pressures are calculated using a pressure-overclosure relationship.

$$\frac{Pressure}{Overclosure} = \frac{(1-\nu)E}{(1+\nu)(1-2\nu)}\frac{1}{t}$$

Table 5.12: Material properties of the cartilage geometries.

Tissue Name	E (MPa)	Poisson's ratio	Thickness (mm)
Femoral Cartilage	12 *[DKB10]* (page 92)	0.45 *[DKB10]* (page 92)	3 *[LKST15]* (page 93)
Medial Tibial Cartilage	12 *[DKB10]* (page 92)	0.45 *[DKB10]* (page 92)	3 *[LKST15]* (page 93)
Lateral Tibial Cartilage	12 *[DKB10]* (page 92)	0.45 *[DKB10]* (page 92)	3 *[LKST15]* (page 93)
Patellar Cartilage	12 *[DKB10]* (page 92)	0.45 *[DKB10]* (page 92)	3 *[LKST15]* (page 93)

5.5.4 Menisci

The model includes two meniscus geometries. The menisci are modeled as transversely isotropic linearly elastic *[DKB10]* (page 92). The circumferential elastic modulus is greater than the axial and radial values. Young's modulus and Poisson's ration in the axial direction is equal to radial direction.

Table 5.13: Material properties of the menisci geometries.

Tissue Name	$E_{circumferential}$ (MPa)	$\nu_{circumferential}$	$E_{axial} = E_{radial}$ (MPa)	$\nu_{axial} = \nu_{radial}$
Medial Meniscus	120 *[DKB10]* (page 92)	0.45 *[DKB10]* (page 92)	20 *[DKB10]* (page 92)	0.3 *[DKB10]* (page 92)
Lateral Meniscus	120 *[DKB10]* (page 92)	0.45 *[DKB10]* (page 92)	20 *[DKB10]* (page 92)	0.3 *[DKB10]* (page 92)

5.5.5 Mass Properties

Mass properties are required because we are using an explicit finite element model. Nominal masses are assigned to reduce the amount of intertial effects in the model. Every ligament node is assigned a mass of 0.0001 kg. The cartilage and menisci are assigned a density of 0.000001 kg/mm^2. The bones are rigid bodies, however the connector elements that are rigidly attached to the bones have a rotational inertia of $I_{11} = I_{22} = I_{33} = 0.0001$ kg*mm^2, and $I_{12} = I_{23} = I_{13} = 0.0$.

5.6 Interactions and Ties

5.6.1 Ineraction - Ligaments and Tendons

These interactions are defined for both spring and continuum representation of ligaments and tendons.

Contact

A pressure-overclosure relationship is defined between the connective tissue and bodies that the tissue may contact. Contact damping is also specified so collisions between the tissues and contact surfaces is not perfectly elastic. This

reduces the oscillation of the connective tissues in the simulation. To save on computational cost, interactions are only defined between connective tissues and nearby bodies Table 5.14.

Table 5.14: Ligament and tendon interactions with other bodies in the simulation.

Name	Femur	Tibia	Patella	Femoral Carti-lage	Tibial Carti-lage	Patellar Carti-lage	Medial Menis-cus	Lateral Menis-cus
amACL	x	x		x	x		x	x
plACL	x	x		x	x		x	x
alPCL	x	x		x	x		x	x
pmPCL	x	x		x	x		x	x
sMCLProx	x	x		x	x		x	
sMCLDist	x	x		x	x		x	
dMCL	x	x		x	x		x	
LCL	x			x				
ALL	x	x		x	x			x
PFL	x	x		x	x			x
OPL	x	x		x	x			x
MPFL	x		x			x		
LPFL	x		x			x		
Patellar Tendon	x	x		x				
Quadriceps Tendon	x			x				

A linear pressure-overclosure relationship is specified, where the interaction between the bone surface and a ligament node begins when the node has a clearance of 0.01 mm (i.e the node is not yet touching or overclosing the surface). Specifically, the relationship is a contact force-overclosure relationship. This is a force-overclosure relationship, and not a pressure-overclosure relationship because the ligament surface is defined as a node-surface. As the node over-closure increases, the contact force increases at a rate of 990 N/mm.

The Abaqus input for this interaction is defined as:

```
*Surface Behavior, pressure-overclosure=TABULAR
0.0e3, -0.01
1.0e3, 1.0
*Contact Damping, definition=DAMPING COEFFICIENT
0.25,
```

Ties/Connections

Insertion sites

The nodes that define each ligament/tendon fiber's insertion are rigidly tied to the corresponding bone's fixed coordinate system.

If in the future, a ligament and/or tendon is being modeled as a continuum, then the nodes at the ligament/tendon's insertion will be defined with a nearest neighbor search between the body that the tissue inserts into and the surface nodes of the ligament/tendon.

dMCL and Meniscus Ties

The deep MCL (*MCL Anatomy* (page 21)) inserts into the medial meniscus. To simulate this anatomy, one node from each fiber in the sMCL mesh are rigidly tied to the surface of the medial meniscus. These nodes are identified from the reference simulation results (*Reference State* (page 54)). It is assumed that the dMCL is in contact with the medial meniscus in the reference simulation results. The dMCL mesh will be refined until a every fiber has at least one node in contact with the medial meniscus. The nodes that are tied to the medial meniscus are defined with a nearest neighbor search.

If in the future, the dMCL is being modeled as a continuum, then the dMCL geometry should have ties to the medial meniscus. The surface nodes that are closest to the medial meniscus (defined with a nearest neighbor search) will be rigidly tied to the medial meniscus' surface.

5.6.2 Interaction - Bone, Cartilage, Meniscus

Contact between the articulating surfaces and menisci is defined with a frictionless pressure-overclosure relationship. There are

1. Femoral cartilage - tibial cartilage
2. Femoral cartilage - lateral meniscus
3. Femoral cartilage - medial meniscus
4. Femoral cartilage - patellar cartilage
5. Tibial cartilage - lateral meniscus
6. Tibial cartilage - medial meniscus

Cartilage Contact

The cartilage is modeled as a rigid body, and contact pressures are calculated using pressure-overclosure relationship *[LKST15]* (page 93)[halloran_comparison_2005]. It is assumed that the cartilage has a constant thickness of 3 mm *[LKST15]* (page 93).

$$\frac{Pressure}{Overclosure} = \frac{(1-\nu)E}{(1+\nu)(1-2\nu)}\frac{1}{t}$$

Where $\nu = 0.45$, $t = 3$ mm *[LKST15]* (page 93), and $E = 12$ MPa *[DKB10]* (page 92).

Menisci Contact

A pressure-overclosure relationship is used to model the contact interaction between the articulating surfaces and the menisci. A "softened" nonlinear pressure-overclosure relationship Fig. 5.8 is used to promote the stability of the model.

```
*SURFACE BEHAVIOR, PRESSURE-OVERCLOSURE=EXPONENTIAL
0.01, 0.1, 75
```

The above specifies a pressure-overclosure relationship. The first value (c_0 in Fig. 5.8) specifies that two surfaces begin to interact when the surfaces are 0.01 mm apart (out of contact), and reach a contact pressure of 0.1 MPa (p_0 in Fig. 5.8) when the surfaces are in contact with zero overclosure. The maximum pressure is set to 225 MPa (K_{max} in Fig. 5.8). This maximum pressure is derived from an elastic foundation equation

$$\frac{Pressure}{Overclosure} = \frac{(1-\nu)E}{(1+\nu)(1-2\nu)}\frac{1}{t}$$
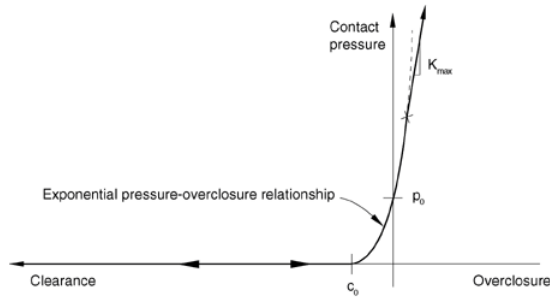
Fig. 5.8: The exponential pressure overclosure relationship from the Abaqus 6.14 documentation.

where $\nu = 0.45$, $t = 3$, and $E = 60$ MPa. Note that $t = 3$ assumes a uniform thickness of 3 mm, which approximates cartilage thickness *[LKST15]* (page 93). Also note that E is five times larger than a normal value for cartilage (12 MPa *[DKB10]* (page 92)). This is increased to limit potential overclosure between surfaces while limiting the maximum pressure-overclosure stiffness.

Ties/Connections

The cartilage and meniscal attachemnts are defined as being perfectly bonded to the bone.

The medial meniscus has ties with the dMCL. This is described elsewhere (*dMCL and Meniscus Ties* (page 72)).

SIMULATION STEPS AND BOUNDARY CONDITIONS

This document describes the specific steps that are used in an Abaqus FE simulation. Each documented step should describe the

- Description: the general purpose of the step

- Interactions: the interactions that are activate in this step

- Kinematic boundary conditions: the kinematic boundary conditions that are being assigned, and where they are being applied

- Kinetic boundary conditions: the external loads that are being applied to the model, and where they are being applied

6.1 Simulation Incrementation (time-step)

The time-step for the simulation defines the incrementation through the simulation's steps. This value will be automatically determined by the Abaqus software.

The automatic controls for the time-step are dependant on the smallest element size in the solid meshes. If the simulation is unstable, or the time-step is prohibitively small, then the solid geometry (meniscus) with the smallest element will be remeshed.

If remeshing is not sufficient to yield a simulation with a reasonably large time-step, then mass scaling will be used to increase the time steps used in the simulation.

6.2 Step Time

The total amount of time that is specified for each step is referred to as *step time*. Unless noted in the step's description, the total time for each step is 1 second.

6.3 Simulation Loading Cases

The steps that makeup an FE simulation for different loading cases:

6.3.1 Reference Simulation

This section describes the specific steps and boundary conditions that are being used during an Abaqus FE simulation that is used to define the reference ligament meshes (described here: *Reference State* (page 54)).

Note: The femur, tibia, patella, cartilage, and menisci do not move or deform in this simulation. They remain in the same position as in the MR image throughout. The purpose of this simulation is to define the position of ligament and tendon mesh nodes so they do not overclose any other bodies.

In this simulation:

- The femur, tibia, patella, cartilage, and menisci are fixed in all DOF
- The femur, tibia, patella, cartilage, and menisci are rigid
- Ligaments and tendons are defined with a prestrain of -5%

There are three steps for this simulation:

Initial settle

Ligaments may be overclosing other bodies by a large amount at the beginning of a simulation (due to the way that the ligament meshes are defined). Additionally, the ligaments may be assigned a prestrain where they will be carrying load at the start of the simulation. During pilot testing it was noticed that ligaments are more stable if there is an initial step where there are no active interactions between the ligaments and other surfaces.

The total time for this step is 0.01 seconds.

Interactions

There are no ligament interactions, and the other geometry is rigid and fixed, so there are no need to define interactions in this step.

Kinematic Boundary Conditions

Femur

The femur is fixed in all degrees of freedom throughout this step.

Tibia

The tibia is fixed in all degrees of freedom throughout this step.

Patella

The proximal nodes in the quadriceps tendon will be fixed in all degrees freedom in this step.

The patella is fixed in all degrees of freedom throughout this step.

Kinetic Boundary Conditions

Femur

No external loads are applied to the femur in this step.

Tibia

No external loads are applied to the tibia in this step.

Patella

No external loads are applied to the patella or the quadriceps tendon in this step.

Wrap bones

The ligament and tendon meshes are defined based on their insertion sites, and they may be overclosing other bodies in the simulation. This step activates the ligament and tendon interactions with the femur, tibia, and patella. These bodies are the first to have ligament interactions because their kinematics will remain fixed.

The total time for this step is 0.1 seconds.

Interactions

The ligament/tendon interactions with the osseous femur, tibia, and patella are activated. Interactions of the ligaments with the menisci and cartilage are still inactive in this step because the amount of overclosure may lead to instability.

Table 6.1: Active interactions between different bodies and structures during the *Wrap bones* step.

Name	Femur	Tibia	Patella	Femoral Cartilage	Tibial Cartilage	Patellar Cartilage	Medial Meniscus	Lateral Meniscus
amACL	x	x						
plACL	x	x						
alPCL	x	x						
pmPCL	x	x						
sMCLProx	x	x						
sMCLDist	x	x						
dMCL	x	x						
LCL	x							
ALL	x	x						
PFL	x	x						
OPL	x	x						
MPFL	x		x			x		
LPFL	x		x			x		
Patellar Tendon	x	x						
Quadriceps Tendon	x							

Kinematic Boundary Conditions

Femur

The femur is fixed in all degrees of freedom throughout this step.

Tibia

The tibia is fixed in all degrees of freedom throughout this step.

Patella

The proximal nodes in the quadriceps tendon will be fixed in all degrees freedom in this step.

The tibia is fixed in all degrees of freedom throughout this step.

Kinetic Boundary Conditions

Femur

No external loads are applied to the femur in this step.

Tibia

No external loads are applied to the tibia in this step.

Patella

No external loads are applied to the patella or the quadriceps tendon in this step.

Wrap soft tissue

The previous step activated ligament interactions with the bones, and this step activates ligament interaction with the cartilage and menisci.

The total time for this step is 0.1 seconds.

Interactions

The interactions from the previous step are still active, and the ligament/tendon interactions with the cartilage and menisci are activated. This step activates the remaining interactions that are being defined for the simulation.

Table 6.2: Active interactions between different bodies and structures during the *Wrap soft tissue* step.

Name	Femur	Tibia	Patella	Femoral Cartilage	Tibial Cartilage	Patellar Cartilage	Medial Meniscus	Lateral Meniscus
amACL	x	x		x	x		x	x
plACL	x	x		x	x		x	x
alPCL	x	x		x	x		x	x
pmPCL	x	x		x	x		x	x
sMCLProx	x	x		x	x		x	
sMCLDist	x	x		x	x		x	
dMCL	x	x		x	x		x	
LCL	x			x				
ALL	x	x		x	x			x
PFL	x	x		x	x			x
OPL	x	x		x	x			x
MPFL	x		x			x		
LPFL	x		x			x		
Patellar Tendon	x	x		x				
Quadriceps Tendon	x			x				

Kinematic Boundary Conditions

Femur

The femur is fixed in all degrees of freedom throughout this step.

Tibia

The tibia is fixed in all degrees of freedom throughout this step.

Patella

The proximal nodes in the quadriceps tendon will be fixed in all degrees freedom in this step.

The patella is fixed in all degrees of freedom throughout this step.

Kinetic Boundary Conditions

Femur

No external loads are applied to the femur in this step.

Tibia

No external loads are applied to the tibia in this step.

Patella

No external loads are applied to the patella or the quadriceps tendon in this step.

6.3.2 Passive Flexion

This section describes the specific steps and boundary conditions that are being used during an Abaqus FE simulation of passive flexion.

There are four steps in the passive flexion simulation cycle:

1. *Initial settle* (page 79)

2. *Load Patella* (page 80)

3. *Initial orientation to 0 flexion* (page 81)

4. *Passive flexion* (page 82)

Initial settle

Before this simulation, the ligament and tendon meshes have been defined from the results of the *reference simulation* (page 74), so there is no overclosure between the ligaments, tendons and other bodies.

The total time for this step is 0.01 seconds.

Interactions

All of the desired interactions are active in this step.

Table 6.3: Active interactions between different bodies and structures during the *Wrap soft tissue* step.

Name	Femur	Tibia	Patella	Femoral Carti-lage	Tibial Carti-lage	Patellar Carti-lage	Medial Menis-cus	Lateral Menis-cus
amACL	x	x		x	x		x	x
plACL	x	x		x	x		x	x
alPCL	x	x		x	x		x	x
pmPCL	x	x		x	x		x	x
sMCLProx	x	x		x	x		x	
sMCLDist	x	x		x	x		x	
dMCL	x	x		x	x		x	
LCL	x			x				
ALL	x	x		x	x			x
PFL	x	x		x	x			x
OPL	x	x		x	x			x
MPFL	x		x			x		
LPFL	x		x			x		
Patellar Tendon	x	x		x				
Quadriceps Tendon	x			x				
Femoral Cartilage					x	x	x	x
Tibial Cartilage							x	x

Kinematic Boundary Conditions

The rigid bodies are fixed in all degrees of freedom.

Femur

The femur is fixed in all degrees of freedom throughout this step.

Tibia

The tibia is fixed in all degrees of freedom throughout this step.

Patella

The proximal nodes in the quadriceps tendon will be fixed in all degrees freedom in this step.

The patella is fixed in all degrees of freedom throughout this step.

Kinetic Boundary Conditions

There are no external loads.

Femur

No external loads are applied to the femur in this step.

Tibia

No external loads are applied to the tibia in this step.

Patella

No external loads are applied to the patella or the quadriceps tendon in this step.

Load Patella

The patella was fixed in the previous step. This step removes the kinematic constraint on the patella, and loads the quadriceps tendon with a nominal load.

The total time for this step is 0.25 seconds.

Interactions

The interactions from the previous step are still active. All of the desired interactions should still be active in this step.

Kinematic Boundary Conditions

Femur

The femur is fixed in all degrees of freedom throughout this step.

Tibia

The tibia is fixed in all degrees of freedom throughout this step.

Patella

The proximal nodes in the quadriceps tendon are no longer fixed, they have no boundary conditions (note that their motion is still constrained with the *patellar quadriceps connector* (page 63)).

No kinematic boundary conditions are specified for the patella.

Kinetic Boundary Conditions

Femur

No external loads are applied to the femur in this step.

Tibia

No external loads are applied to the tibia in this step.

Patella

A 20 N load is applied to the *patellar quadriceps connector* (page 63). This load is linearly increased from 5 N to 20 N throughout this step.

Initial orientation to 0 flexion

This step moves the femur from it's initial position to 0 degrees flexion. The femur's flexion angle is controlled, and is free to move in other degrees of freedom. There is a nominal 20 N compressive load applied to the femur throughout this step.

Interactions

The orientation of the knee at the end of this step is orientation at the beginning of the passive flexion test. As such, all of the interactions that are desired for the passive flexion test are active during this step. These interactions are still active from the previous steps.

Kinematic Boundary Conditions

Femur

For the passive flexion test, the femur will be unconstrained in all directions except for rotation about the flexion axis. The angle about the femur's flexion axis will be assigned throughout this step.

The initial orientation of the knee is known after the femur and tibia coordinate systems are defined with respect to the MR image's coordinate system (more details in *Coordinate Systems* (page 55)). The initial flexion angle is used to define the kinematic boundary condition for the femur during the initial step. The rotation is applied to the *connector element that corresponds to the flexion axis* (page 61).

- **Change the flexion from the initial value to zero**
    - The femur is free to move in other degrees of freedom

Tibia

The tibia will be fixed in all degrees of freedom.

Patella

No kinematic boundary conditions are applied to the patella or the quadriceps tendon.

Kinetic Boundary Conditions

Femur

To reduce the instability in the simulation, a nominal 20 Ncompressive force will be applied to the femur during this step. This force will be applied to the *connector element that corresponds to the SI axis* (page 61). No other external forces will be applied to the femur.

Tibia

No external loads are applied to the tibia in this step.

Patella

To reduce the potential for instability, a 20 N load is applied to the *patellar quadriceps connector element* (page 63). This load is maintained at 20 N throughout this step.

Passive flexion

This step simulates passive flexion. The femur is kinematically controlled in flexion, and free to move in other degrees of freedom.

The total time for this step is 2 seconds.

Interactions

The interactions from the previous step are maintained in this step. All of the desired interactions for the simulation are active in this step.

Table 6.4: Active interactions between different bodies and structures during the *Passive flexion* step.

Name	Femur	Tibia	Patella	Femoral Cartilage	Tibial Cartilage	Patellar Cartilage	Medial Meniscus	Lateral Meniscus
amACL	x	x		x	x		x	x
plACL	x	x		x	x		x	x
alPCL	x	x		x	x		x	x
pmPCL	x	x		x	x		x	x
sMCLProx	x	x		x	x		x	
sMCLDist	x	x		x	x		x	
dMCL	x	x		x	x		x	
LCL	x			x				
ALL	x	x		x	x			x
PFL	x	x		x	x			x
OPL	x	x		x	x			x
MPFL	x		x			x		
LPFL	x		x			x		
Patellar Tendon	x	x		x				
Quadriceps Tendon	x			x				
Femoral Cartilage					x	x	x	x
Tibial Cartilage							x	x

Kinematic Boundary Conditions

Femur

For the passive flexion test, the femur will be unconstrained in all directions except for rotation about the flexion axis. The angle about the femur's flexion axis will be assigned throughout this step.

- **Passive flexion step: Increase the flexion angle from 0 to 90 degrees**
    - The femur is free to move in other degrees of freedom

Tibia

The tibia will be fixed in all degrees of freedom in this step.

Patella

No kinematic boundary conditions are applied to the patella or the quadriceps tendon.

Kinetic Boundary Conditions

Femur

To reduce potential instability in the simulation, a nominal compressive force of 20 N will be applied to the femur during this step. This force will be applied along the joint coordinate system's SI axis, which is the tibia's fixed SI axis. No other external forces will be applied to the femur.

Tibia

No external loads are applied to the tibia in this step.

Patella

To reduce the potential for instability, a 20 N load is applied to the *patellar quadriceps connector element* (page 63). This load is maintained at 20 N throughout this step.

MODEL OUTPUTS

This document describes the outputs that are measured from the simulation results. Time is used to index the application of external loads and prescribed displacements/motions. The model outputs can be measured at specific time points throughout the test cycle. Custom Python scripts are used to extract these measurements from the simulation's results file (.odb for Abaqus).

7.1 Contact

Contact measurements can be directly measured from the simulation. Between each contact pair (Table 7.1) the contact metrics are:

- Total contact area

- Total contact force (magnitude)

- Contact pressure distribution

Table 7.1: The contact pairs where contact area and total contact force are measured from.

Femoral cartilage	Tibial cartilage - medial
Femoral cartilage	Tibial cartilage - lateral
Femoral cartilage	Patellar cartilage

7.2 Joint Kinematics

The *connector elements* (page 61) are used to measure joint kinematics from the simulation results. The connector elements are aligned with the joint's coordinate system, so joint translations and rotation are directly related to each connector's translation and rotation. Note that the connector's initial position is defined when the joint is in the image state (i.e. the joint position/orientation in the MR image), so the initial joint position/orientation should be taken into account when measuring joint kinematics.

7.3 Ligament Force

The ligament force is defined as the magnitude of force carried by the ligament. It is taken as the sum of forces magnitudes carried by each ligament fiber. Each fiber's force is taken as the average force magnitude carried by the elements in the fiber. The elements in each fiber should carry a similar force magnitude, however the forces may be different due to ligaments wrapping around surfaces.

ANNOTATED BIBLIOGRAPHY

This section is for internal MCLS lab use. It summarizes information gathered from the literature.

8.1 Continuum Ligaments

[DKB10] (page 92) modeled four tibiofemoral ligaments (ACL, PCL, MCL, LCL), and four patellofemoral ligaments and tendons (MPL, LPL, quadriceps tendon, and patellar tendon). The figures also appear to show a medial patellar retinaculum, however the text does not describe structures or their material properties. The tibiofemoral ligaments, MPL, and LPL were modeled as fiber reinforces structures with a transversely isotropic hyperelastic material model. The quadriceps and patellar tendon were modeled with a neo-Hooken model.

[NBJvdG+17] (page 93) modeled the ACL, PCL, MCL, LCL, and patellar tendon were modeled with a Holzapfel-Gesser-Ogden (HGO) hyperelastic material model. The fiber orientation of the ACL was split into two groups (anterior and posterior). Thermal loading was used to apply initial strain, with a negative expansion coefficient assigned to each ligament.

8.2 Cartilage

[PCMD06] **(page 94) modeled cartilage as a single phase linear elastic material**

- E = 5 Mpa
- $\nu = 0.46$

[KwonOhRyongKangKyoungTakSonJuhyun+13] **(page 94) and** *[KKS+17]* **(page 93) cited** *[PCMD06]* **(page 94) in their methods, a**

- E = 20 Mpa
- $\nu = 0.46$

[KKS+17] (page 93) modeled the interface between the cartilage and bone as fully bonded. A pressure-overclosure relationship was used to model articular contact.

[DKB10] **(page 92) modeled the cartilage as isioropic linearly elastic**

- E = 12 Mpa
- $\nu = 0.45$

[DHRJ03] **(page 93) modeled the artilage as isotropic linear elastic. Frictionless contact was modeled. Thier convergence study s**

- E = 15 Mpa

- $\nu = 0.475$

[LKST15] **(page 93) modeled cartilage contact with a nonlinear elastic foundation formulation.**

- E = 5 Mpa

- $\nu = 0.45$

- 3 mm uniform thickness

[NBJvdG+17] **(page 93) modeled the cartilage as a nonlinear Neo-Hookean hyperelastic isotropic material.**

- $C_{10} = 0.86$ MPa

- $D = 0.048 MPa^{-1}$

$$\psi = C_{10}(I_1 - 3) + \frac{1}{2D}(J - 1)^2$$

8.3 Meniscus

[PCMD06] **(page 94) modeled the meniscus as a single phase linear elastic material**

- E = 59 Mpa

- $\nu = 0.49$

[KKS+17] (page 93) modeled the meniscus as homogeneous linearly elastic and transversely isotropic. A hexahedral mesh was aligned to the circumferential direction of the model to define local element coordiante systems. Linear springs were used to attach meniscal horns to bone. A pressure-overclosure relationship was used to model articular contact.

[DKB10] **(page 92) modeled the menisci as transversely isotropic linearly elastic**

- $E_{cir} = 120$ Mpa

- $\nu_{cir} = 0.45$

- $E_{axial} = E_{transverse} = 20$ Mpa

- $\nu_{axial} = \nu_{transverse} = 0.3$

[DKB10] **(page 92) modeled the meniscal horns as isotropic, linearly elastic, citing that their properties were poorly understood**

- E = 120 Mpa

- $\nu = 0.45$

[NBJvdG+17] (page 93) modeled the meniscus with a Holzapfel-Gesser-Ogden (HGO) hyperelastic model. Meniscal attachments were modeled as bundles of tension-only nonlinear springs

Table 8.1: Meniscal attachment properties [NBJvdG+17]

Attachment Name	Stiffness (N/mm)	Number of Springs
Horn	400	4
anterior transverse ligament	Not reported	3
anterior and posterior meniscofemoral ligaments	49	1

[DHRJ03] (page 93) performed a sensitivity study on how meniscal properties affect contact metrics. The meniscal horn attachments were modeled as linear springs. Frictionless contact was modeled. Thier convergence study showed that 4 layers of elements were needed to model the meniscus.

The experimental component of the study used pressure-sensitive film to measure contact under 400 N and 1200 N compressive loads at 0 and 15 degrees flexion. A finite element model was developed, and a simplified sampling technique was used to define how sensitive the contact metrics were to assigned material properties.

Table 8.2: Meniscal sensitivity parameters from [DHRJ03]

Parameter	Initial Value	Lower Bound	Upper Bound
Shear modulus $G_{r\theta} = G_{rz}$ (MPa)	57.5	22.7	77.7
Transverse ligament stiffness (N/mm)	200	50	900
Total stiffness of horn attachment (N/mm)	2000	500	30000
Poisson's ratio $\nu_{r\theta} = \nu_{z\theta}$	0.3	0.1	0.35
Poisson's ratio ν_{rz}	0.2	0.1	0.4
$E_r = E_z$ (MPa)	20	15	60
E_θ (MPa)	150	100	200

This study concluded that the contact metrics were sensitive to the meniscal circumferential modulus (E_θ), axial/radial modulus ($E_r = E_z$), and the total horn stiffness.

[DBA+06] V. B. Duthon, C. Barea, S. Abrassart, J. H. Fasel, D. Fritschy, and J. Ménétrey. Anatomy of the anterior cruciate ligament. *Knee Surgery, Sports Traumatology, Arthroscopy*, 14(3):204–213, March 2006. URL: http://link.springer.com/article/10.1007/s00167-005-0679-9, doi:10.1007/s00167-005-0679-9.

[PZ07] Wolf Petersen and Thore Zantop. Anatomy of the Anterior Cruciate Ligament with Regard to Its Two Bundles. *Clinical Orthopaedics and Related Research®*, 454:35, January 2007. URL: https://journals.lww.com/clinorthop/Fulltext/2007/01000/Anatomy_of_the_Anterior_Cruciate_Ligament_with.9.aspx, doi:10.1097/BLO.0b013e31802b4a59.

[TLG+18] Yasutaka Tashiro, Gian Andrea Lucidi, Tom Gale, Kanto Nagai, Elmar Herbst, James J. Irrgang, Yasuharu Nakashima, William Anderst, and Freddie H. Fu. Anterior cruciate ligament tibial insertion site is elliptical or triangular shaped in healthy young adults: high-resolution 3-T MRI analysis. *Knee Surgery, Sports Traumatology, Arthroscopy*, 26(2):485–490, February 2018. URL: https://link.springer.com/article/10.1007/s00167-017-4607-6, doi:10.1007/s00167-017-4607-6.

[AGBE05] A. A. Amis, C. M. Gupte, A. M. J. Bull, and A. Edwards. Anatomy of the posterior cruciate ligament and the meniscofemoral ligaments. *Knee Surgery, Sports Traumatology, Arthroscopy*, 14(3):257–263, October 2005. URL: http://link.springer.com/article/10.1007/s00167-005-0686-x, doi:10.1007/s00167-005-0686-x.

[AZW+12] Colin J Anderson, Connor G Ziegler, Coen A Wijdicks, Lars Engebretsen, and Robert F LaPrade. Arthroscopically Pertinent Anatomy of the Anterolateral and Posteromedial Bundles of the Posterior Cruciate Ligament:. *The Journal of Bone and Joint Surgery-American Volume*, 94(21):1936–1945, November 2012. URL: http://content.wkhealth.com/linkback/openurl?sid=WKPTLP:landingpage&an=00004623-201211070-00003, doi:10.2106/JBJS.K.01710.

[LaP07] Robert F. LaPrade. The Anatomy of the Medial Part of the Knee. *The Journal of Bone and Joint Surgery (American)*, 89(9):2000, September 2007. URL: http://jbjs.org/cgi/doi/10.2106/JBJS.F.01176, doi:10.2106/JBJS.F.01176.

[LYG+10] Fang Liu, Bing Yue, Hemanth R. Gadikota, Michal Kozanek, Wanjun Liu, Thomas J. Gill, Harry E. Rubash, and Guoan Li. Morphology of the medial collateral ligament of the knee. *Journal of orthopaedic surgery and research*, 5(1):69, 2010. URL: https://josr-online.biomedcentral.com/articles/10.1186/1749-799X-5-69.

[LLWE03] Robert F. LaPrade, Thuan V. Ly, Fred A. Wentorf, and Lars Engebretsen. The posterolateral attachments of the knee. *The American Journal of Sports Medicine*, 31(6):854–860, 2003. URL: http://journals.sagepub.com/doi/abs/10.1177/03635465030310062101.

[CVM+13] Steven Claes, Evie Vereecke, Michael Maes, Jan Victor, Peter Verdonk, and Johan Bellemans. Anatomy of the anterolateral ligament of the knee. *Journal of Anatomy*, 223(4):321–328, October 2013. URL: http://onlinelibrary.wiley.com/doi/10.1111/joa.12087/abstract, doi:10.1111/joa.12087.

[LLWE03] Robert F. LaPrade, Thuan V. Ly, Fred A. Wentorf, and Lars Engebretsen. The posterolateral attachments of the knee. *The American Journal of Sports Medicine*, 31(6):854–860, 2003. URL: http://journals.sagepub.com/doi/abs/10.1177/03635465030310062101.

[HSM+17] Mandy Hedderwick, Mark D. Stringer, Liam McRedmond, Grant R. Meikle, and Stephanie J. Woodley. The oblique popliteal ligament: an anatomic and MRI investigation. *Surgical and Radiologic Anatomy*, 39(9):1017–1027, September 2017. URL: http://link.springer.com/10.1007/s00276-017-1838-7, doi:10.1007/s00276-017-1838-7.

[LaP07] Robert F. LaPrade. The Anatomy of the Posterior Aspect of the Knee: An Anatomic Study. *The Journal of Bone and Joint Surgery (American)*, 89(4):758, April 2007. URL: http://jbjs.org/cgi/doi/10.2106/JBJS.F.00120, doi:10.2106/JBJS.F.00120.

[SDM04] Robert N. Steensen, Ryan M. Dopirak, and William G. Mcdonald. The Anatomy and Isometry of Themedial Patellofemoral Ligament: Implications for Reconstruction. *The American Journal of Sports Medicine*, 32(6):1509–1513, September 2004. URL: http://journals.sagepub.com/doi/10.1177/0363546503261505, doi:10.1177/0363546503261505.

[KCM+18] Bradley M. Kruckeberg, Jorge Chahla, Gilbert Moatshe, Mark E. Cinque, Kyle J. Muckenhirn, Jonathan A. Godin, Taylor J. Ridley, Alex W. Brady, Elizabeth A. Arendt, and Robert F. LaPrade. Quantitative and Qualitative Analysis of the Medial Patellar Ligaments: An Anatomic and Radiographic Study , Quantitative and Qualitative Analysis of the Medial Patellar Ligaments: An Anatomic and Radiographic Study. *The American Journal of Sports Medicine*, 46(1):153–162, January 2018. URL: https://doi.org/10.1177/0363546517729818, doi:10.1177/0363546517729818.

[noa] Patellofemoral Joint. URL: https://www.physio-pedia.com/Patellofemoral_Joint.

[CZE+17] Sercan Capkin, Gulsah Zeybek, Ipek Ergur, Can Kosay, and Amac Kiray. An anatomic study of the lateral patellofemoral ligament. *Acta Orthopaedica et Traumatologica Turcica*, 51(1):73–76, January 2017. URL: http://www.sciencedirect.com/science/article/pii/S1017995X16300220, doi:10.1016/j.aott.2016.07.009.

[SDW+17] Kalpit N. Shah, Steven F. DeFroda, James Kristopher Ware, Sarath C. Koruprolu, and Brett D. Owens. Lateral Patellofemoral Ligament: An Anatomic Study. *Orthopaedic Journal of Sports Medicine*, December 2017. URL: https://www.ncbi.nlm.nih.gov/pmc/articles/PMC5718311/, doi:10.1177/2325967117741439.

[LAF12] Julienne Lippe, Amy Armstrong, and John P. Fulkerson. Anatomic Guidelines for Harvesting a Quadriceps Free Tendon Autograft for Anterior Cruciate Ligament Reconstruction. *Arthroscopy*, 28(7):980–984, July 2012. URL: https://www.arthroscopyjournal.org/article/S0749-8063(12)00041-2/abstract, doi:10.1016/j.arthro.2012.01.002.

[noa06] Jumper's Knee. December 2006. URL: http://radsource.us/jumpers-knee/.

[DWP+14] Geoffrey F. Dervin, Timothy Whitehead, Phil Poitras, Milton Parai, and Hakim Louati. The Effect of Medial Release of the Distal Patellar Tendon Insertion on Lateral Patella Translation and Residual Insertion Strength: A Cadaveric Study. *The Journal of Arthroplasty*, 29(3):525–529, March 2014. URL: http://www.sciencedirect.com/science/article/pii/S0883540313005627, doi:10.1016/j.arth.2013.07.044.

[KCM+18] Bradley M. Kruckeberg, Jorge Chahla, Gilbert Moatshe, Mark E. Cinque, Kyle J. Muckenhirn, Jonathan A. Godin, Taylor J. Ridley, Alex W. Brady, Elizabeth A. Arendt, and Robert F. LaPrade. Quantitative and Qualitative Analysis of the Medial Patellar Ligaments: An Anatomic and Radiographic Study , Quantitative and Qualitative Analysis of the Medial Patellar Ligaments: An Anatomic and Radiographic Study. *The American Journal of Sports Medicine*, 46(1):153–162, January 2018. URL: https://doi.org/10.1177/0363546517729818, doi:10.1177/0363546517729818.

[NRLC+02] Ph Neyret, A. H. N. Robinson, B. Le Coultre, C. Lapra, and P. Chambat. Patellar tendon length–the factor in patellar instability? *The Knee*, 9(1):3–6, February 2002.

[LAF12] Julienne Lippe, Amy Armstrong, and John P. Fulkerson. Anatomic Guidelines for Harvesting a Quadriceps Free Tendon Autograft for Anterior Cruciate Ligament Reconstruction. *Arthroscopy*, 28(7):980–984, July 2012. URL: https://www.arthroscopyjournal.org/article/S0749-8063(12)00041-2/abstract, doi:10.1016/j.arthro.2012.01.002.

[WJH09] Andrew C. Waligora, Norman A. Johanson, and Bruce Elliot Hirsch. Clinical Anatomy of the Quadriceps Femoris and Extensor Apparatus of the Knee. *Clinical Orthopaedics and Related Research®*, 467(12):3297–3306,

December 2009. URL: https://link.springer.com/article/10.1007/s11999-009-1052-y, doi:10.1007/s11999-009-1052-y.

[noa18] Meniscofemoral ligaments - Humphery and Wisberg Ligaments. January 2018. URL: http://boneandspine.com/meniscofemoral-ligaments/.

[GSM+02] Chinmay Gupte, A Smith, Ian Mcdermott, Anthony Bull, Rhidian Thomas, and A A Amis. Meniscofemoral ligaments revisited. Anatomical study, age correlation and clinical implications. *The Journal of bone and joint surgery. British volume*, 84:846–51, September 2002. doi:10.1302/0301-620X.84B6.0840846.

[KHC+94] T. Kusayama, C. D. Harner, G. J. Carlin, J. W. Xerogeanes, and B. A. Smith. Anatomical and biomechanical characteristics of human meniscofemoral ligaments. *Knee surgery, sports traumatology, arthroscopy: official journal of the ESSKA*, 2(4):234–237, 1994.

[YH91] M. Yamamoto and K. Hirohata. Anatomical study on the menisco-femoral ligaments of the knee. *The Kobe Journal of Medical Sciences*, 37(4-5):209–226, October 1991.

[noa18] Meniscofemoral ligaments - Humphery and Wisberg Ligaments. January 2018. URL: http://boneandspine.com/meniscofemoral-ligaments/.

[GSM+02] Chinmay Gupte, A Smith, Ian Mcdermott, Anthony Bull, Rhidian Thomas, and A A Amis. Meniscofemoral ligaments revisited. Anatomical study, age correlation and clinical implications. *The Journal of bone and joint surgery. British volume*, 84:846–51, September 2002. doi:10.1302/0301-620X.84B6.0840846.

[KHC+94] T. Kusayama, C. D. Harner, G. J. Carlin, J. W. Xerogeanes, and B. A. Smith. Anatomical and biomechanical characteristics of human meniscofemoral ligaments. *Knee surgery, sports traumatology, arthroscopy: official journal of the ESSKA*, 2(4):234–237, 1994.

[YH91] M. Yamamoto and K. Hirohata. Anatomical study on the menisco-femoral ligaments of the knee. *The Kobe Journal of Medical Sciences*, 37(4-5):209–226, October 1991.

[JCP+12] Adam M. Johannsen, David M. Civitarese, Jeffrey R. Padalecki, Mary T. Goldsmith, Coen A. Wijdicks, and Robert F. LaPrade. Qualitative and Quantitative Anatomic Analysis of the Posterior Root Attachments of the Medial and Lateral Menisci. *The American Journal of Sports Medicine*, 40(10):2342–2347, October 2012. URL: https://doi.org/10.1177/0363546512457642, doi:10.1177/0363546512457642.

[LER+14] Christopher M. LaPrade, Michael B. Ellman, Matthew T. Rasmussen, Evan W. James, Coen A. Wijdicks, Lars Engebretsen, and Robert F. LaPrade. Anatomy of the Anterior Root Attachments of the Medial and Lateral Menisci , Anatomy of the Anterior Root Attachments of the Medial and Lateral Menisci: A Quantitative Analysis , A Quantitative Analysis. *The American Journal of Sports Medicine*, 42(10):2386–2392, October 2014. URL: https://doi.org/10.1177/0363546514544678, doi:10.1177/0363546514544678.

[ASC+16] Azhar A. Ali, Sami S. Shalhoub, Adam J. Cyr, Clare K. Fitzpatrick, Lorin P. Maletsky, Paul J. Rullkoetter, and Kevin B. Shelburne. Validation of predicted patellofemoral mechanics in a finite element model of the healthy and cruciate-deficient knee. *Journal of Biomechanics*, 49(2):302–309, January 2016. URL: http://www.sciencedirect.com/science/article/pii/S0021929015007265, doi:10.1016/j.jbiomech.2015.12.020.

[BA15] Eric A. Branch and Adam W. Anz. Distal Insertions of the Biceps Femoris , Distal Insertions of the Biceps Femoris: A Quantitative Analysis , A Quantitative Analysis. *Orthopaedic Journal of Sports Medicine*, 3(9):2325967115602255, September 2015. URL: https://doi.org/10.1177/2325967115602255, doi:10.1177/2325967115602255.

[ASC+16] Azhar A. Ali, Sami S. Shalhoub, Adam J. Cyr, Clare K. Fitzpatrick, Lorin P. Maletsky, Paul J. Rullkoetter, and Kevin B. Shelburne. Validation of predicted patellofemoral mechanics in a finite element model of the healthy and cruciate-deficient knee. *Journal of Biomechanics*, 49(2):302–309, January 2016. URL: http://www.sciencedirect.com/science/article/pii/S0021929015007265, doi:10.1016/j.jbiomech.2015.12.020.

[LaP07] Robert F. LaPrade. The Anatomy of the Medial Part of the Knee. *The Journal of Bone and Joint Surgery (American)*, 89(9):2000, September 2007. URL: http://jbjs.org/cgi/doi/10.2106/JBJS.F.01176, doi:10.2106/JBJS.F.01176.

[ASC+16] Azhar A. Ali, Sami S. Shalhoub, Adam J. Cyr, Clare K. Fitzpatrick, Lorin P. Maletsky, Paul J. Rullkoetter, and Kevin B. Shelburne. Validation of predicted patellofemoral mechanics in a finite element model of the healthy and cruciate-deficient knee. *Journal of Biomechanics*, 49(2):302–309, January 2016. URL: http://www.sciencedirect.com/science/article/pii/S0021929015007265, doi:10.1016/j.jbiomech.2015.12.020.

[GS83] E. S. Grood and W. J. Suntay. A Joint Coordinate System for the Clinical Description of Three-Dimensional Motions: Application to the Knee. *Journal of Biomechanical Engineering*, 105(2):136–144, May 1983. URL: http://dx.doi.org/10.1115/1.3138397, doi:10.1115/1.3138397.

[AW12] Shahram Amiri and David R. Wilson. A Computational Modeling Approach for Investigating Soft Tissue Balancing in Bicruciate Retaining Knee Arthroplasty. 2012. URL: https://www.hindawi.com/journals/cmmm/2012/652865/, doi:10.1155/2012/652865.

[HBMA+06] P. Hansen, J. Bojsen-Moller, P. Aagaard, M. Kjaer, and S. P. Magnusson. Mechanical properties of the human patellar tendon, in vivo. *Clinical Biomechanics*, 21(1):54–58, January 2006. URL: http://www.sciencedirect.com/science/article/pii/S0268003305001774, doi:10.1016/j.clinbiomech.2005.07.008.

[HHD+14] Mirco Herbort, Christian Hoser, Christoph Domnick, Michael J. Raschke, Simon Lenschow, Andre Weimann, Clemens Kösters, and Christian Fink. MPFL reconstruction using a quadriceps tendon graft: Part 1: Biomechanical properties of quadriceps tendon MPFL reconstruction in comparison to the Intact MPFL. A human cadaveric study. *The Knee*, 21(6):1169–1174, December 2014. URL: http://www.sciencedirect.com/science/article/pii/S0968016014001719, doi:10.1016/j.knee.2014.07.026.

[KHC+94] T. Kusayama, C. D. Harner, G. J. Carlin, J. W. Xerogeanes, and B. A. Smith. Anatomical and biomechanical characteristics of human meniscofemoral ligaments. *Knee surgery, sports traumatology, arthroscopy: official journal of the ESSKA*, 2(4):234–237, 1994.

[MSIA09] Azhar M. Merican, Sanjay Sanghavi, Farhad Iranpour, and Andrew A. Amis. The structural properties of the lateral retinaculum and capsular complex of the knee. *Journal of Biomechanics*, 42(14):2323–2329, October 2009. URL: https://www.ncbi.nlm.nih.gov/pmc/articles/PMC2764350/, doi:10.1016/j.jbiomech.2009.06.049.

[NBJvdG+17] Hamid Naghibi Beidokhti, Dennis Janssen, Sebastiaan van de Groes, Javad Hazrati, Ton Van den Boogaard, and Nico Verdonschot. The influence of ligament modelling strategies on the predictive capability of finite element models of the human knee joint. *Journal of Biomechanics*, 65:1–11, December 2017. URL: http://www.sciencedirect.com/science/article/pii/S0021929017304529, doi:10.1016/j.jbiomech.2017.08.030.

[SVL+16] Colin R. Smith, Michael F. Vignos, Rachel L. Lenhart, Jarred Kaiser, and Darryl G. Thelen. The Influence of Component Alignment and Ligament Properties on Tibiofemoral Contact Forces in Total Knee Replacement. *Journal of Biomechanical Engineering*, 138(2):0210171–02101710, February 2016. URL: https://www.ncbi.nlm.nih.gov/pmc/articles/PMC4844247/, doi:10.1115/1.4032464.

[AW12] Shahram Amiri, David R. Wilson, Shahram Amiri, and David R. Wilson. A Computational Modeling Approach for Investigating Soft Tissue Balancing in Bicruciate Retaining Knee Arthroplasty, A Computational Modeling Approach for Investigating Soft Tissue Balancing in Bicruciate Retaining Knee Arthroplasty. *Computational and Mathematical Methods in Medicine, Computational and Mathematical Methods in Medicine*, 2012, 2012:e652865, October 2012. URL: http://www.hindawi.com/journals/cmmm/2012/652865/abs/,http://www.hindawi.com/journals/cmmm/2012/652865/abs/, doi:10.1155/2012/652865, 10.1155/2012/652865.

[DKB10] Yasin Y. Dhaher, Tae-Hyun Kwon, and Megan Barry. The effect of connective tissue material uncertainties on knee joint mechanics under isolated loading conditions. *Journal of Biomechanics*, 43(16):3118–3125, December 2010. URL: http://www.sciencedirect.com/science/article/pii/S0021929010004380, doi:10.1016/j.jbiomech.2010.08.005.

[ELS+14] Michael B. Ellman, Christopher M. LaPrade, Sean D. Smith, Matthew T. Rasmussen, Lars Engebretsen, Coen A. Wijdicks, and Robert F. LaPrade. Structural Properties of the Meniscal Roots. *The American Journal of Sports Medicine*, 42(8):1881–1887, August 2014. URL: https://doi.org/10.1177/0363546514531730, doi:10.1177/0363546514531730.

[EKH+15] Joseph A. Ewing, Michelle K. Kaufman, Erin E. Hutter, Jeffrey F. Granger, Matthew D. Beal, Stephen J. Piazza, and Robert A. Siston. Estimating patient-specific soft-tissue properties in a TKA knee. *Journal of Or-

thopaedic Research, pages n/a–n/a, September 2015. URL: http://onlinelibrary.wiley.com/doi/10.1002/jor.23032/abstract, doi:10.1002/jor.23032.

[HCA+16] Michael D. Harris, Adam J. Cyr, Azhar A. Ali, Clare K. Fitzpatrick, Paul J. Rullkoetter, Lorin P. Maletsky, and Kevin B. Shelburne. A Combined Experimental and Computational Approach to Subject-Specific Analysis of Knee Joint Laxity. *Journal of Biomechanical Engineering*, 138(8):081004–081004, June 2016. URL: http://dx.doi.org/10.1115/1.4033882, doi:10.1115/1.4033882.

[KSL+16] Mohammad Kia, Kevin Schafer, Joseph Lipman, Michael Cross, David Mayman, Andrew Pearle, Thomas Wickiewicz, and Carl Imhauser. A Multibody Knee Model Corroborates Subject-Specific Experimental Measurements of Low Ligament Forces and Kinematic Coupling During Passive Flexion. *Journal of Biomechanical Engineering*, 138(5):051010–051010, March 2016. URL: http://dx.doi.org/10.1115/1.4032850, doi:10.1115/1.4032850.

[LKST15] Rachel L. Lenhart, Jarred Kaiser, Colin R. Smith, and Darryl G. Thelen. Prediction and Validation of Load-Dependent Behavior of the Tibiofemoral and Patellofemoral Joints During Movement. *Annals of Biomedical Engineering*, 43(11):2675–2685, April 2015. URL: http://link.springer.com/article/10.1007/s10439-015-1326-3, doi:10.1007/s10439-015-1326-3.

[MEHW16] Steve A. Maas, Ahmet Erdemir, Jason P. Halloran, and Jeffrey A. Weiss. A general framework for application of prestrain to computational models of biological materials. *Journal of the Mechanical Behavior of Biomedical Materials*, 61:499–510, August 2016. URL: http://www.sciencedirect.com/science/article/pii/S1751616116300765, doi:10.1016/j.jmbbm.2016.04.012.

[NBJvdG+17] Hamid Naghibi Beidokhti, Dennis Janssen, Sebastiaan van de Groes, Javad Hazrati, Ton Van den Boogaard, and Nico Verdonschot. The influence of ligament modelling strategies on the predictive capability of finite element models of the human knee joint. *Journal of Biomechanics*, 65:1–11, December 2017. URL: http://linkinghub.elsevier.com/retrieve/pii/S0021929017304529, doi:10.1016/j.jbiomech.2017.08.030.

[SVL+16] Colin R. Smith, Michael F. Vignos, Rachel L. Lenhart, Jarred Kaiser, and Darryl G. Thelen. The Influence of Component Alignment and Ligament Properties on Tibiofemoral Contact Forces in Total Knee Replacement. *Journal of Biomechanical Engineering*, 138(2):021017–021017, January 2016. URL: http://dx.doi.org/10.1115/1.4032464, doi:10.1115/1.4032464.

[DKB10] Yasin Y. Dhaher, Tae-Hyun Kwon, and Megan Barry. The effect of connective tissue material uncertainties on knee joint mechanics under isolated loading conditions. *Journal of Biomechanics*, 43(16):3118–3125, December 2010. URL: http://www.sciencedirect.com/science/article/pii/S0021929010004380, doi:10.1016/j.jbiomech.2010.08.005.

[DHRJ03] Tammy L. Haut Donahue, M. L. Hull, Mark M. Rashid, and Christopher R. Jacobs. How the stiffness of meniscal attachments and meniscal material properties affect tibio-femoral contact pressure computed using a validated finite element model of the human knee joint. *Journal of Biomechanics*, 36(1):19–34, January 2003. URL: http://www.jbiomech.com/article/S0021-9290(02)00305-6/abstract, doi:10.1016/S0021-9290(02)00305-6.

[KKS+17] Kyoung-Tak Kang, Sung-Hwan Kim, Juhyun Son, Young Han Lee, Shinil Kim, and Heoung-Jae Chun. Probabilistic evaluation of the material properties of the in vivo subject-specific articular surface using a computational model. *Journal of Biomedical Materials Research Part B: Applied Biomaterials*, 105(6):1390–1400, August 2017. URL: http://onlinelibrary.wiley.com/doi/10.1002/jbm.b.33666/abstract, doi:10.1002/jbm.b.33666.

[LKST15] Rachel L. Lenhart, Jarred Kaiser, Colin R. Smith, and Darryl G. Thelen. Prediction and Validation of Load-Dependent Behavior of the Tibiofemoral and Patellofemoral Joints During Movement. *Annals of Biomedical Engineering*, 43(11):2675–2685, April 2015. URL: http://link.springer.com/article/10.1007/s10439-015-1326-3, doi:10.1007/s10439-015-1326-3.

[NBJvdG+17] Hamid Naghibi Beidokhti, Dennis Janssen, Sebastiaan van de Groes, Javad Hazrati, Ton Van den Boogaard, and Nico Verdonschot. The influence of ligament modelling strategies on the predictive capability of finite element models of the human knee joint. *Journal of Biomechanics*, 65:1–11, December 2017. URL: http://linkinghub.elsevier.com/retrieve/pii/S0021929017304529, doi:10.1016/j.jbiomech.2017.08.030.

[PCMD06] E. Peña, B. Calvo, M. A. Martínez, and M. Doblaré. A three-dimensional finite element analysis of the combined behavior of ligaments and menisci in the healthy human knee joint. *Journal of Biomechanics*, 39(9):1686–1701, January 2006. URL: http://www.jbiomech.com/article/S0021-9290(05)00211-3/abstract, doi:10.1016/j.jbiomech.2005.04.030.

[KwonOhRyongKangKyoungTakSonJuhyun+13] Kwon Oh-Ryong, Kang Kyoung-Tak, Son Juhyun, Kwon Sae-Kwang, Jo Seung-Bae, Suh Dong-Suk, Choi Yun-Jin, Kim Ho-Joong, and Koh Yong-Gon. Biomechanical comparison of fixed- and mobile-bearing for unicomparmental knee arthroplasty using finite element analysis. *Journal of Orthopaedic Research*, 32(2):338–345, October 2013. URL: https://onlinelibrary.wiley.com/doi/full/10.1002/jor.22499, doi:10.1002/jor.22499.